Towards Automated Lake Ice Classification using Dual Polarization RADARSAT SAR Imagery

by

Junqian Wang

A thesis
presented to the University of Waterloo
in fulfillment of the
thesis requirement for the degree of
Master of Science
in
Geography

Waterloo, Ontario, Canada, 2018

AUTHOR'S DECLARATION

I hereby declare that I am the sole author of this thesis. This is a true copy of the thesis, including any required final revisions, as accepted by my examiners.

I understand that my thesis may be made electronically available to the public.

Abstract

Lake ice, as one of the most important component of the cryosphere, is a valuable indicator of climate change and variability. The Laurentian Great Lakes are the world's largest supply of freshwater and their ice cover has a major impact on regional weather and climate, ship navigation, and public safety. Monitoring detailed ice conditions on large lakes requires the use of satellite-borne synthetic aperture radar (SAR) data that provide all-weather sensing capabilities, high resolution, and large spatial coverage. Ice experts at the Canadian Ice Service (CIS) have been manually producing operational Great Lakes image analysis charts based on visual interpretation of the SAR images. Ice services such as the CIS would greatly benefit from the availability of an automated or semi-automated SAR ice classification algorithm.

We investigated the performance of the unsupervised segmentation algorithm "glocal" iterative region growing with semantics (IRGS) for lake ice classification using dual polarized RADARSAT-2 imagery. Here, the segmented classes with arbitrary labels are manually labelled based on visual interpretation. IRGS was tested on 26 RADARSAT-2 scenes acquired over Lake Erie during winter 2014, and the results were validated against the manually produced CIS image analysis charts. Analysis of various case studies indicated that the "glocal" IRGS algorithm can provide a reliable ice-water classification using dual polarized images with a high overall accuracy of 90.2%. The improvement of using dual-pol as opposed to single-pol images for ice-water discrimination was also demonstrated. For lake ice type classification, most thin ice types were effectively identified but thick and very thick lake ice were often confused due to the ambiguous relation between backscatter and ice types. Texture features could be included for further improvement. Overall, our "glocal" IRGS classification results are close to visual interpretation by ice analysts and would have expected to be closer if they could draw ice charts at a more detailed level.

Acknowledgements

I would first like to express my sincere gratitude to my supervisor Prof. Claude Duguay for his patience, motivation, and inspiration. He always makes himself available whenever I have questions about my research or writing. This thesis could not have been written without his continuous support and guidance.

I would also like to express my appreciation to Dr. David Clausi, Dr. Stephen Howell, and Dr. Andrea Scott who agreed to be my committee members. My appreciation also extends to Dr. David Clausi, Mingzhe Jiang, and Michael Stone from the Vision and Image Processing lab at University of Waterloo for providing access and help with the MAGIC software. I would also like to thank Véronique Pinard from the Canadian Ice Service for providing image analysis charts, answering my countless questions, and help with the validation.

Many thanks to Kevin Kang, Marie Hoekstra, Lein Wang, and Janine Baijnath for their help with my thesis through discussions. Special thanks to Mike Lackner (MAD helpdesk) for providing timely technical support and software issues.

Lastly, I would like to thank my parents and friends Liuyi Guo, Jingyi Liu, Yue Zhao, and Pan Liu for their unconditional encouragements throughout my graduate study. I would also like to thank my landlord Kaveh Fazli for offering me a ride on my defense day.

Table of Contents

List of Figures

List of Tables

Chapter 1
General Introduction

1.1 Introduction

Lakes cover around 2% of the Earth's surface, with most of them located in the Northern Hemisphere and covering a total area of 790,000 km^2 (Brown & Duguay, 2010). According to Duguay et al. (2003), 15-40% of the arctic and sub-arctic tundra areas of the Northern Hemisphere are covered by lakes. Therefore, lake ice is one of the most important components of cryosphere due to its large spatial coverage in high-latitude regions (Brown & Duguay, 2010). The presence, thickness, and timing of lake ice cover formation and decay can affect the functioning of lake ecosystems (Bernhardt, Engelhardt, Kirillin, & Matschullat, 2012). Lake ice cover isolates water from the atmosphere, restricts energy exchange, reduces light penetration, and limits wave mixing and evaporation (Choiński, Ptak, Skowron, & Strzelczak, 2015). As a result, lake ice can influence the chemical and biological processes in the lake such as algal blooms and aquatic organisms (Adrian, Walz, Hintze, Hoeg, & Rusche, 1999; Dibike, Prowse, Bonsal, Rham, & Saloranta, 2012). Lake ice is also a valuable indicator of climate change and variability since it is sensitive to changing climatic conditions, especially air temperature (Brown & Duguay, 2010; Duguay et al., 2006; Livingstone & Adrian, 2009; Soja, Kutics, & Maracek, 2014).

Compared to the expensive ground-based observations, satellite remote sensing can provide large spatial coverage and frequent temporal resolution for lake monitoring. Optical and infrared sensors such as NASA's Moderate-Resolution Imaging Spectroradiometer (MODIS), Landsat Thematic Mapper and Multispectral Scanner, and the National Ocean and Atmospheric Administration's (NOAA) Advanced Very High Resolution Radiometer (AVHRR) can provide satisfactory observations over lakes under daytime clear-sky conditions. During winter months, however, these optical and infrared sensors are limited by reduced daylight hours and persistent cloud cover over northern lakes. Passive microwave sensors such as the Scanning Multichannel Microwave Radiometer (SMMR), the Special Sensor Microwave Imager (SSM/I), and the Advanced Microwave Scanning Radiometer (AMSR) can monitor lakes regardless of clouds and darkness with high temporal resolution, but their relatively coarse spatial resolution is not enough for detailed analysis of lake ice. With high spatial resolution and all-weather sensing capabilities, satellite synthetic aperture radar (SAR) sensors such as TerraSAR-X, Canadian Space Agency's (CSA) RADARSAT-1/2, and

European Space Agency's (ESA) ERS-1/2, ENVISAT, and Sentinel-1 are well suited for lake ice monitoring.

The Laurentian Great Lakes are the world's largest supply of freshwater covering an area of 245,000 km^2. Monitoring ice conditions on the Great Lakes is important for the shipping industry and marine resource management (Leshkevich & Nghiem, 2013). The Canadian Ice Service (CIS) has been generating weekly Great Lakes ice cover products since 1973. As a common operational area of interest to Canada and the U.S., the CIS and the U.S. National Ice Center (NIC) have shared responsibility for ice charting of the Great Lakes (Bertoia et al., 2004). Operational ice analysis charts are manually produced by experienced ice analysts based on visual interpretation of satellite images, supported by meteorological data and visual observations from ship and aircraft (CIS, 2005). Satellite SAR imagery with wide spatial coverage is the prime data source for operational ice charting. Although ice analysis charts can provide reliable qualitative ice conditions, the manual production is subjective, time-consuming, and expensive. Furthermore, these charts only provide regional information of ice conditions so that users cannot pinpoint the exact locations of each ice type (Ochilov & Clausi, 2012). Since a large volume of data will be available with the future RADARSAT Constellation Mission (RCM), which will provide better spatial and temporal coverage, it will be increasingly challenging for ice analysts to visually interpret many images for operational purposes. Therefore, an effective automated or semi-automated pixel-level ice classification algorithm is of great interest to operational ice services.

Numerous efforts have been made to automate the ice charting process. However, most of them have not achieved the timeliness and accuracy of operational requirements. An unsupervised segmentation algorithm called iterative region growing with semantics (IRGS) was proposed by Yu and Clausi (2008) for SAR sea ice classification. IRGS has been integrated into the MAp-Guided Ice Classification (MAGIC) System (Clausi, Qin, Chowdhury, Yu, & Maillard, 2010). Among other unsupervised approaches, IRGS has shown robust performance for operational SAR sea-ice classification and has been validated by CIS ice analysts (Ochilov & Clausi, 2012). IRGS has also been successfully tested by Surdu et al. (2014) for grounded and floating ice classification on shallow lakes of the North Slope of Alaska. Recently, a hierarchical approach based on the IRGS algorithm named "glocal" IRGS was proposed for ice-water classification (Leigh, Wang, & Clausi, 2014). By performing segmentation individually on smaller polygons, sea ice and open water were well

separated. This promising algorithm is worth testing for lake ice classification using dual-polarization SAR imagery.

1.2 Research Objectives

The main goal of this research is to evaluate the performance of the semi-automated "glocal" IRGS algorithm for lake ice classification using dual polarized RADARSAT-2 imagery. The classification results are evaluated against the Great Lakes image analysis charts provided by the CIS. To achieve the research goal, the study is divided into three objectives: 1) to evaluate the performance of the "glocal" IRGS algorithm for ice-water discrimination; 2) to examine the capability of the "glocal" IRGS algorithm to separate thickness-based ice types identified by the CIS; and 3) to test the advantages of using dual-pol (HH and HV) images as opposed to single-pol (HH) images for lake ice classification.

1.3 Thesis Outline

Chapter 2 provides detailed background information about lake ice formation and decay process, introduction to SAR, factors that affect radar backscatter, SAR signatures of the Great Lakes, challenges for SAR ice classification, operational ice charting at the CIS, previous studies on SAR ice mapping, and a brief introduction to IRGS. Chapter 3 evaluates the "glocal" IRGS ice classification algorithm over Lake Erie using dual polarization RADARSAT-2 imagery. Chapter 4 summarizes the main findings of the study, identifies the limitations of the algorithm, and provides suggestions for future work.

Chapter 2
Background

This chapter provides background knowledge on SAR ice mapping. Firstly, the physical processes involved in lake ice formation and decay as well as how climatic and non-climatic factors affect lake ice cover at each stage of ice development are presented. An introduction to the factors affecting SAR backscatter and scattering mechanisms are provided, followed by a description of SAR signatures of the Great Lakes and challenges for SAR ice classification. A detailed description of operational ice observation and the analysis process leading to the generation of ice charts at the CIS are then presented. Finally, a review of previous SAR ice mapping studies is provided, followed by a brief description of the IRGS algorithm used in this thesis.

2.1 Lake Ice Formation and Decay

The "energy surplus or deficit in the energy balance" determines the formation, growth, and decay of lake ice cover (Brown & Duguay, 2010, p. 672). The transfer of energy between water, ice, snow, and the atmosphere is governed by the first law of the thermodynamics (Brown & Duguay, 2010). The first law of thermodynamics is the law of conservation of energy discovered around 1850, which states that the total energy of an isolated system is constant, it can neither be created nor destroyed (Truesdell, 1971). Williams (1965) proposes that the energy transfer for ice growth and decay is mainly controlled by heat exchange with the atmosphere, heat storage in the water, and heat from inflows of water. With a decrease in air temperature, the surface water loses heat to the atmosphere. As the surface water cools, it becomes denser and sinks to the deeper portion of the lake. This process continues until the whole lake body cools to 4°C, which is the temperature of maximum density of freshwater (Brown & Duguay, 2010). Further cooling allows the lower-density water layer to stay at the surface and when it cools to the freezing point, initial skim ice will first form on the lake surface (Jeffries, Morris, & Duguay, 2012).

Subsequent ice thickening can create congelation ice and snow ice on freshwater lakes. Congelation ice forms at the bottom of the ice cover where water freezes at the ice-water interface and loses heat through the ice to the atmosphere (Figure 2-1, 1 and 2) (Jeffries, Morris, & Duguay, 2012). Congelation ice is also known as "black ice" because it has high optical depth allowing light to transmit to the subsurface water, which makes it visually transparent (Martin O Jeffries & Morris, 2006). Snow ice typically forms at the top of the ice cover when slush freezes at the snow-ice

interface (Jeffries et al., 2012). As shown in Figure 2-1 (3 and 4), the bubble-filled slush forms at the top of ice cover when the accumulated snow presses the ice cover below the water level that underlying water flows up to the ice surface through ice fractures and soaks the bottom of snow cover (Jeffries & Morris, 2006). Snow ice can also form when snowfall occurs during initial freeze-up or liquid precipitation falls through snow cover to the ice surface (Brown & Duguay, 2010). Snow ice is often referred to as "white ice" because it contains a large amount of bubbles that causes a high albedo and strong light scattering (Jeffries et al., 2012). According to Bengtsson (1986), snow ice tends to form close to the shores as a result of wind redistribution while black ice tends to form in the center part of the lake. During winter, the formation of both snow ice and congelation ice determines the thermodynamic thickening of the lake ice cover. Jeffries and Morris (2006) showed that the growth of black ice at the bottom of the ice and the formation of snow ice on top of ice is due to "the negative temperature gradients in the ice and snow (black ice) and snow alone (snow ice)" which brings the conductive heat flow from the ice layer up to the atmosphere (p. 803). Therefore, the ice growth rate and ice thickness is controlled by the conductive heat flow in thermodynamic thickening (Jeffries & Morris, 2006).

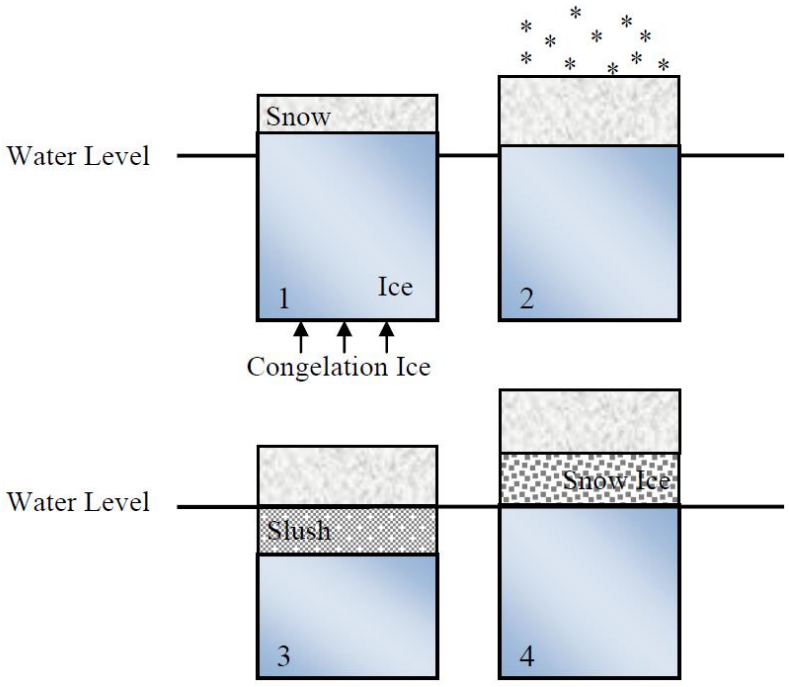

Figure 2-1: The formation of congelation ice and snow ice. (Source: Kheyrollah Pour, 2011)

The timing from initial ice cover formation to final melting, and ice cover duration is named ice phenology (Bernhardt et al., 2012). Ice phenology is generally divided into freeze-up and break-up processes. Freeze-up is defined as the time period between initial ice formation and complete ice coverage, and break-up refers to the time period between the beginning of ice melt and complete disappearance of ice (Jeffries et al., 2012). Ice phenology and ice thickness are affected by a number of climatic and non-climatic factors that control ice formation and decay (Brown & Duguay, 2010). Brown and Duguay (2010) provide a comprehensive review of the interactions between lake ice and climate. They indicate that ice phenology is primarily controlled by variations in air temperature, whereas ice thickness is more associated with the snow accumulation regime on ice cover. The following sections provide a review of how climatic and non-climatic factors affect lake ice cover at each stage of development.

2.1.1 Climatic and Non-Climatic Factors

2.1.1.1 Climatic factors

Climatic factors that determine ice phenology and ice thickness are typically the local weather conditions including air temperature, snow accumulation, wind, and cloud cover (Bernhardt et al., 2012; Brown & Duguay, 2010; Duguay et al., 2006; George, 2013; Jeffries et al., 2012; Williams, 1965).

Air temperature has shown to be the dominant factor that affect ice phenology (Brown & Duguay, 2010; Duguay et al., 2006; Soja, Kutics, & Maracek, 2014; Williams, 1965). Early studies have used accumulated degree days (freezing and thawing degree days) to predict the freeze-up and break-up dates (Burbidge & Lauder, 1957; Mackay, 1961; Williams, 1965). Williams (1965) found that the surface water temperature is almost linearly correlated with air temperature during the first stage of cooling and this relationship was used to determine the date at which a sheltered lake cools to 4°C. Research by Soja et al. (2014) also found that there is a significant correlation between surface water temperature and air temperature, and the surface water temperature is strongly associated with ice-on and ice-off dates. Their results showed that up to 54% (Lake Neusiedl) and 74% (Lake Balaton) of the variance of ice cover duration can be explained by winter air temperatures. They showed that air temperature is positively correlated with solar radiation. As identified by Soja et al. (2014), ice duration has a significant negative relationship with sunshine hours. The amount of solar radiation input on a lake is highly dependent on its geographical location (Bernhardt et al., 2012; Brown &

Duguay, 2010), but the relationship between air temperature and latitude has been found to be nonlinear (Weyhenmeyer, Meili, & Livingstone, 2004). Duguay et al. (2006) compared recent ice phenology trends across Canada with trends in air temperature from 1966 to 1995. They found that freeze-up/break-up dates were strongly correlated with 0 ºC isotherm dates at many lake locations in Canada. At Lake Mendota (Madison, Wisconsin), a 1 ºC mean air temperature change in November and December was found to correspond in a 4.3-day change in freeze-up date, and a 1 ºC mean air temperature change from January to March to a 3.3-day change in break-up dates (Robertson, Ragotzkie, & Magnuson, 1992).

Snow accumulation can influence ice phenology especially during ice thickening and break-up processes (Brown & Duguay, 2010; Soja et al., 2014; Williams, 1965). A study by Adams (1976) demonstrated how snowfall events can advance the timing of initial ice formation on lakes. However, since snow has lower thermal conductivity (0.08-0.54 $Wm^{-2} K^{-1}$) compared to ice (2.24 $Wm^{-2} K^{-1}$) (Sturm, Holmgren, König, & Morris, 1997), snow accumulating on ice cover can slow down the growth rate of ice as a result of its insulating properties (Brown & Duguay, 2010). During spring melt, snow can act as an insulator and delay ice break-up. Additionally, since the presence of snow can initiate the growth of snow ice, the higher surface albedo of snow ice leads to lower solar radiation absorption which can also delay ice break-up (Brown & Duguay, 2010; Soja et al., 2014). The depth of snow primarily depends on occurrence and intensity of snowfall. Soja et al. (2014) found that snow depth and snow days are strongly correlated, with a correlation coefficient of 0.85 and that snow conditions can highly influence break-up and ice cover duration (Duguay et al., 2003). Snow conditions can also be affected by wind redistribution, resulting in higher amounts of snow and snow ice appearing near the shores than the center of the lake (Bengtsson, 1986; Soja et al., 2014).

Wind is another important climatic factor that affects both ice freeze-up and break-up processes (Brown & Duguay, 2010; Duguay et al., 2006). During the initial ice formation, wind can enhance the turbulent mixing of surface water with warmer sub-surface water which may delay the initial formation of skim ice (Soja et al., 2014; Williams, 1965). Although Yao et al. (2013) argue that the enhanced turbulent mixing induced by wind can accelerate water cooling and can thereby promote freeze-up, Soja et al. (2014) point out that this argument is only valid when considering "the total heat energy balance for the whole epilimnion" (p. 130). Wind is also a "frequent disturbance" affecting the formation of the first ice (Jeffries et al., 2012, p. 390). Wind stress can mechanically break the initial formed skim ice, resulting in ice fractures, and delay the thickening of ice cover (Brown & Duguay,

2010; Williams, 1965). Although the heat exchange with atmosphere is the dominant factor influencing ice break-up, under some circumstances the mechanical action of wind can be more important (Williams, 1965). Once ice cover forms on the lake surface, wind exposure can enhance ice growth by further increasing the heat loss of the ice surface (Brown & Duguay, 2010). The snow density and snow depth on the ice cover can also be altered by wind (Jeffries & Morris, 2006).

The presence of cloud cover is another climatic control that affects ice growth and decay (Arp, Jones, & Grosse, 2013; Brown & Duguay, 2010; Maykut & Untersteiner, 1971). Clouds can reflect incoming shortwave radiation away from the Earth's surface during the day, leading to lower air temperature than clear-sky conditions (Wang, Liu, & Bao, 2016). However, clouds can also trap the emitted longwave radiation, resulting in warmer atmosphere especially at night (Brown & Duguay, 2010). The overall cooling or warming effect of cloud cover is determined by which process dominates (Wang & Key, 2005). In high-latitudes regions where solar radiation is limited during the winter, the energy balance of ice growth and decay is mainly controlled by longwave radiation (Brown & Duguay, 2010). The presence of clouds reduces longwave radiation losses and can therefore slow down the ice growth and advance ice decay. The condition of the cloud cover has been considered in many lake ice models such as the FLake model (Freshwater Lake model) and the Canadian Lake Ice Model (CLIMo) (Duguay et al., 2003).

2.1.1.2 Non-climatic Factors

Non-climatic factors that control ice cover formation and decay include lake morphometry (lake depth, area, volume, and fetch), lake elevation, lake turbidity, and inflow from rivers and land runoff (Bernhardt et al., 2012; Brown & Duguay, 2010; Soja et al., 2014; Williams, 1965).

Lake morphometry related factors such as lake depth, area, volume, and fetch are important determinants of ice phenology, especially during freeze-up (Brown & Duguay, 2010). Lake depth is the most important lake morphometry parameter because it determines the amount of heat storage in a lake (Williams, 1965). Deeper lakes have larger thermal inertia because they can accumulate higher amount of heat during the summer and fall (Choiński et al., 2015). The more heat stored in the lake, the longer it takes to cool the water and eventually freeze (Jeffries & Morris, 2007). Ice cover on the Laurentian Great Lakes provides a good example of the impact of lake depth and volume on ice formation. The deeper Lake Superior usually has a lower ice fraction compared to the shallower Lake Erie even though the air temperature is colder over Lake Superior. The effect of lake depth on freeze-up has been found to be more important than break-up, which is primarily driven by air temperature

(Williams & Stefan, 2006). However, Duguay et al. (2003) found that for shallow, low volume lakes in the high-latitude areas, lake depth is a significant factor controlling break-up dates. Lake fetch (the longest distance over a lake surface that the wind is able to generate waves) can also indirectly affect the appearance of ice cover (Jeffries et al., 2012). An early study by Scott (1964) showed that as initial ice forms on the lake surface, the bulk temperature on small lakes is generally around 2 to 3 ºC, while the bulk temperature on most large lakes has to be lower than 1 ºC. In addition to heat storage capacity, lake morphometry also has an impact on wind fetch and water circulation (Jeffries & Morris, 2007).

Several studies have found that lake elevation also affects ice phenology (Brown & Duguay, 2010; Jensen et al., 2007; Livingstone & Adrian, 2009). Jensen et al. (2007) demonstrated that in the Laurentian Great Lakes region, later freeze-up dates are experienced over large low elevation lakes. According to Livingstone and Adrian (2009), lakes located at lower elevation generally have shorter ice cover duration. The reason that elevation has an influence on the timing of ice growth and decay could be explained by the changing air temperature and atmospheric pressure with elevation.

The water turbidity of lake is another non-climatic factor that has been identified to affect ice formation and decay, especially during freeze-up (Bernhardt et al., 2012). Bernhardt et al. (2012) report that clear lakes can store more heat because they allow deeper penetration of the radiation compared to more turbid lakes. They used "Secchi-depth" to measure the degree of turbidity and compared modelled ice phenology variables for 38 Berlin-Brandenburg lakes. Results showed that clear lakes (larger Secchi-depth) had more ice-free winters and experienced later freeze-onset dates than more turbid lakes.

Inflow from rivers and land runoff can also influence ice phenology (Brown & Duguay, 2010; Howell, Brown, Kang, & Duguay, 2009; Williams, 1965). Inflow from streams can create currents and mechanically break the initially formed ice cover (Brown & Duguay, 2010). Inputs from warmer rivers and land runoff can also add additional heat into the lake and delay ice formation (Williams, 1965). Howell, Brown, Kang, and Duguay (2009) demonstrate that the inflow from Slave River causes a fracture in Great Slave Lake ice cover which contributes to advancing the timing of break-up (Figure 2-2).

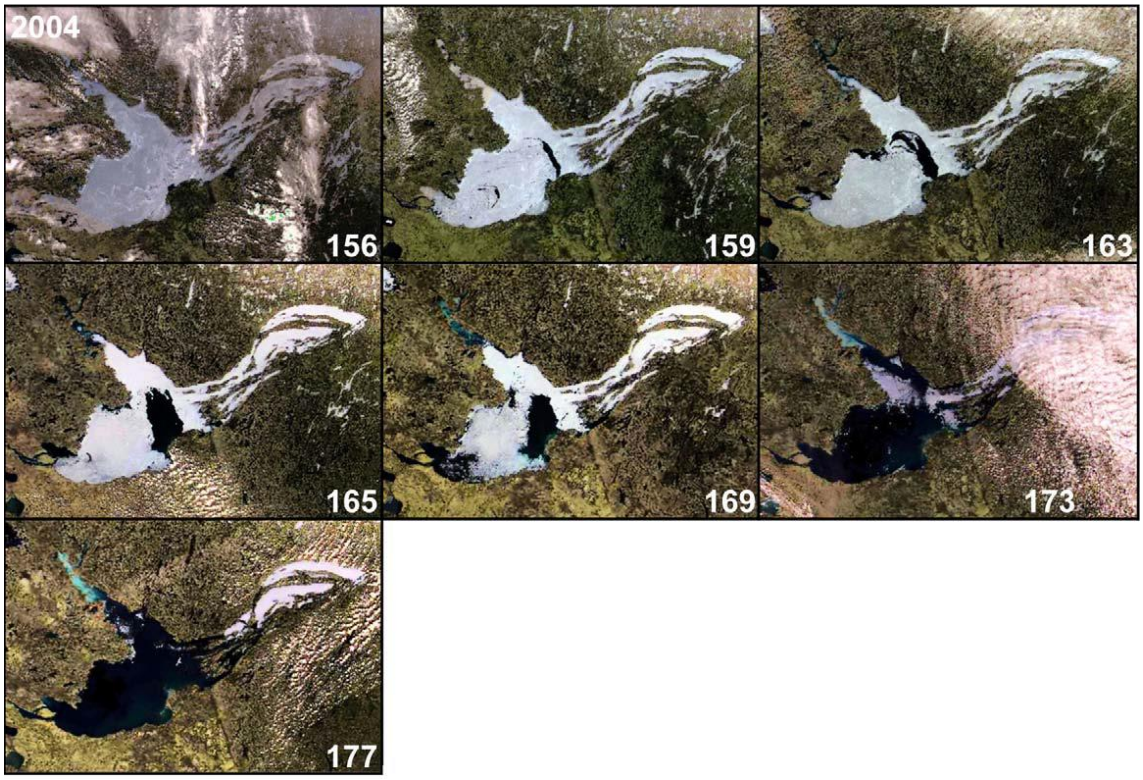

Figure 2-2: MODIS imagery of Great Slave Lake during ice break-up. (Source: Howell et al., 2009)

2.1.2 Ice Phenology Trends

Since lake ice is sensitive to a number of climatic factors, long-term changes in the timing of ice freeze-up and break-up can be used as an indicator of climate variability and change (Duguay et al., 2006; Livingstone & Adrian, 2009; Magnuson et al., 2000). Lake phenology has been proven to be a good proxy for regional air temperature (Livingstone, 1997). Magnuson et al. (2000) indicated that there was a high consistency between lake ice duration and air temperature trends in the Northern Hemisphere from 1846 to 1995. The timescale for lake ice trend analysis is a crucial factor in assessing climate warming (Benson et al., 2012; Brown & Duguay, 2010). Long-term records of warming trends may be related to the end of Little Ice Age since 1800s (Brown & Duguay, 2010; Futter, 2003). Additionally, Benson et al. (2012) examined ice phenology trends for recent 30-year (1975-2005), 100-year (1905-2005), and 150-year (1855-2005) periods. Ice variables for the 30-year trends were steeper than the 100- and 150- year periods, and the 100-year trends were less apparent than for the 150-year period (Benson et al., 2012). Different rates of ice phenology trends were also found in the Laurentian Great Lakes region, with a shorter time period (1975-2004) showing steeper

trends in earlier break-up dates and later freeze-up dates (Jensen et al., 2007) than the trends over the longer period (1846-2000) investigated by Magnuson et al., (2000).

In many parts of the Northern Hemisphere, warming climate conditions have resulted in earlier occurrence of lake ice break-up dates in the past few decades (Benson et al., 2012; Duguay et al., 2006; Magnuson et al., 2000). Research by Choiński et al. (2015) examined ice cover trends from 18 polish lakes between 1961 and 2010. Results show later formation of complete ice cover by 1.2 days per decade and earlier disappearance of ice by 5.6 days per decade. Soja et al. (2014) observed ice phenology trends of two Central European steppe lakes from 1926 to 2012. Both lakes exhibited a significant trend towards earlier ice-off and shorter ice duration. Similar trends have been found by Benson et al. (2012) and Magnuson et al. (2000), who reported trends towards later freeze-up and earlier break-up in the past 60 decades for numerous lakes in the Northern Hemisphere. For lakes in the Southern Ontario, recent trends toward earlier break-up and shorter ice duration were also observed from 1853 to 2001 (Futter, 2003).

Although trends towards later freeze-up and earlier break-up dates have been documented for many northern lakes, some studies have shown no significant ice phenology trends especially for freeze-up dates (Blenckner et al., 2004; Duguay et al., 2006). The response of freeze-up to climate is weaker because freeze-up is also dependent on lake morphometry (Jeffries & Morris, 2007). As Futter (2003) conclude, the timing of ice-off is probably a more useful indicator of climate change than ice-on.

2.2 Synthetic Aperture Radar

2.2.1 SAR Basics

SAR is a form of radar that transmits microwave signal and receives the energy backscattered from the terrain. For a real aperture radar system, the azimuth resolution is inversely correlated to the antenna length and therefore is limited by the size of the antenna that can be installed aboard an airplane or satellite. Synthetic aperture radar utilizes the motion of aircraft and the Doppler principle to synthesize a long antenna using a short antenna. The development of SAR is an evolutionary advancement in radar remote sensing providing relatively high spatial resolution. For example, RADARSAT-2 measurements provide a spatial resolution of up to 1 m in Spotlight mode.

The amount of power received at the SAR sensor is a product of the power per unit area at target, effective scattering area of the target, spreading loss of reradiated signal, and the effective antenna

receiving area (Moore, 1983). The mathematical radar equation combining all these factors is expressed as:

$$P_r = \frac{P_t G_t \cdot \sigma \cdot A_r}{(4\pi)^2 \cdot R^4} \tag{2.1}$$

where P_r is the power received, P_t is the transmitted power to the target, G_t is the antenna gain, σ is the effective scattering area of the target (also called the radar cross-section), A_r is the antenna receiving area, and R is the range distance between the transmitter and the target (Jensen, 2007).

It is the radar backscatter coefficient, also called sigma nought (σ^0), which measures the scattering behavior of the terrain. It represents the amount the radar cross-section σ scattered back to the receiver per unit area (A) and is expressed as:

$$\sigma^0 = \frac{\sigma}{A} \tag{2.2}$$

2.2.2 Factors that Affect Radar Backscatter

The backscatter intensity is dependent on the surface roughness and dielectric properties of the medium. Surface roughness is a strong factor that influences the radar backscatter. A smooth surface acts like a specular reflector where most of the energy is reflected away and only a small amount of radar backscattered to the sensor. For a rougher surface, the incident wave interacts with the surface with diffuse scattering in all directions which will produce a brighter radar return. Another factor that affects radar return is the electrical characteristics of the medium, which can be measured by the complex dielectric constant (Jensen, 2007). It is a measure of the ability of a material to conduct electrical energy, which will influence its ability to absorb, transmit, and reflect microwave energy. Water has a very high dielectric constant of approximately 80 and thus reflects most of the radar energy at the water surface. The dielectric constant of freshwater ice is around 2.2 to 4.5 depending on the bubble content (Drai, 2000; Duguay, Pultz, Lafleur, & Drai, 2002). For sea ice, the dielectric constant is higher than freshwater ice due to the salinity. The dielectric constant of sea ice has shown almost linear correlation with the brine volume (Vant, Ramseier, & Makios, 1978). Therefore, lake ice and multiyear sea ice tend to have higher backscatter because their near zero salinity allows the volume scattering within ice. First-year smooth sea ice appears dark in SAR imagery because the high near-surface salinity resulting in high dielectric constant that prevents radar signal from penetrating the surface and are reflected away.

The measured backscatter can be a result of surface scattering, volume scattering and to a more limited extent double-bounce scattering (Atwood et al., 2015). Surface scattering occurs at the surface of a homogeneous medium. Volume scattering occurs when the medium is inhomogeneous with varying dielectric constant that allows the incidence wave to penetrate through the surface. The backscatter of lake ice comes from both surface scattering at the air/ice and ice/water interfaces as well as volume scattering that interacts with bubbles within ice (Duguay et al., 2002). Snow cover accumulated on ice contributes some volume scattering, but very little for dry snow and barely influence the signal of ice (Ulaby, Moore, & Fung, 1986). Early research have attributed the high backscatter of floating ice in the shallow lakes to double-bounce scattering from the ice/water interface and the columnar bubbles (Jeffries, Wakabayashiz, & Weeks, 2001; Jeffries, Morris, Weeks, & Wakabayashi, 1994; Matsuoka et al., 1999). However, a recent study by Atwood et al. (2015) explored the scattering mechanism of ice in shallow Arctic lakes using polarimetric satellite and ground-based radar. They found that single bounce at the rough lake ice/water interface that has high dielectric contrast rather than double-bounce is the dominant scattering mechanism contributing to the strong backscatter of lake ice.

2.2.3 SAR Signatures of the Great Lakes

A comprehensive library of C-band backscatter signatures of lake ice together with in situ measurements was compiled by Nghiem and Leshkevich (2007) during cruises as part of 1997 Great LAkes Winter Experiment (GLAWEX'97) (February to March 1997) on Lake Superior. In this experiment, the Jet Propulsion Laboratory (JPL) C-band polarimetric scatterometer was mounted on two icebreaker vessels to measure the backscatter signatures of various ice types and calm open water. The measurements included multiple polarizations with incidence angle ranges from 0 to 60º applicable to ERS, RADARSAT, and ENVISAT satellites. Figure 2-3 shows the HH backscatter for various lake ice types and calm open water. Modeled backscatter of open water under different wind speeds are shown as cyan curves.

Since open water can be treated as a homogeneous medium in the microwave region and that only surface scattering is present (Ulaby et al., 1982), the backscatter of open water is highly dependent on incidence angle and wind-induced surface roughness. Backscatter of open water increases as the incidence angle decreases and wind speed increases. For calm open water, specular reflection at the water surface reflects away most of the radar energy producing a low radar return (Figure 2-3). Backscatter of calm water at large incidence angles increases because wind effect is stronger for far

range measurements that are far away from the ship (Nghiem & Leshkevich, 2007). Under windy conditions, the rough water surface is able to reflect radar energy back to the receiver. As shown in Figure 2-3, higher HH backscatter is modeled with increasing wind speed.

The backscatter signatures from GLAWEX'97 for ice types included brash ice, pancake ice, stratified ice, lake ice with crusted snow, consolidated ice floes, and new lake (black) ice (Figure 2-3). These are the common ice types observed on the Great Lakes during GLAWEX'97 with different thickness, snow cover, surface conditions or stratifications. The backscatter of brash ice is the highest among other ice types because brash ice is heavily rafted and ridged that can reach up to 5 m thick. Pancake ice, stratified ice, lake ice with crusted snow, and consolidated ice floes have very similar backscatter signatures. New lake ice has the lowest backscatter compared to other ice types and backscatter decreases steeply with increasing incidence angle. This can be explained by the dominant specular reflection at the smooth black ice surface that reflects away most of the signal. In general, all the ice types have a decreasing trend towards larger incidence angle but the slope is less steep than open water.

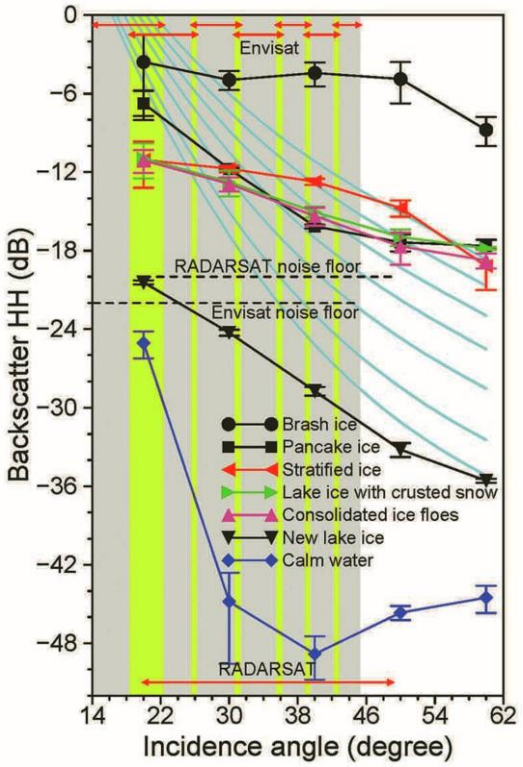

Figure 2-3: HH backscatter signatures of Great Lakes ice and open water. The cyan curves represents backscatter of open water under wind speeds of 2 m/s, 4 m/s, 8 m/s, 12 m/s, 16 m/s, 20 m/s, and 24 m/s (lower to upper). The ranges of incidence angles for RADARSAT and

ENVISAT is marked in red double arrows. The background grey and yellow bands denote non-overlapping and overlapping ranges of incidence angles of ENVISAT SAR, respectively. (Source: Nghiem & Leshkevich, 2007)

2.3 Challenges for SAR Ice Classification

Incidence angle and wind effects over water are the main factors that complicate SAR ice classification. The co-polarized backscatter for ice and open water is incidence angle dependent (Geldsetzer et al., 2010). As incidence angle decreases, stronger radar return is observed especially for open water. On the other hand, the co-polarized backscatter of open water is highly dependent on wind speed and direction (Shokr, 2009). Wind-induced ripples over water can increase the surface roughness and thereafter result in higher backscatter that is close to that of ice, as shown in Figure 2-3. This high backscatter variability makes it difficult to separate open water from lake ice robustly. Previous studies have shown that VV backscatter is more sensitive to wind effects on water surfaces than HH backscatter (Long, Collyer, & Arnold, 1996; Sobiech & Dierking, 2013). Cross-polarized backscatter over water varies with wind speed but is independent of wind direction (Vachon & Wolfe, 2011). Thus, cross-polarized data is less sensitive to wind effects than co-polarized data and is well suited for separating old ice and open water (Arkett, Flett, De Abreu, & Gillespie, 2006; Duguay, Bernier, Gauthier, & Kouraev, 2015). Cross-polarization data can also provide more information about surface roughness structure and make it easier to delineate ice floes (Arkett et al., 2006; Ramsay et al., 2004). However, discriminating new ice from open water can be difficult with cross-polarizated images because the signal-to-noise ratio is relatively low (Geldsetzer et al., 2010). In this case, small (steep) incidence angles in co-polarized images can be used to improve the separability between new ice and open water. Therefore, it is expected that dual-polarization data can largely improve SAR ice interpretation, particularly ice-water discrimination at small incidence angles.

Classifying lake ice types is also a challenging task due to the overlapping backscatter signatures of different ice types. Although different naming conventions of lake ice have been used, the correlation between backscatter coefficient and ice types is still ambiguous. For operational ice mapping, ice thickness is the most important ice variable when classifying ice types. However, it is practically challenging to identify different thickness of ice based only on SAR images since surface (and subsurface) conditions of ice can largely influence the returned signal. Ice with the same thickness can have large radar return from heavily ridged surface or much lower backscatter from smooth ice surface.

Interpreting SAR images during ice decay is difficult because wet snow and melting ice on the ice surface will absorb most of the radar signal and obscure the signal from reaching the ice underneath. Melt conditions result in a dark tone for all ice types in the SAR images. Therefore, distinguishing decaying ice from open water and new ice from SAR imagery can be problematic.

2.4 Operational Ice Observation and Analysis at the Canadian Ice Service

Operational ice services from numerous nations routinely issue ice analysis charts, iceberg conditions, warnings, and forecasts in support of safe maritime operations in ice-covered waters (Bertoia et al., 2004). Various national ice centers have different geographic regions of interest but they work in similar ice charting manners. Their goal is to provide accurate and timely ice conditions mainly for safe ship navigation. Most centers produce ice analysis charts based primarily on visual interpretation of satellites imagery supplemented by aerial and shipboard visual observations as well as meteorological information.

Optical and thermal satellites are suitable for ice monitoring, but are hampered by constant cloud cover. Passive microwave sensors provide near daily and all weather imagery, but are limited by coarse resolution. With all weather day-and-night sensing capabilities and high spatial resolution, radar remote sensing has been of strong interest to ice centers since the technology was developed (Bertoia & Ramsay, 1998). Back in early 1970s, airborne real aperture radars were used for ice pack mapping, and in the 1980s and 1990s, airborne synthetic aperture radar was used operationally (Bertoia et al., 2004). Since the launch of ESA's ERS-1 (July 1991) and CSA's RADARSAT-1 (November 1995), SAR data has been quickly adopted by Canadian and U.S. ice services as well as a few European ice services as the primary data source for ice monitoring. More recent multi-polarization SAR systems such as ENVISAT, RADARSAT-2, and Sentinel-1 have also been included at ice services to improve ice-water and ice type discrimination. Among other data sources, SAR imagery is considered the principle and most suitable data for operational ice mapping to support navigation safety (Bertoia et al., 2004). However, analyzing SAR imagery during melt season can be difficult due to the absorption of signal by surface melt water on ice.

The CIS produces three types of ice charts: image analysis charts, daily ice charts, and regional ice charts. Image analysis charts are the product of the analysis of operationally significant SAR imagery in near real time (within 4 hours of acquisition). Daily ice charts are valid at 18:00 UTC every day and are produced by ice forecasters based on various data sources including satellite images, reports

from ship and aircraft, as well as climatology and weather conditions. Regional ice charts are weekly products that have a complete coverage of a certain region. They are valid on Mondays and are produced based on all available data during the week.

Since the Great Lakes are an area of common operational interest to Canada and U.S., the CIS and NIC have shared responsibility for ice charting in the Great Lakes region (Bertoia et al., 2004). The production of ice analysis charts is coordinated between the two ice services. The image analysis charts are produced only at the CIS primarily for the Canadian Coast Guard ice offices and ice breakers to facilitate ship escorts and routings through ice (CIS, 2005). For the daily ice charts, the CIS produces charts from Fridays to Mondays and the NIC produces charts from Tuesdays to Thursdays. Although ice analysis charts have not been verified systematically, they provide the most reliable and accurate ice information for the Great Lakes. The following section focuses on the CIS Great Lakes image analysis charts, how to interpret the charts, and the need for automated ice mapping algorithm.

2.4.1 Great Lakes Image Analysis Charts

The CIS receives approximately 11,000 SAR images annually from various platforms such as RADARSAT-2 and Sentinel-1 satellites (ERS-1/2, ENVISAT, RADARSAT-1 in the past) (CIS, 2005). The CIS produces image analysis charts through visual interpretation of operationally significant SAR imagery in near real time (within 4 hours of acquisition). Based on any daily available SAR images, image analysis charts are first produced and given to ice forecasters to supplement the production of daily and regional ice charts. Compared to daily ice charts, image analysis charts are less generalized and are a more detailed analysis of SAR imagery. The spatial extent of image analysis charts varies depending on the footprint of the SAR imagery and on the operational requirements. Currently, RADARSAT-2 ScanSAR mode and Sentinel-1 Extra Wide mode images are the main data source for ice charting. These SAR images have a wide spatial coverage of up to 500-km range. Before analysis, they are projected in either Lambert or Polar projections and then a 2 × 2 block average is applied to reduce image resolution to approximately 100 meter for archival purposes.

Trained ice analysts have sound knowledge of the tone, texture, and spatial context of the ice features that allow them to extract ice concentration, ice type, and ice topography from SAR imagery. Based on their knowledge, they manually draw lines and polygons through visual interpretation of SAR imagery using Polaris, which is a digital image display and vector drawing tool based on

ArcGIS. For multi-polarization data, simple RGB composite (i.e. HH-HH-HV, HH-HV-HV) is often used to enhance visual display. As mentioned earlier, visual interpretation SAR imagery can be challenging during the melting season if liquid water is present on the ice surface. Therefore, ice analysts also rely on historic ice patterns (previous charts) and weather conditions to ensure accurate and consistent image analysis. In addition, accumulated freezing degree days (AFDD) is often used to estimate ice thickness particularly for thicker ice types. Since the charts are for operational use, ice analysts always try to generalize the information and sometimes overestimate the ice extent.

2.4.2 Interpreting Image Analysis Charts

Image analysis charts are region-based polygon maps drawn by experienced ice experts from SAR imagery. For each polygon, qualitative ice conditions are provided in the form of an oval shape "egg code" (Figure 2-4). The standard World Meteorological Organization (WMO) egg code reports total concentration, partial concentration, stage of development (age), and form of ice without identifying the exact location of each ice type. The top value C_t in the egg code is the total ice concentration in the polygon area. The second line is the partial concentration for each corresponding ice type (stage of development). The third line lists the stage of development of ice from the thickest (S_o) to thinner ice types (S_d, S_e), of which their concentrations are reported in the second line. The fourth line reports the predominant form of ice (floe size) for each corresponding stage of development. All ice concentrations are reported in tenths. Table 2-1 and Table 2-2 show the standard lake-ice stage of development coding and the coding for forms of ice, respectively.

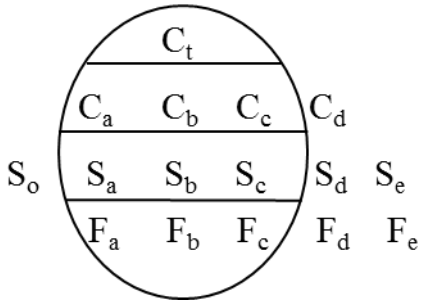

Figure 2-4: The WMO egg code for each polygon.

Table 2-1: Coding for lake-ice stages of development

Stage of development	Thickness (cm)	Ice-type code
New lake ice	< 5	1
Thin lake ice	5 - 15	4
Medium lake ice	15 - 30	5

Thick lake ice	30 - 70	7
Very thick lake ice	> 70	1·

Table 2-2: Coding for forms of ice

Description	>Width	Code
Pancake ice	-	0
Small ice cake, brash ice, agglomerated brash	< 2 meters	1
Ice cake	2 - 20 meters	2
Small floe	20 - 100 meters	3
Medium floe	100 - 500 meters	4
Big floe	500 - 2,000 meters	5
Vast floe	2 - 10 kilometers	6
Giant floe	> 10 kilometers	7
Fast ice	-	8
Icebergs, growlers or floebergs	-	9
Undetermined, unknown or no form	-	X

Image analysis charts are color-coded using the international WMO code in total concentration (CT) or stage of development (SD) of ice in the area. The color code CT shows the total ice concentration in each ice analysis polygon, and the color code SD represents the stage of development of ice with the highest partial concentration in that polygon. Figure 2-5 shows an example of the Eastern Great Lakes image analysis chart color-coded in CT and SD on February 18, 2016. Fast ice is defined as the ice that is fastened to the shore and is colored in grey.

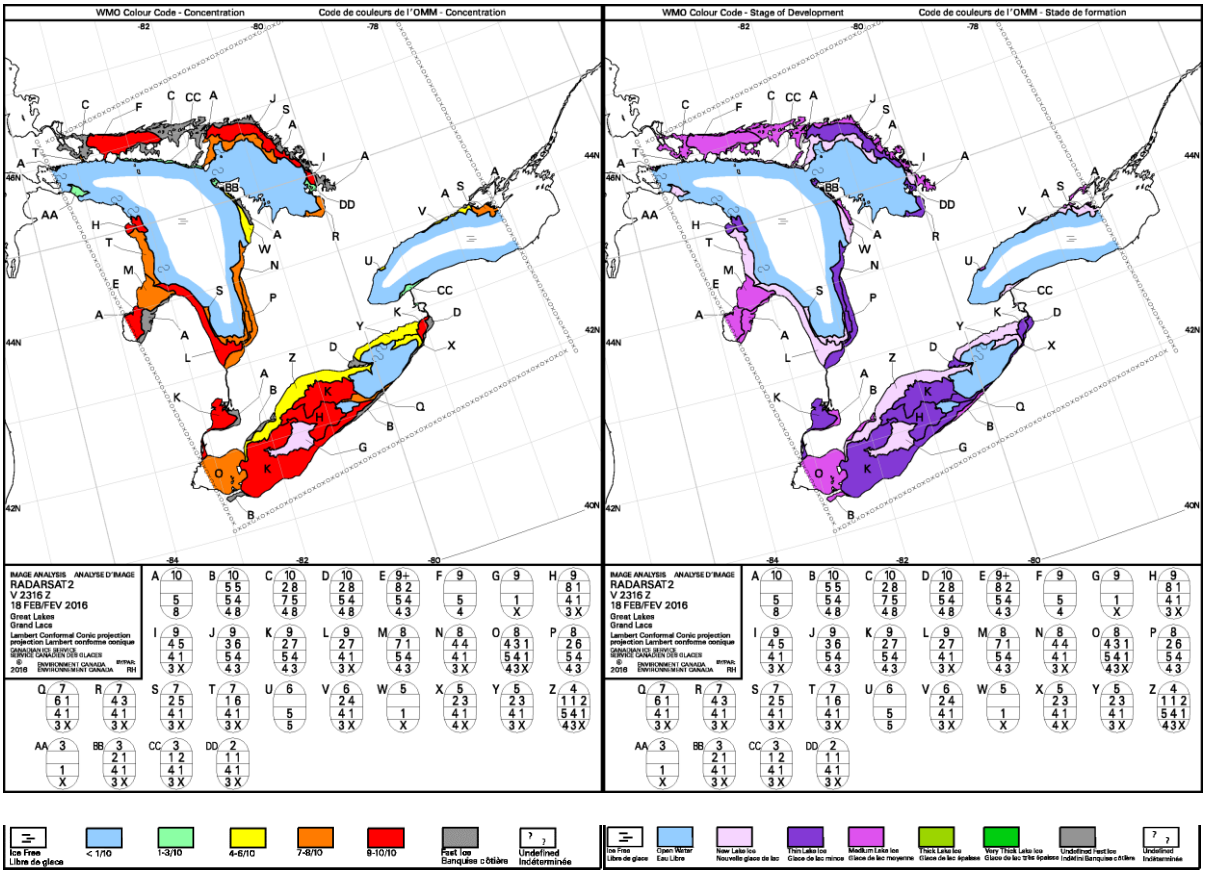

Figure 2-5: The CIS Great Lakes Image analysis chart on February 18, 2016 color-coded in CT (left) and SD (right).

2.4.3 The Need for Automated Algorithm

Currently, manual analysis of satellite images remains the main mode of operational ice charting at most ice centers. However, manual production is subjective, time-consuming, and expensive. At the CIS, it takes ice analyst a few hours to produce a complete ice analysis chart for the Great Lakes region. Since ice analysts have their individual practice of ice charting, a different interpretation can be made by a different ice analyst. Presently, there are seven ice analysts at the CIS in charge of the ice charting. Additionally, the level of detail and accuracy of the charts are quite low. Quantitative assessments have demonstrated the erroneous and subjective nature of the CIS ice analysis charts (Ochilov & Clausi, 2012; Shokr, 2009). Therefore, operational ice services have been seeking for effective and accurate information extraction and analysis techniques using (semi)-automated algorithms to release the ice analysts and allow them to focus on more important decision-making tasks. However, many of the past publications on the development and improvement of image

segmentation, expert-system, and data fusion methods have not met the accuracy and timeliness required for operational analysis (Bertoia et al., 2004).

2.5 Previous Studies on SAR Ice Mapping

Most of the early work on Great Lakes ice mapping was done through visual interpretation of remote sensing data due to the large geographic area of the lakes (Rondy, 1971; Schertler et al., 1975). Since the mid-1970s, numerous Great Lakes ice cover studies have been conducted including field studies, image processing, and freshwater ice classification algorithms using Landsat, AVHRR, ERS-1/2, and RADARSAT data (Leshkevich, 1985; Nghiem, Leshkevich, & Kwok, 1998). However, many of the early satellite ice interpretation algorithms were subjective (Leshkevich & Nghiem, 2013). In 2007, a comprehensive C-band lake ice backscatter signature library was compiled from the radar data from a 1997 field experiment campaign (GLAWEX'97) together with in situ measurements (Nghiem & Leshkevich, 2007). The authors utilized this library for Great Lakes ice mapping with single-polarized ERS-2 and RADARSAT images through supervised classification (Leshkevich & Nghiem, 2007). However, the algorithm needs further improvement because open water in single polarization data has a large backscatter range depending on the wind conditions and incidence angle. With the launch of advanced multi-polarization SAR satellites, Leshkevich and Nghiem (2013) were able to advance their Great Lakes ice classification algorithm with multi-polarization RADARSAT-2 quad-pol and ENVISAT ASAR dual-pol data. They first discriminated ice from open water using a HH backscatter threshold of -3 dB for small incident angles and a VV/HH ratio of 3.1 as a threshold for large incidence angles. Once the ice/water mask was created, the calibrated ice backscatter library was then used to classify the ice types through supervised classification. Their results proved that multi-polarization data can better identify ice types and open water than single-polarized data with less ambiguity caused by different wind speed and direction over water (Leshkevich & Nghiem, 2013).

Developing automated or semi-automated ice classification algorithms from SAR imagery is a long-standing goal for researchers as well as operational ice services. Various approaches have been explored, including simple backscatter thresholding, neural network (NN), Markov random fields (MRF), Bayesian approach, expert system, *k*-means, support vector machines (SVM), and maximum likelihood (ML). The most straightforward method for retrieving ice information from SAR data is to identify backscatter thresholds. Backscatter thresholds are usually determined by obtaining the mean and standard deviation values of randomly selected homogeneous regions. Previous studies have

achieved reasonable ice-water classification results by applying thresholds of SAR backscatter intensities (Geldsetzer, Van Der Sanden, & Brisco, 2010; Leshkevich & Nghiem, 2013). However, thresholds are generally not robust and constrained by incidence angle and wind conditions. A study by Geldsetzer, Sanden, and Brisco (2010) established backscatter thresholds to discriminate decaying lake ice from open water on the shallow lakes in the northern Yukon using dual-pol RADARSAT-2 imagery. A HH backscatter threshold of -21.35 dB was used prior to initial break-up and a HV backscatter threshold of -24.35 dB during break-up. However, their thresholds are not robust due to the high inter-lake and temporal variability of radar backscatter. Sobiech and Dierking (2013) evaluated the performance of unsupervised *k*-means classification approach and a fixed-threshold method for separating decaying freshwater ice and water from RADARSAR-2 and TerraSAR-X images. They demonstrated that results of the unsupervised *k*-means approach were similar to those of the threshold method. Since unsupervised classification does not require prior analysis of training samples and is easy to implement, it is believed to be superior to the threshold method (Sobiech & Dierking, 2013).

Numerous efforts have been made to automate SAR-based ice mapping; however, the majority of the work has focused on sea ice. Early work by Kwok, Rignot, and Holt (1992) applied unsupervised ISODATA classification followed by cluster labelling utilizing seasonal look-up tables of different ice types. This algorithm has been implemented at the Alaska SAR Facility. Gill (2003) developed a semi-automatic SAR sea ice classification algorithm using fuzzy rules on AMPLITUDE, GAMMA-pdf, PMR, and ENTROPY derived from Gray-Level Co-occurrence Matrix (GLCM). The algorithm classifies the data over Arctic sea ice into 8 classes, including both near-range and far-range calm water, wind-roughed water, and low and high concentration sea ice. Soh, Tsatsoulis, Gineris, and Bertoia, (2004) developed an intelligent SAR sea ice image analysis system named Advanced Reasoning using Knowledge for Typing Of Sea ice (ARKTOS). This fully automatic system can mimic the reasoning process of ice experts by extracting objects or features and using rule-based system to classify the segments. An algorithm based on segment-wise thresholding of local backscatter autocorrelation was proposed by Karvonen, Similä, and Mäkynen (2005) for Baltic Sea ice and open water discrimination. Their algorithm has been used operationally at the Finnish Ice Service for operational sea ice mapping. Shokr (2009) compiled an ice type backscatter database using visual RADARSAT image analysis at the CIS. Backscatter equations for open water and ice types as a function of incidence angle were derived using both heterogeneous and homogeneous areas from the ice analysis polygons. This quantitative assessment also tested the robustness of operational

SAR analysis by identifying anomalies in the CIS visual analysis. A texture-based automatically trained ML classifier from RADARSAT-1 and ENVISAT ASAR images was developed for ice-ocean discrimination (Haarpaintner & Solbø, 2007). Their results were significantly improved by dividing the images into narrow incidence angle ranges. An automatic NN-based algorithm and a Bayesian algorithm trained with texture features were used for SAR sea ice classification in the Central Arctic (Zakhvatkina, Alexandrov, Johannessen, Sandvenand, & Frolov, 2013). The result of NN classification provided over 80% of correspondence with expert visual analysis of SAR images. Recently, Zakhvatkina et al. (2017) developed a fully automated ice-water classification algorithm based on dual-polarized RADARSAT-2 images. They used backscatter values and GLCM texture features to train a SVM classifier. More than 2700 SAR images were classified to achieve an average accuracy of 91%.

Most of the past studies on SAR ice mapping chose supervised algorithms because they can be trained and automated. However, training data can be biased and often cannot capture all the variability of different classes. Although unsupervised classification produces arbitrary classes that only require manual labelling, it does not require prior analysis of training samples and can efficiently adapt to varying backscatter (Yu & Clausi, 2007). Research by Yu and Clausi (2008) proposed an unsupervised SAR sea-ice classification algorithm called iterative region growing with semantics (IRGS). This algorithm is an edge-based method which uses edge penalty functions and a region growing technique (Yu & Clausi, 2008). IRGS has been successfully used by Surdu et al. (2014) for grounded and floating ice classification on shallow lakes of the North Slope of Alaska. Recently, Leigh, Wang, and Clausi (2014) proposed an automated ice-water discrimination algorithm using dual polarization RADARSAT-2 imagery. They implemented the region-based "glocal" IRGS on HV polarization followed by the automated labelling with pixel-based SVM algorithm using texture features.

2.6 Iterative Region Growing using Semantics

IRGS is an image segmentation algorithm integrated into the MAGIC System developed by the Vision and Image Processing Research Group at University of Waterloo (Clausi et al., 2010) and is the algorithm retained in this thesis. It is an unsupervised classification algorithm that identifies homogeneous regions with arbitrary class labels. IRGS is a MRF-based algorithm that accounts for spatial relationships and uses Gaussian statistics to model backscatter characteristics (Leigh et al., 2014). This algorithm has been tested on SAR sea ice classification and it is indicated that IRGS can

produce homogeneous regions that are generally consistent with visual interpretation (Yu & Clausi, 2007, 2008). Since IRGS is a region-based algorithm, it is less affected by speckle noise compared to pixel-based algorithms. A more in depth description of the IRGS algorithm can be found in Yu (2006).

IRGS incorporates edge strength to the traditional MRF model, and proceeds labelling and region merging in an iterative manner. Firstly, IRGS over-segments the scene into small homogeneous regions using a watershed algorithm and a region adjacency graph (RAG) is built on these regions. Then, a class label is assigned to each region using an MRF model. These initially identified regions rather than individual pixels are used for further classification. Region properties are computed using Gaussian statistics (mean and covariance) of all pixels in a region (Leigh, 2013). Adjacent regions with the same class label are then merged greedily until the system energy is minimized (Ochilov & Clausi, 2012). The region-based labelling and merging processes are iterated until merging cannot be performed or the maximum number of iterations is reached. Here, the edge strength between each pair of adjacent regions is considered in the segmentation and classification that an increased edge penalty is used for each new iteration (Yu & Clausi, 2007).

For large SAR scenes that are on the order of 500 km wide, the statistics for a class can vary across the scene as a result of incidence angle effect and intra-scene class variations. To minimize the non-stationarities introduced from large scenes, Leigh, Wang, and Clausi (2014) proposed a hierarchical classification approach based on the proposed IRGS algorithm called "glocal". This method combines the "high-detail local" and "large-scale global" information (Leigh et al., 2014, p. 5532). By performing segmentation separately on smaller polygons, the class statistics for each polygon can be considered stationary.

Chapter 3
Semi-automated classification of lake ice cover using dual polarization RADARSAT-2 imagery

3.1 Introduction

Lake ice is one of the most important components of cryosphere with its large spatial coverage in high-latitude regions (Brown & Duguay, 2010). Lake ice is also a robust indicator of climate change and variability due to its sensitivity to changing climatic conditions (Brown & Duguay, 2010; Duguay et al., 2006; Livingstone & Adrian, 2009). The Laurentian Great Lakes have the world's largest freshwater surface covering an area of 245,000 km^2. Ice cover of the Great Lakes has a strong impact on the regional climate, navigation, economic activities, and public safety (Leshkevich & Nghiem, 2013). Knowledge of ice conditions and variability on the Great Lakes is especially important for the shipping industry and marine resource management.

Monitoring detailed ice conditions on large lakes requires the use of satellite-borne Synthetic Aperture Radar (SAR) data that provide all-weather sensing capabilities, high resolution, and large spatial coverage. For many ice centers, SAR is considered the only satellite data source suitable for operational ice mapping to support navigation safety (Bertoia et al., 2004). C-band satellite SAR data from RADARSAT-1, ERS-1/2, and ENVISAT have been intensively used as the prime data source for sea ice mapping in the last two decades (Zakhvatkina, Korosov, Muckenhuber, Sandven, & Babiker, 2017). With better ice-water discrimination and ice edge detection capabilities, multi-polarization data from Sentinel-1 and RADARSAT-2 can further improve the ability for ice monitoring (Ramsay et al., 2004). Using RADARSAT-2 quad-pol and ENVISAT ASAR dual-pol data, Leshkevich and Nghiem (2013) successfully advanced their Great Lakes ice classification algorithm utilizing the backscatter signature library established from the 1997 Great LAkes Winter Experiment (GLAWEX97).

Different ice types and open water can be identified from the analysis of SAR images. Due to the lack of suitable automated algorithms, the Canadian Ice Service (CIS) and U.S. National Ice Center (NIC) have been manually producing Great Lakes ice charts for operational purposes based mainly on SAR images with ancillary data. Ice charts can provide reliable region-based ice type and ice concentration information. However, the visual interpretation of SAR images is coarse, time-consuming, and subjective. With the growing number of SAR missions such as the newly launched

Sentinel-1A/B and the upcoming RADARSAT Constellation Mission, a dramatic increase of satellite imagery is becoming available for lake ice mapping. The large data volume is constrained by the inefficient manual interpretation. Therefore, an automated or semi-automated ice classification algorithm is desired to assist the CIS ice charting process.

Numerous efforts have been made to automate ice mapping from SAR data, with a particular focus on sea ice. Various types of algorithms have been applied, including simple backscatter thresholding, neural network (NN), Bayesian approach, expert system, *k*-means, support vector machines (SVM), maximum likelihood (ML), and Markov random fields (MRF). Algorithms based only on backscatter coefficient are often constrained by the ambiguous correlation between backscatter and ice/water features. Different ice types with varying surface roughness can have overlapping backscatter ranges with open water depending on wind conditions (Shokr, 2009). Therefore, additional SAR statistics such as local mean and variance (Shokr, Jessup, & Ramsay, 1999) and texture features (Karvonen, Cheng, Vihma, Arkett, & Carrieres, 2012; Leigh, Wang, & Clausi, 2014; Zakhvatkina et al., 2017) have been utilized to improve the classification.

Early work by Kwok, Rignot, and Holt (1992) used unsupervised ISODATA classification followed by cluster labelling using seasonal look-up tables of different ice types. This algorithm was implemented at the Alaska SAR Facility. Gill (2003) proposed a semi-automatic sea ice classification algorithm using fuzzy rules on SAR amplitude data and entropy derived from Gray-Level Co-occurrence Matrix (GLCM). The algorithm classifies data over the Arctic Ocean into calm water, wind-roughed water, and low and high concentration sea ice. An intelligent system called Advanced Reasoning using Knowledge for Typing Of Sea ice (ARKTOS) was developed for SAR sea ice image analysis (Soh et al., 2004). This fully automatic system can mimic the reasoning process of ice experts by extracting objects or features and using rule-based system to classify the segments. Karvonen, Similä, and Mäkynen (2005) developed an algorithm based on segment-wise thresholding of local backscatter autocorrelation for discriminating open water and Baltic Sea ice. Their algorithm has been adopted at the Finnish Ice Service for operational sea ice classification. A texture-based automatically trained ML classifier was developed from RADARSAT-1 and ENVISAT ASAR images for ice-ocean discrimination (Haarpaintner & Solbø, 2007). By dividing the images into narrow incidence angle ranges, their results were significantly improved. A study by Geldsetzer, Sanden, and Brisco (2010) established backscatter thresholds to distinguish decaying lake ice from open water using dual-pol RADARSAT-2 imagery. However, their thresholds are not robust enough

due to the high interlake and temporal variability of radar backscatter. Recently, Zakhvatkina et al. (2017) developed a fully automatic ice-water classification algorithm based on dual-polarized RADARSAT-2 images. The authors achieved an average accuracy of 91%. They trained a SVM classifier with backscatter values and GLCM texture features. Similar texture-based training was also previously applied to a NN-based algorithm for sea ice classification in the Central Arctic (Zakhvatkina, Alexandrov, Johannessen, Sandvenand, & Frolov, 2013).

Most of the aforementioned studies on SAR ice classification have used supervised classification based on SAR statistics. Although supervised classification can be implemented automatically, the training data are generally biased due to the high interclass and intraclass variability of backscatter (Ochilov & Clausi, 2012). Additionally, well trained algorithms often perform best on specific geographic regions or seasons and thus cannot be widely applied. Unlike supervised classification, the unsupervised approach does not require a priori knowledge of the feature of investigation. While the arbitrary classes generated from an unsupervised algorithm often need manual labelling, it is believed to be a superior approach to many supervised methods since it does not require prior analysis of training samples and is easy to implement (Sobiech & Dierking, 2013).

Recently, an unsupervised classification algorithm named "glocal" iterative region growing with semantics (IRGS) based on the published IRGS algorithm was proposed and used for sea ice-water classification (Leigh et al., 2014). This is a hierarchical region-based method that minimizes the effect of incidence angle variation by performing segmentation separately on smaller polygons. Leigh et al. (2014) have used the "glocal" IRGS algorithm on HV polarization imagery and obtained well discriminated sea ice and open water segments. It has been shown that for SAR sea-ice image segmentation, IRGS can produce homogeneous regions that are relatively consistent with visual interpretation (Yu & Clausi, 2008). Among other unsupervised approaches, IRGS has shown robust performance for operational SAR sea-ice classification and has been validated by the CIS ice experts (Ochilov & Clausi, 2012). IRGS was also successfully used by Surdu et al. (2014) for grounded and floating ice classification on shallow lakes of the North Slope of Alaska. Although the multivariate version of IRGS algorithm is applicable (Qin & Clausi, 2010), it has not been comprehensively tested on dual-pol images for ice mapping. This promising algorithm is also worth testing on large lakes.

Hence, the objective of this study is to investigate the performance of the semi-automated "glocal" IRGS for lake ice classification on Lake Erie using dual polarized (HH and HV) RADARSAT-2 imagery. Here, ice-water and ice type classification are conducted separately. The performance of the

algorithm on dual-pol data as opposed to single polarization is also tested. Classification results are validated against Great Lakes image analysis charts provided by the CIS.

3.2 Study Area

The selected lake for this study, Lake Erie, is the fourth largest of the Great Lakes by surface area (Figure 3-1). It is located in northeastern North America, on the border of Canada and United States. Lake Erie lies between 78º to 94º W with a surface area of 25,655 km^2 and an average depth of 19 m. It is the shallowest and smallest by volume of the Great Lakes. Lake depth determines the amount of heat stored in the lake body and thus is an important factor for ice freeze-up (Williams, 1965). Deeper lakes have greater heat storage capacity so that they take longer to cool down and eventually freeze (Jeffries & Morris, 2007). Therefore during winter, the Great Lakes do not usually freeze over completely except the shallowest Lake Erie (Cordeira & Laird, 2008).

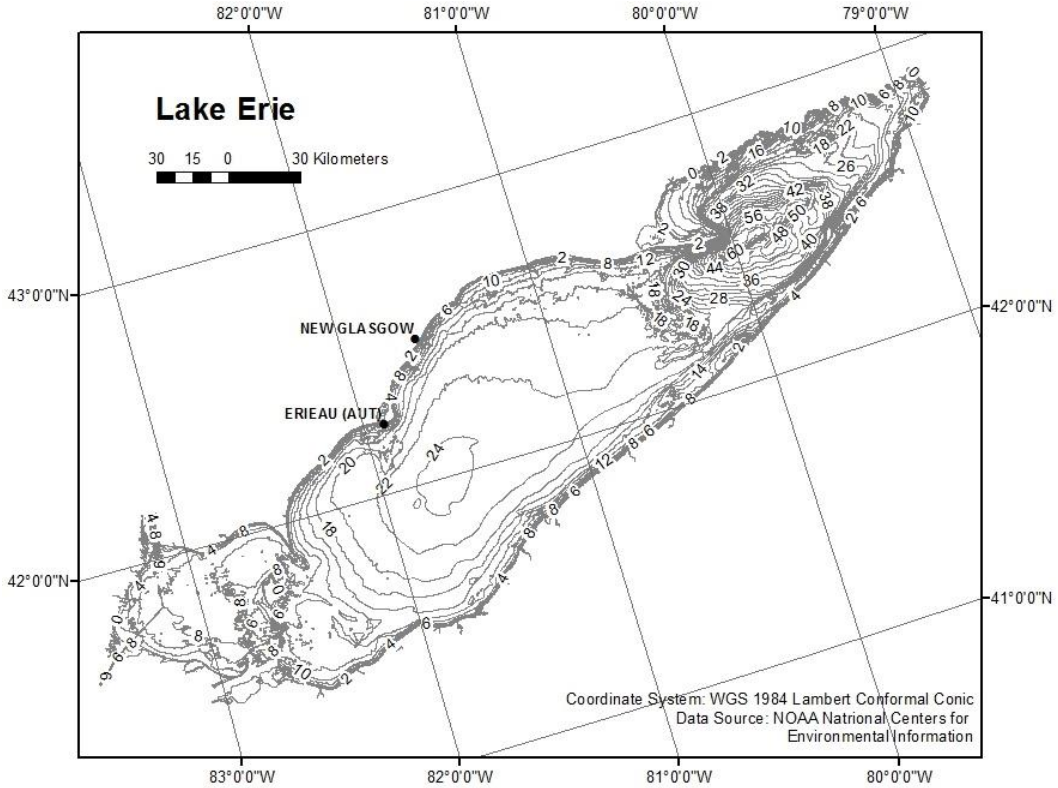

Figure 3-1: Bathymetry of Lake Erie. Lake depth contours are in meters. The locations of the New Glasgow and ERIEAU (AUT) weather stations are shown by black dots.

For the past five years (2013-2017), the mean winter air temperature and mean annual temperature recorded at the New Glasgow weather station, near the northern shore of Lake Eire (Figure 3-1), was -2.68 ºC and 9.25 ºC respectively (Table 3-1). The period of analysis is the cold winter of 2013-2014

which experienced an average winter temperature of -6.36 ºC. During that winter, the constant low temperature caused 92.5% of the Great Lakes to become frozen by early March, which is the second largest ice coverage since 1973 (NOAA/GLERL, 2014). The daily minimum and maximum air temperatures in the area of Lake Erie during this winter is shown in Figure 3-2. The hourly air temperature at the time of each RADARSAT-2 image acquisition used in the study is also shown. Ascending and descending scenes are acquired at 6 pm and 6 am local time, respectively.

Table 3-1: Seasonal mean air temperature (ºC) for winter (DJF), spring (MAM), summer (JJA), and fall (SON) recorded at New Glasgow weather station (42°30'52.062" N, 81°38'10.092" W).

	Winter (DJF)	Spring (MAM)	Summer (JJA)	Fall (SON)	Annual Temp
2013	-1.38	6.96	19.90	10.54	9.00
2014	-6.36	5.33	19.44	9.91	7.08
2015	0.71	6.56	19.19	12.55	9.75
2016	0.56	7.41	20.97	13.10	10.51
2017	-0.22	7.73	20.31	11.78	9.90
Mean	-2.68	5.46	19.96	11.58	9.25

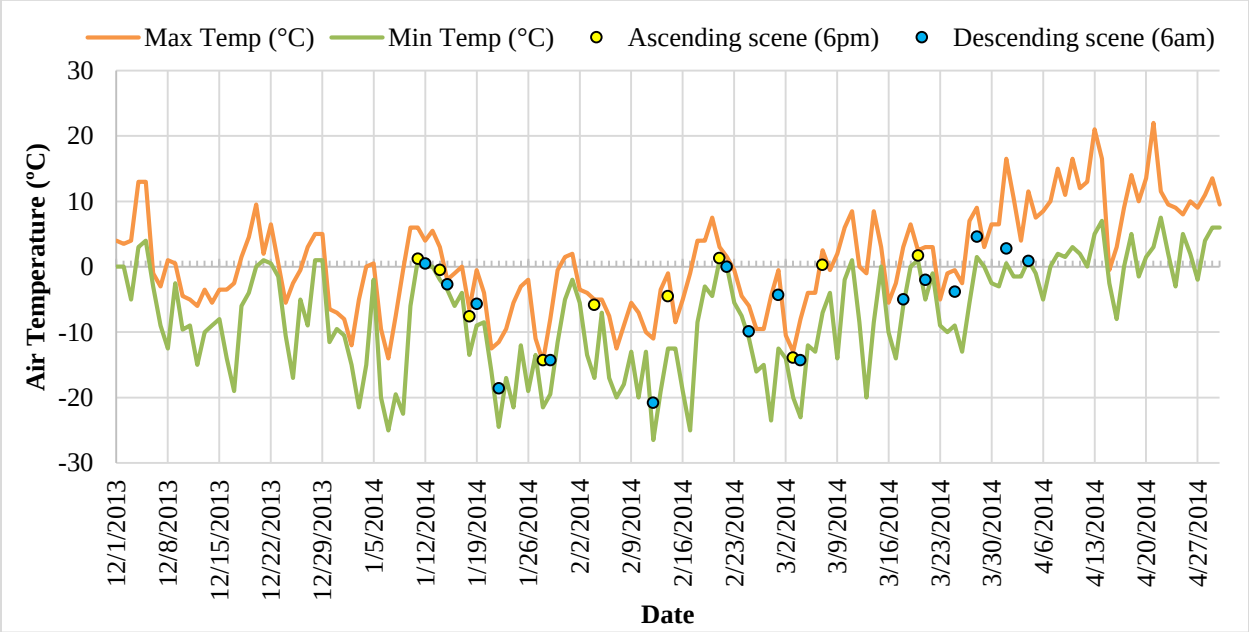

Figure 3-2: Lake Erie min (green) and max (orange) daily air temperature during the winter 2013-2014 measured at the New Glasgow weather station (42°30'52.1"N 81°38'10.1"W). Hourly air temperature of the RADARSAT-2 acquisitions measured at the ERIEAU (AUT) weather station (42°15'00.4"N, 81°54'00.5"W) is shown as yellow and blue dots for ascending (6 pm) and descending (6 am) scene, respectively.

3.3 Data

3.3.1 Synthetic aperture radar

Dual co- and cross- polarized (HH+HV) C-band RADARSAT-2 ScanSAR Wide A images obtained from the Canadian Space Agency were used in the study for lake ice classification. They have a nominal pixel spacing of 50 m × 50 m and a scene size of 500 km × 500 km in both range and azimuth directions. With a wide spatial coverage, ScanSAR Wide mode has been the main mode used by the CIS for operational lake ice monitoring. The incidence angle of the images ranges from 20° to 49°. The temporal resolution is around 1-3 days with varying incidence angle ranges. A total of 26 scenes acquired over Lake Erie from January to April 2014 with varying ice and wind conditions were selected to test the algorithm (Figure 3-3).

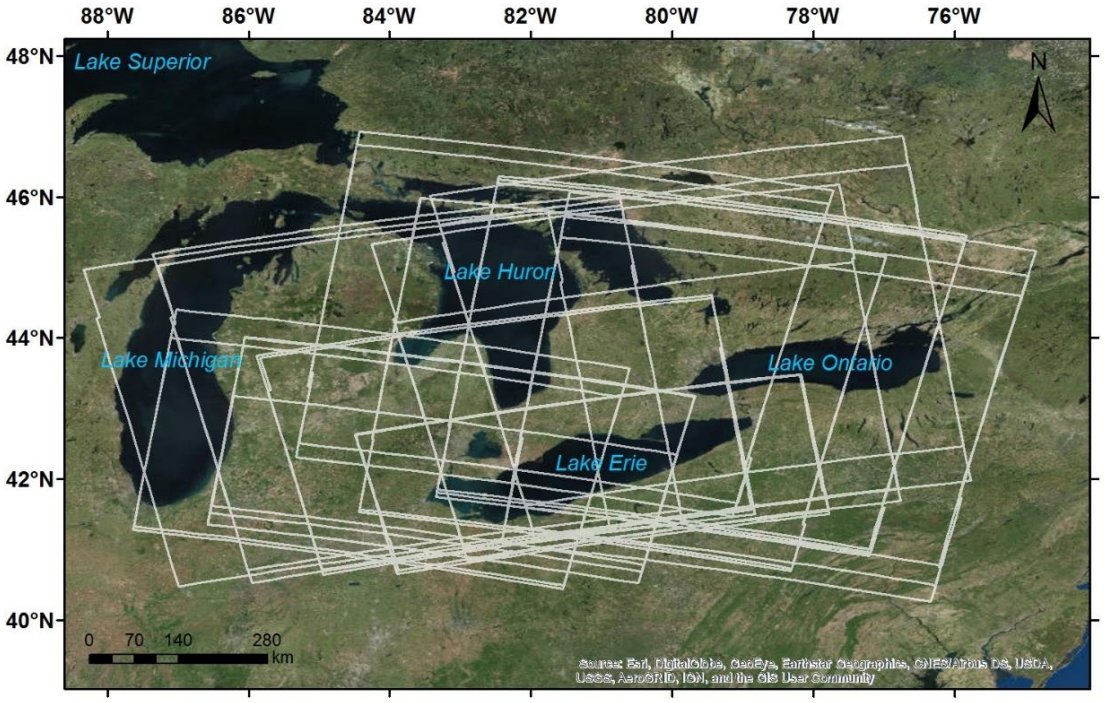

Figure 3-3: Map of Lake Erie. Coverage of the 26 RADARSAT-2 scenes is shown in white.

An example of a RADARSAT-2 scene is shown in Figure 3-4. This scene was acquired on January 19, 2014 during the ice freeze-up period. The scene covers Lake Erie (bottom), part of Georgian Bay (top), and Lake Ontario (right). Various ice types on Lake Erie are well captured at HH polarization. As shown, HV polarization is less sensitive to incidence angle and wind-induced open water surface roughness in contrast to HH polarization. The original images were downsampled from

approximately 10,000 × 10,000 pixels to 5,000 × 5,000 pixels by performing a 2 × 2 block averaging (100-m pixel spacing). This reduces the image size by a factor of 4 which increases the computational efficiency. This is the same procedure followed at the CIS for ice charting from SAR imagery.

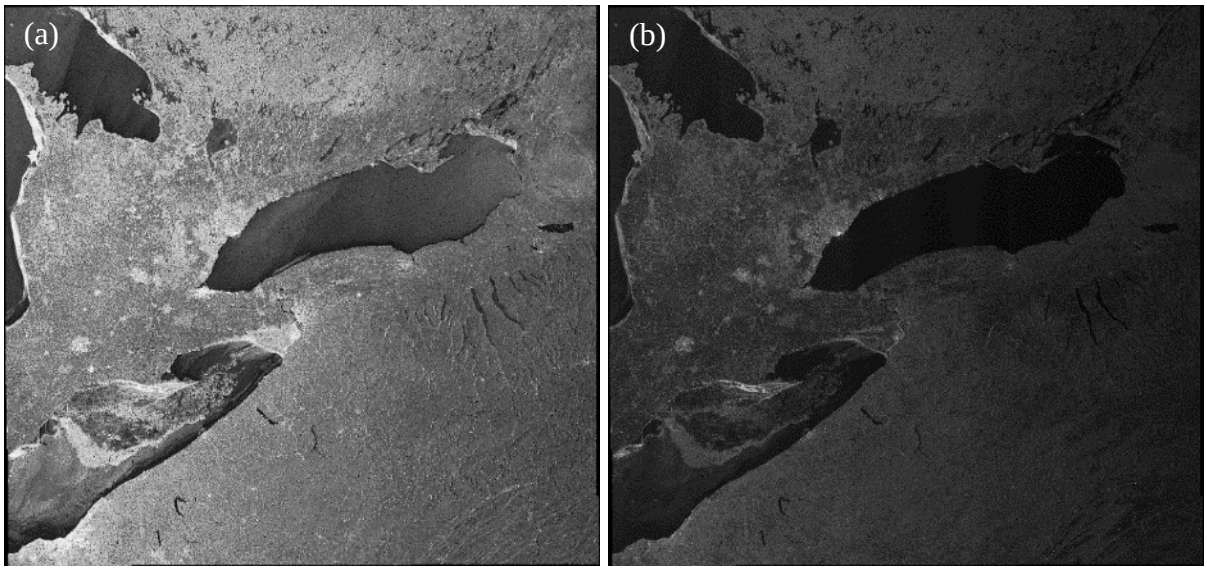

Figure 3-4: RADARSAT-2 SCW scene acquired on January 19, 2014. (a) HH polarization; (b) HV polarization.

3.3.2 CIS image analysis charts

The Great Lakes image analysis charts acquired from the CIS were used for validation of the classification results. They are produced through visual interpretation of the ice conditions from operationally significant SAR imagery in near real time (within 4 hours of acquisition). Visual interpretation of SAR imagery is conducted by an experienced ice analyst through a digital image display and vector drawing tool. In addition to SAR imagery, historic ice patterns and meteorological conditions are also analyzed to support the ice charting. Ice analysts manually draw polygons on the SAR image and for each polygon, the ice types and their estimated concentrations are reported in an oval shape "egg code". The egg code is the World Meteorological Organization (WMO) standard which lists total concentration, partial concentration, stage of development (ice type), and form of ice without identifying the exact location of each ice type. The ice types in the charts follow the WMO standard thickness-based categories. The standard lake-ice stage of development coding is given in Table 3-2.

Table 3-2: Description of lake-ice stages of development

Stage of development	Thickness (cm)	Ice-type code
New lake ice	< 5	1
Thin lake ice	5 – 15	4
Medium lake ice	15 – 30	5
Thick lake ice	30 – 70	7
Very thick lake ice	> 70	1·

Image analysis charts are color-coded using the international WMO code for total concentration (CT) or stage of development (SD) of ice in the area. The total ice concentration is often monitored for weather forecasting while stage of development is more useful for operational purposes such as ship navigation. Color code CT represents the estimated total ice concentration (in tenths) in each manually drawn polygon. Fast ice that is fastened to the shore is 100 percent concentration by definition. Color code SD is the ice type that has highest partial concentration in that polygon. The color code for CT is used when concentration is more variable than stage of development, while the color code for SD is intended to be used when stage of development is more variable than concentration (CIS, 2016). An example of the Eastern Great Lakes image analysis chart color coded as CT and SD drawn from the RADARSAT-2 January 19, 2014 scene (Figure 3-4) is shown in Figure 3-5.

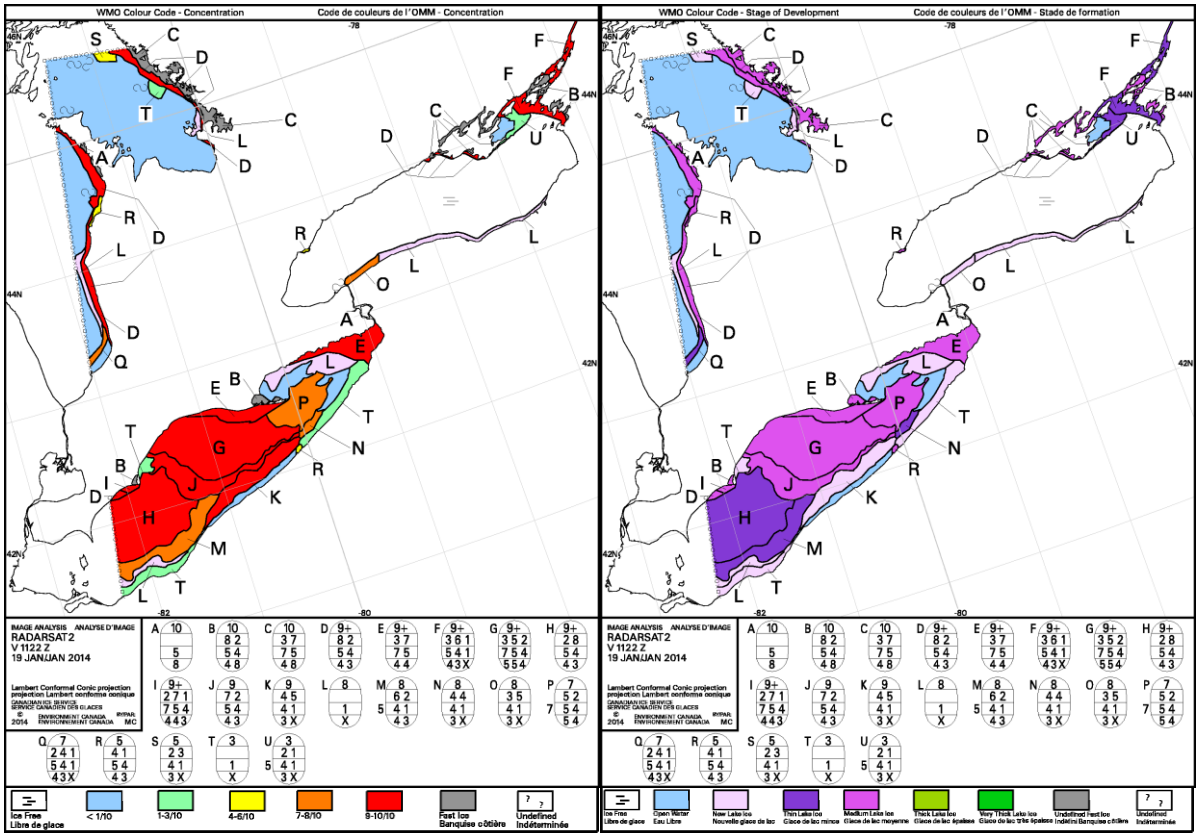

(a) (b)

Figure 3-5: CIS Great Lakes Image analysis chart of January 19, 2014 with (a) WMO CT color code (b) WMO SD color code

3.4 Methodology

3.4.1 "Glocal" iterative region growing with semantics classification

To map lake ice types and open water, image segmentation was performed on the 26 RADARSAT-2 scenes. The hierarchical region-based classification called "glocal" IRGS method was used in the study (Leigh et al., 2014). This is an unsupervised classification method that can identify homogeneous regions with arbitrary class labels. It has been integrated into the MAp-Guided Ice Classification (MAGIC) System developed by the Vision and Image Processing Research Group at University of Waterloo (Clausi et al., 2010).

The "glocal" method used in the study was built upon the IRGS algorithm developed by Yu and Clausi (2008). It is an unsupervised segmentation algorithm proposed for SAR sea-ice mapping. IRGS is an edge-based method which uses edge penalty functions and a region growing technique

(Yu & Clausi, 2008). Basically, IRGS first breaks the scene into small homogeneous regions using a watershed segmentation algorithm and assigns each region a class label using an MRF model (Ochilov & Clausi, 2012). Then, adjacent regions with the same assigned class are merged greedily until the system energy is minimized. The classification and merging process are combined in a iterative manner until the merging cannot be performed further or the maximum number of iterations is reached (Yu, 2006). This algorithm incorporates the edge strength, which improves the adaptivity of the spatial context model to non-stationarity situations (Yu, 2006; Yu & Clausi, 2008). Since IRGS is performed on regions rather than pixels, long range of the spatial interactions between pixels are accounted efficiently (Yu, 2006).

For large lakes such as the Great Lakes, large SAR scenes on the order of 500 km wide are necessary for mapping lake ice. However, such large scenes introduces statistical nonstationarities across the image as a result of the incidence angle effects. To minimize the effects of incidence angle, the hierarchical "glocal" IRGS classification approach which combines the "high-detail local" and "large-scale global" information was introduced (Leigh et al., 2014, p. 5532). The local step divides the image into a number of autopolygons and IRGS classification is performed separately for each autopolygon. The class statistics for each autopolygon can be considered stationary (Leigh et al., 2014). The global step then glues the autopolygons and forms a classification across the whole scene. This hierarchical method identifies homogeneous regions in the full scene with arbitrary class labels.

The "glocal" IRGS classification is performed in the MAGIC system and the flowchart is shown in Figure 3-6. The inputs to the system are HH and HV polarizations of a RADARSAT-2 image and its corresponding landmask that masks out land and other lakes. First, a number of autopolygons (10 × 10 grid) are created on the HV image using the watershed segmentation (Vincent & Soille, 1991). The HV polarization is chosen because it is less sensitive to incidence angle and wind-induced surface roughness. An example of autopolygon segmentation for the January 19, 2014 scene (see original imagery in Figure 3-4) is presented in Figure 3-7a. Each autopolygon is then segmented to five arbitrary classes using IRGS classification based on both HH and HV bands. This step oversegments the image to ensure each class is almost homogeneous. Figure 3-7b shows this classification for each autopolygon. Following this, the global step glues the regions of the local autopolygon classification using IRGS and then completes the full scene classification with arbitrary class labels. Here, different number of arbitrary classes are segmented for the ice-water classification and lake ice type classification.

1) Ice-water classification: The global step glues the autopolygons to 8 classes across the entire scene. Each of the 8 classes is considered homogeneous and contains only water or only ice. An example of the full-scene "glocal" classification is presented in Figure 3-8a.

2) Lake ice type classification: The global step glues the autopolygons to 4 distinct classes across the whole scene. Each of the 4 classes is considered as one of the WMO standard thickness-based ice types.

The last step is to manually label the classes as ice types or water based on visual interpretation of SAR imagery. A labelled ice-water classification of the example scene is shown in Figure 3-8b.

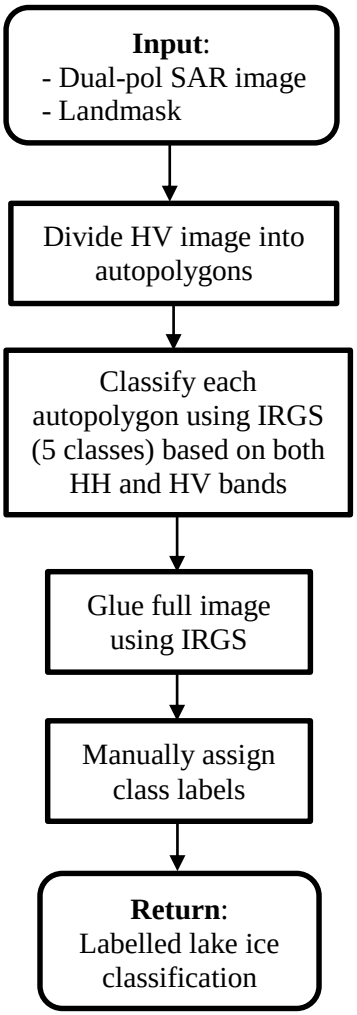

Figure 3-6: "Glocal" IRGS classification flowchart

Experimentation was accomplished to ensure the parameters of "glocal" classification (10 × 10 grid, 5 classes for local, 4 or 8 classes for global) used in the study performed well for the 26 tested

scenes. To oversegment to the most homogenous regions, best ice-water classification results are obtained when 8 classes are segmented. For ice type classification, only 4 classes are segmented because it is difficult to visually label different ice types. The performance of the algorithm was not sensitive to the minor adjustment of parameters.

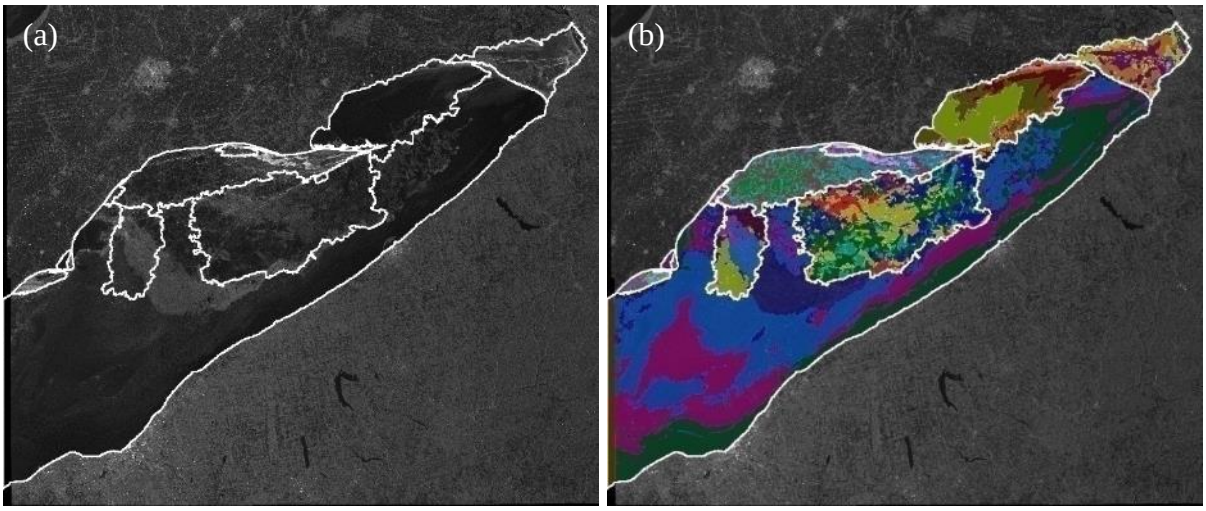

Figure 3-7: Local autopolygon classification of the January 19, 2014 scene. (a) Autopolygon segmentation boundaries in white. (b) IRGS classification of each autopolygon. Five classes are identified in each autopolygon.

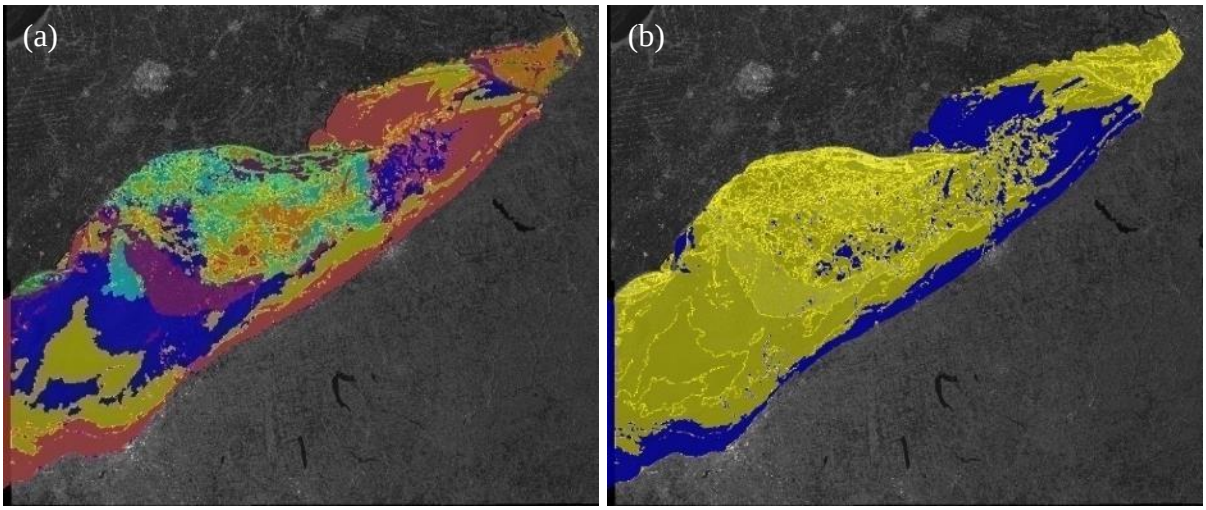

Figure 3-8: (a) "Glocal" IRGS classification (8 classes) of the January 19, 2014 scene. (b) Labelled ice-water classification (ice in yellow, water in blue).

3.4.2 Dual-pol vs. single-pol

The advantage of utilizing dual polarization compared to single polarization for ice observation is evident particularly for ice-water classification. One of the main challenges in discriminating open water from ice is the wind-affected water in co-polarized images. Wind-roughened open water has similar backscatter than ice in a single co-polarized image particularly at small incidence angles, whereas cross-polarization is less sensitive to wind effects and can be useful for ice-water discrimination (Duguay, Bernier, Gauthier, & Kouraev, 2015). However, there is limited ice-water contrast in cross-polarized backscatter because of the relatively low signal-to-noise ratio (Geldsetzer et al., 2010). Therefore, a combined use of co- and cross-polarized data should improve the potential for ice-water classification than using single polarization. With the launch of Sentinel-1A/B and RADARSAT-2, more multi-polarization SAR data are becoming available and increasingly used for operational ice mapping at ice centers. To test the advantages of using the dual-polarization (HH+HV) opposed to single HH polarization, "glocal" IRGS ice-water classification was also performed on only HH-polarized images.

3.5 Results and Discussion

3.5.1 Overall results

The semi-automated "glocal" IRGS classification was tested on 26 ScanSAR Wide RADARSAT-2 scenes and the results were compared against the CIS image analysis charts. The image analysis charts are manually drawn direcly from RADARSAT-2 imagery by trained ice analysts at the CIS. They are currently the most reliable reference data available for the ice cover over the Great Lakes. This study assumes that the CIS image analysis charts represent the "true" lake ice conditions and the absolute difference between the charts and classification results were calculated as the classification error. Figure 3-9 shows an example of the validation process for both ice-water and ice-type classification for the January 19 scene. The HH and HV images are shown in Figure 3-9a and 3-9b. The ice-water and ice type classification results are shown in Figure 3-9e and 3-9h, respectively. For ice-water classification, image analysis charts color coded in CT (Figure 3-9c) were reclassified into lake ice and open water using a total ice concentration threshold of 10% (Figure 3-9d). This is the lowest ice concentration identified by ice analysts. Polygons with ice concentration smaller than 10% were reclassified as open water, otherwise they were considered ice. To perform a quantitative accuracy assessment, error maps based on pixel-by-pixel differences between image analysis charts

and “glocal” IRGS results were generated (Figure 3-9f). For each scene, open water and lake ice correspondence as well as the overall accuracy were obtained. Since image analysis charts are region-based products that have much lower resolution than our pixel-based classification, per-pixel validation was also conducted using 200 random sample points per scene. For lake ice type classification, the image analysis charts color coded in SD (Figure 3-9g) were used for visual comparison. Of the 26 scenes, 12 scenes of Lake Erie were fully ice covered and therefore not included in the ice-water classification. The ice-water and ice type classification results for all scenes are presented in Appendix A and Appendix B, respectively.

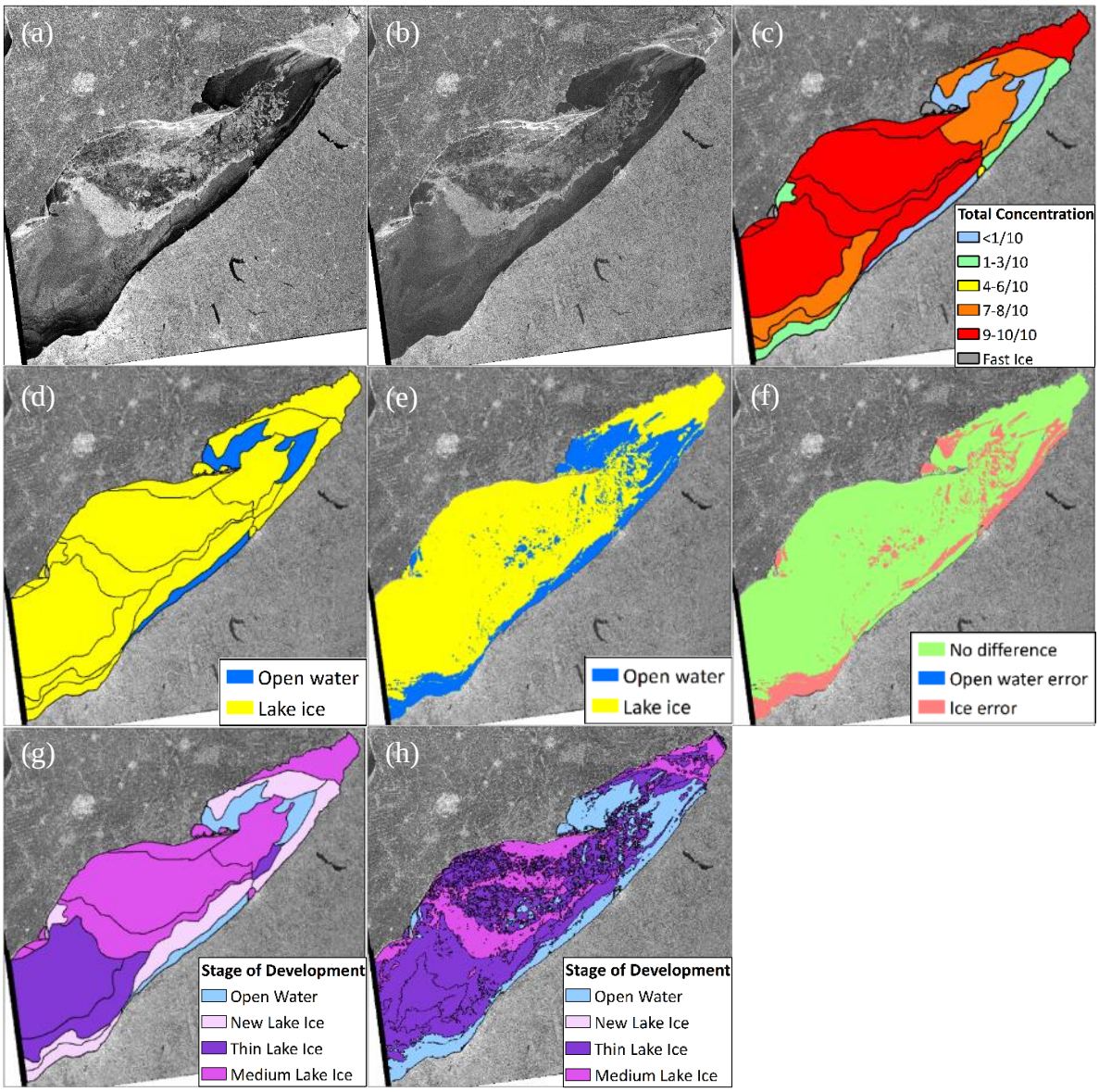

Figure 3-9: Validation process of the classification results against the CIS image analysis charts. (a) Original RADARSAT-2 HH-polarized image acquired on January 19, 2014. (b) Original HV-polarized image. (c) Collocated subset of image analysis chart (color-coded in CT) on the same date. (d) Image analysis chart reclassified into lake ice (ice concentration from 10 to 100%) and open water (ice concentration from 0 to 10%). (e) Labelled ice-water classification result. (f) Error map showing the pixel-by-pixel difference between image analysis chart and ice-water classification result: no difference, open water error (open water misclassified as lake ice), and lake ice error (lake ice misclassified as open water). (g) Image analysis chart color-coded in SD. (h) Labelled ice type classification result.

There is generally a good agreement between the image analysis charts and our ice-water classification results. The average overall accuracy of the ice-water classification is 85.1% and the highest overall accuracy reaches 93.8% (Table 3-3). Most of the errors come from misclassifying ice as open water. Although the HH backscatter for open water is highly dependent on incidence angle as well as wind speed and directions (Shokr, 2009), the "glocal" IRGS algorithm can provide a robust ice-water discrimination in most conditions. The random pixel sampling shows an overall accuracy of 90.2%. Examples of different cases are analyzed in Section 3.5.2.1.

Table 3-3: Accuracy assessment of ice-water classification for 12 scenes.

	Pixel-by-pixel difference with image analysis charts			**Pixel-by-pixel difference against original SAR images (200 randomly selected pixels per scene)**		
SAR acquisition date (M/D/Y)	Overall accuracy	Open water error	Ice error	Overall accuracy	Open water error	Ice error
1/11/2014	84.8%	0.6%	14.5%	92.0%	1.0%	7.0%
1/12/2014	84.1%	7.6%	8.3%	86.0%	5.5%	8.5%
1/14/2014	88.0%	0.5%	11.5%	94.5%	2.0%	3.5%
1/15/2014	87.8%	1.8%	10.4%	89.5%	2.0%	8.5%
1/18/2014	84.9%	0.9%	14.9%	92.0%	2.0%	6.0%
1/19/2014	85.2%	0.1%	14.7%	89.5%	0.5%	10.0%
2/21/2014	91.7%	0.9%	7.4%	96.0%	0.0%	4.0%
2/22/2014	78.9%	0.1%	21.0%	81.0%	0.0%	19.0%
3/25/2014	88.7%	0.7%	10.6%	92.0%	1.0%	7.0%
3/28/2014	89.1%	2.8%	8.1%	88.5%	3.0%	8.5%
4/1/2014	93.8%	0.6%	5.6%	94.5%	1.5%	4.0%
4/4/2014	86.2%	5.7%	8.1%	87.0%	5.5%	7.5%
Average	**86.9%**	**1.9%**	**11.3%**	**90.2%**	**2.0%**	**7.8%**

For comparison between classification using single-pol and dual-pol, results showed that there is generally a slight improvement of using dual-pol rather than single HH polarization (Figure 3-10). Compared with the image analysis charts, the average overall accuracy using single-pol for 12 scenes is 83.4%, which is around 3% lower than the accuracy for dual-pol. The inclusion of HV polarization

can improve the ice-water classification accuracy, especially at small incidence angles where wind-roughed open water tends to be as bright as lake ice. However, a few scenes showed higher accuracy for single-pol than dual-pol mainly owing to the low signal-to-noise ratio in HV image. This implies that if there is a good ice-water contrast in the HH polarization, the contribution of the HV polarization is negligible. Overall, most of the scenes showed little difference (<5%) between using single-pol and dual-pol images. This difference can be ignored because some inconsistencies can be attributed to the low spatial resolution of the image analysis charts. Example of scenes for comparison will be discussed in Section 3.5.2.2.

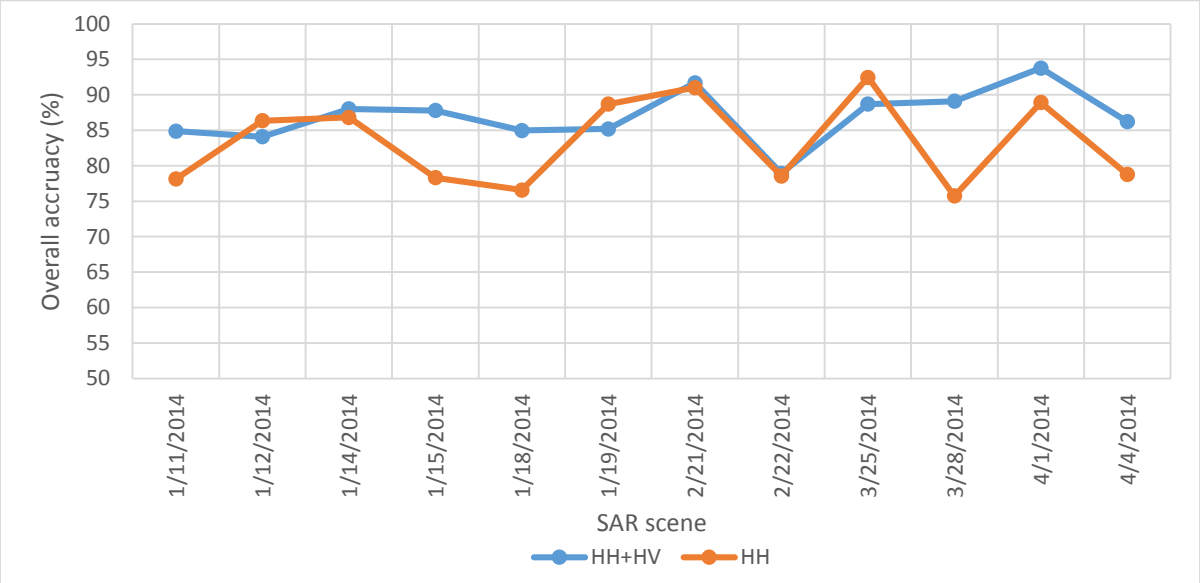

Figure 3-10: Overall accuracy of "glocal" IRGS ice-water classification using dual-polarization (HH+HV) and single-polarization (HH).

The ice type classification results were not quantitatively assessed because image analysis charts are coarse and do not contain heterogeneous ice type polygons. From visual comparison, "glocal" IRGS algorithm can generally identify different ice types with single-pol and dual-pol imagery, particularly when the surface conditions are different for different ice types. New lake ice is often confused with open water due to their similar low backscatter range. Thick lake ice and very thick lake ice appear similar in the SAR imagery, so that they were not discriminated from each other in most cases. Specific scenes are analyzed in Section 3.5.2.3.

The total time for ice classification of Lake Erie in a 5,000 × 5,000 pixel scene is under 10 minutes, which is much faster than the manual ice charting at the CIS. The CIS ice analyst takes around 2 hours to produce a Great Lakes image analysis chart from a large swath SAR image. The local

autopolygon classification takes around 1 minute, the global IRGS gluing takes 30 seconds, and the manual labelling takes about 2-5 minutes depending on the complexity of the scene.

3.5.2 Analysis of specific cases

The performance of lake ice classification can vary with incidence angle, wind speed and direction, as well as ice conditions. Here, a sample of scenes exhibiting different ice and open water conditions are analyzed and discussed.

3.5.2.1 Ice-water classification

The final classification result for the April 1 scene is shown in Figure 3-11. This is an easy scene for ice-water discrimination because there is a good backscatter contrast between open water and lake ice. Although this scene is acquired during the break-up season where the melting ice weakens the backscatter, open water in the far range scatters away most of the radar signal and appears much darker than the decaying lake ice. This scene achieves a high correspondence of 93.8% with the image analysis chart. Differences between the classification results and image analysis charts are found at the ice-water boundary and some cracks between ice floes (Figure 3-11g). This can be attributed to the coarse resolution of the image analysis charts. Errors also appear at the northeastern part of Lake Erie where some fast ice is misclassified as open water (Figure 3-11d and Figure 3-11f).

The scene of January 15, presented in Figure 3-12, is a typical case where Lake Erie is located in the near range. This scene is acquired during the ice freeze-up and mainly contains thin lake ice and medium lake ice. A Landsat-8 image acquired one day before is shown in Figure 3-12e. The seasonally-predominant southwesterly winds push the ice to the northeastern part of the lake. The HH backscatter of open water is highly dependent on the incidence angle with a large increase in backscatter towards smaller incidence angles, as shown in Figure 3-12a towards the right portion of the image. This is because at small incidence angles, surface scattering dominates the scattering mechanism where open water with a high dielectric constant has a stronger reflection of the radar energy than that of ice. With wind-induced surface roughness, open water can have even higher backscatter than the lake ice. Using this ice/water contrast, Leshkevich and Nghiem (2013) successfully separated lake ice and open water using a simple threshold of HH backscatter at small incidence angles. This scene achieves an overall accuracy of 89.5%. Some errors appear at the ice-water boundaries where the contrast of the edges of open water and ice is less evident.

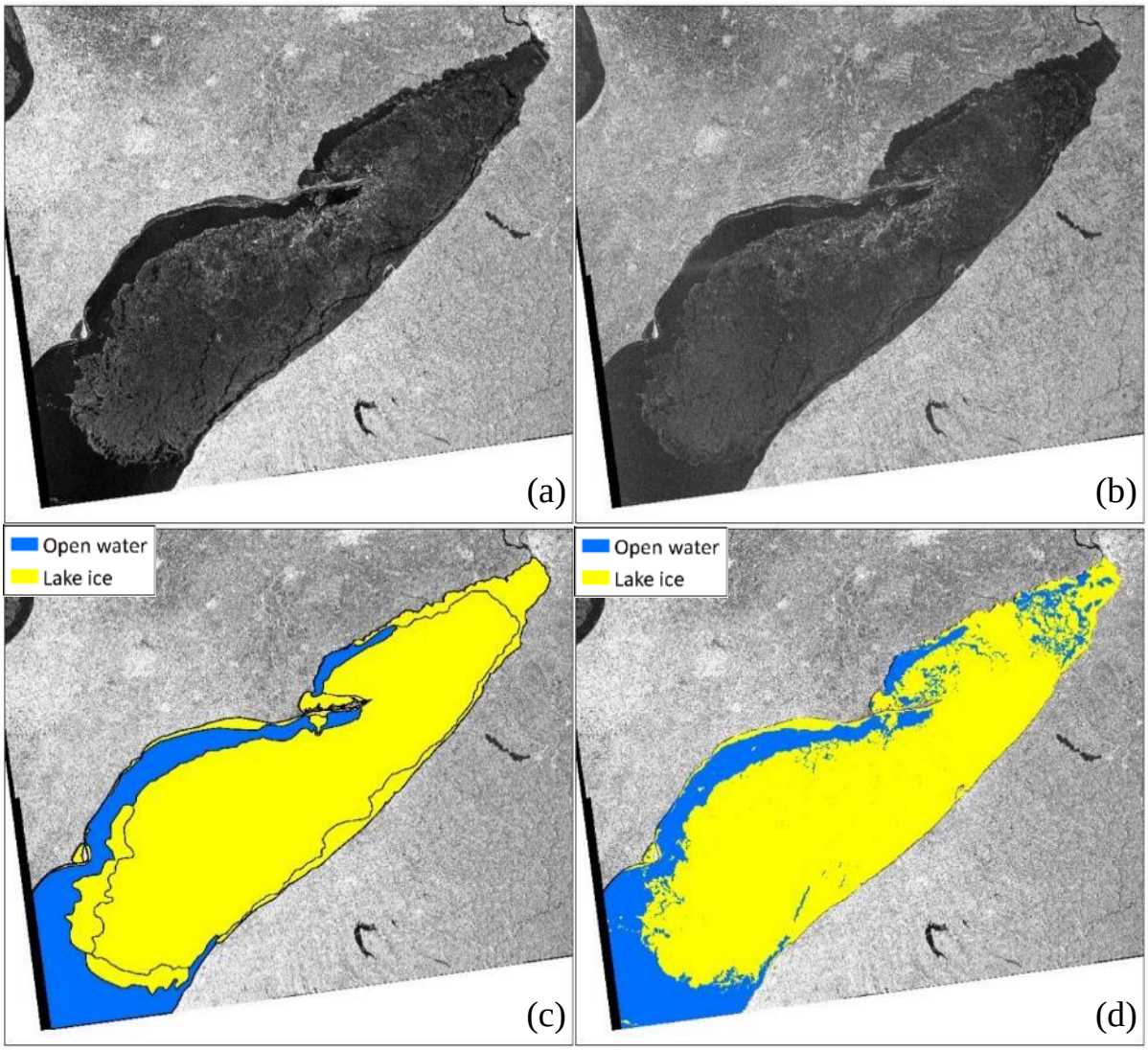

Figure 3-11: (a) Original RADARSAT-2 HH-polarized image acquired on April 1, 2014. (b) Original HV-polarized image. (c) Image analysis chart reclassified into lake ice (ice concentration from 10 to 100%) and open water (ice concentration from 0 to 10%). (d) Labelled ice-water "glocal" IRGS classification.

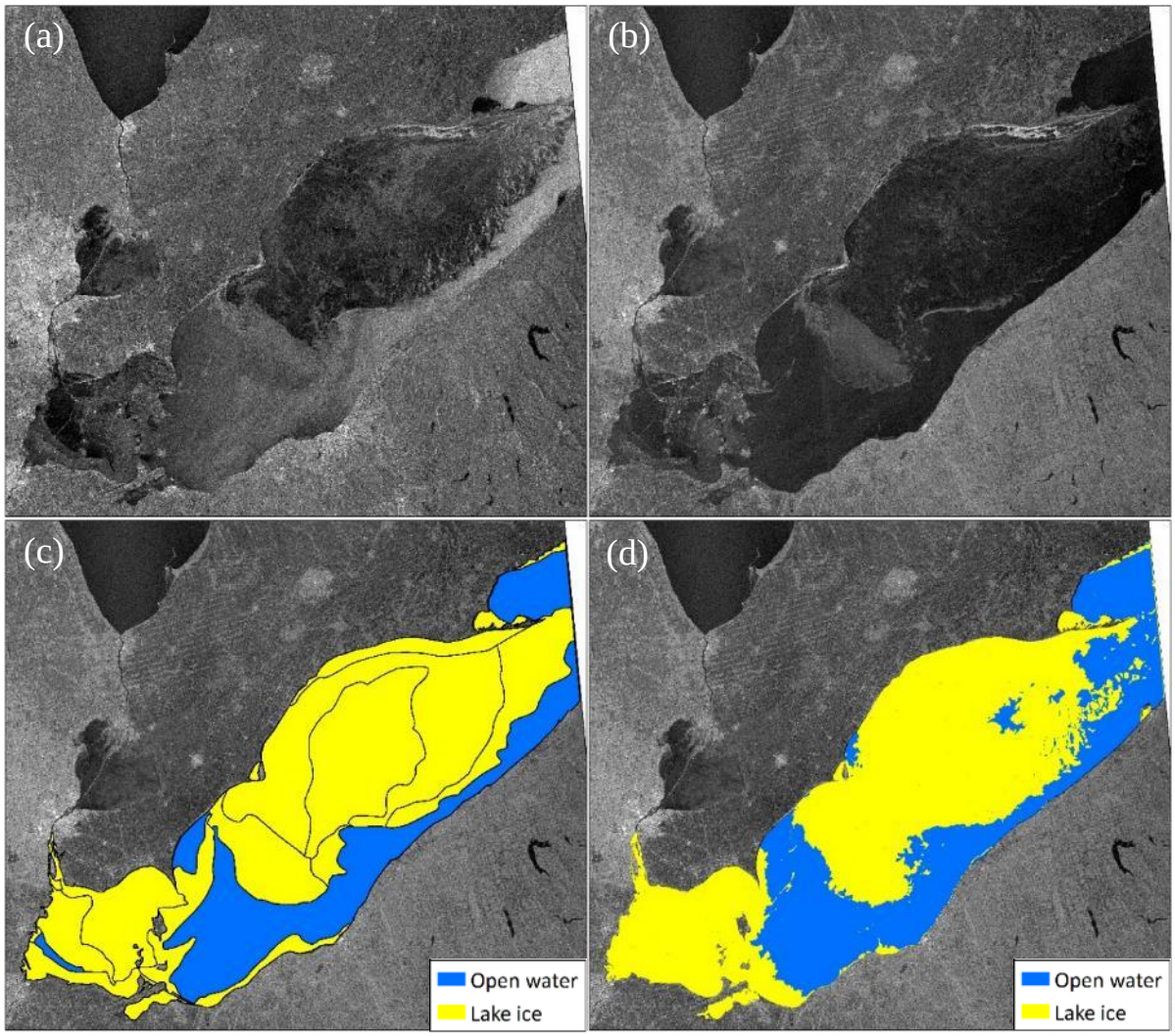
(a)
(b)
(c)
(d)
Open water
Lake ice
Open water
Lake ice

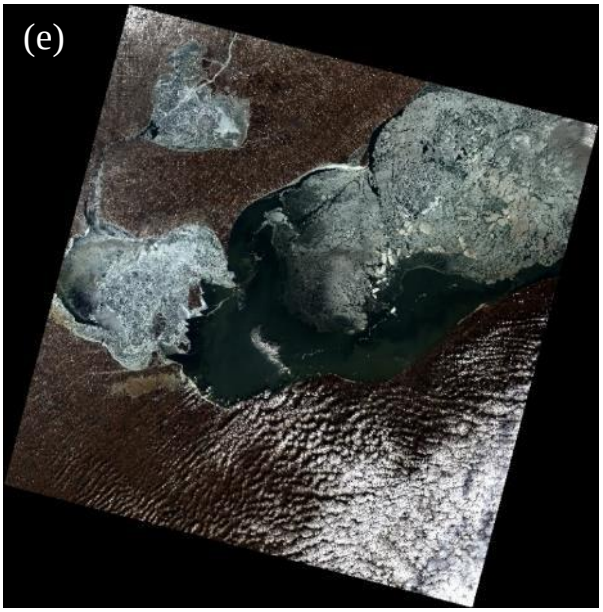

Figure 3-12: (a) Original RADARSAT-2 HH-polarized image acquired on January 15, 2014. (b) Original HV-polarized image. (c) Image analysis chart reclassified into lake ice (ice concentration from 10 to 100%) and open water (ice concentration from 0 to 10%). (d) Labelled ice-water "glocal" IRGS classification. (e) Landsat 8 image acquired on January 14, 2014.

Of the 12 scenes, the scene of April 4 is a fairly difficult scene during spring melt (Figure 3-13). The ice in this scene is mainly very thick lake ice (>70 cm) mixed with 20 to 30% of thick lake ice (30-70 cm). Lake Erie is located in the near-to-middle incidence angle range where open water tends to appear as grey tone with wind-induced surface roughness. Since this scene is acquired during the ice decay season, the melting lake ice has a medium grey tone backscatter which results in a very low contrast with open water. Some open water areas were misclassified as lake ice but the overall accuracy achieved 87.0%. The algorithm also identified cracks in the northeastern part of the lake which were not delineated in the image analysis chart.

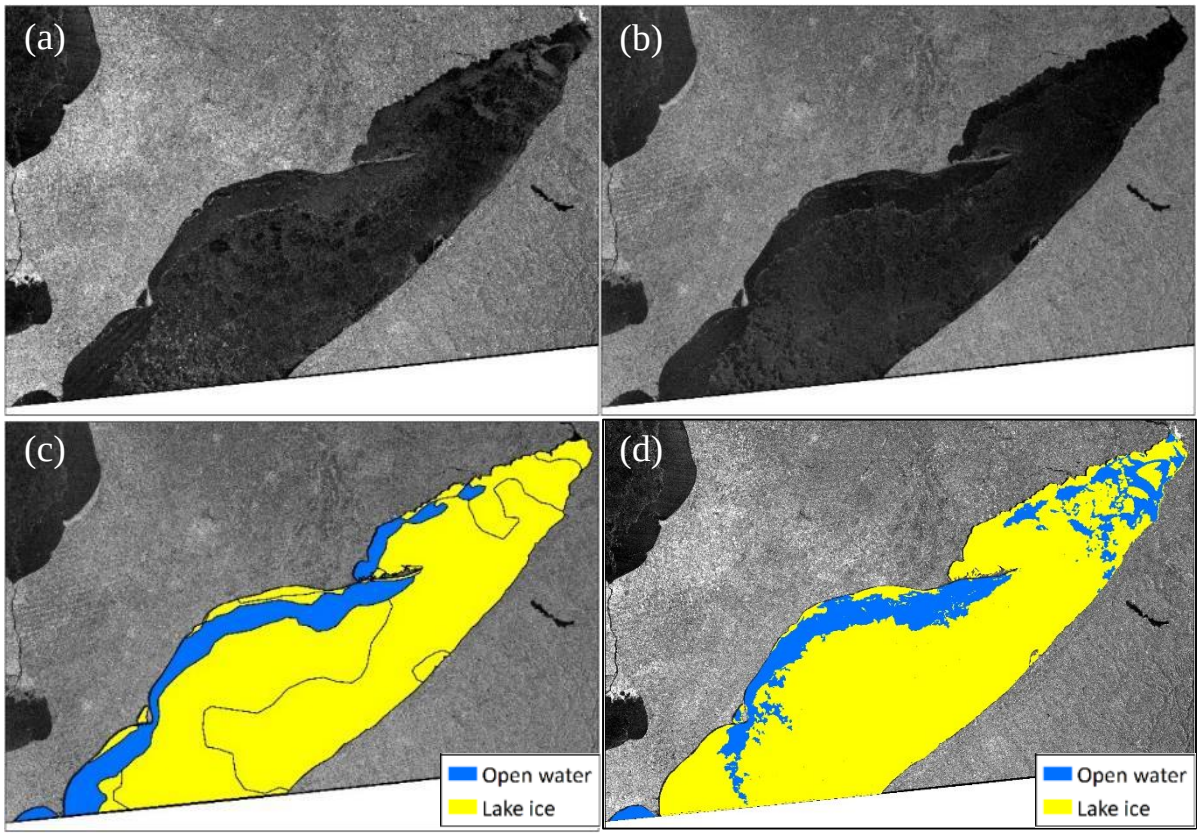

Figure 3-13: (a) Original RADARSAT-2 HH-polarized image acquired on April 4, 2014. (b) Original HV-polarized image. (c) Image analysis chart reclassified into lake ice (ice concentration from 10 to 100%) and open water (ice concentration from 0 to 10%). (d) Labelled ice-water "glocal" IRGS classification.

The scene of February 21 is a case during the spring melt when wet ice and snow or melt ponds on top of the lake ice are present (Figure 3-14). This scene was acquired when the minimum air temperature was higher than the freezing point during that day (Figure 3-3). The decaying lake ice in this scene has relatively low backscatter because melting ice and wet snow on the ice surface absorbs most of the radar signal (Duguay et al., 2002). Since this is a near-range scene, there is generally a good contrast between the bright wind-roughed open water and dark lake ice. However, the bright brash ice with high angular topography in area A of the scene can barely be distinguished from open water at HH polarization but HV can provide a good contrast. As a result, this scene achieves a high overall accuracy of 96.0%.

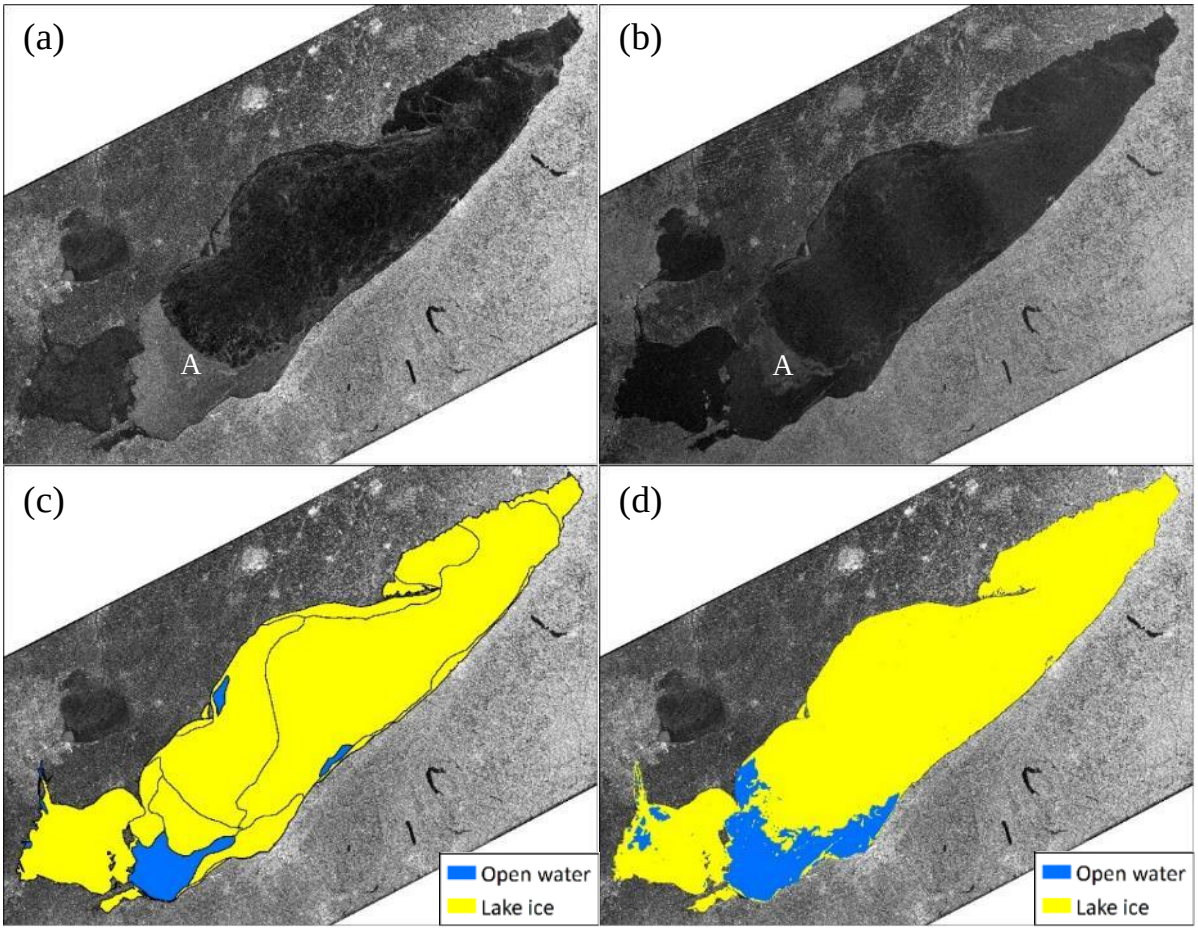

Figure 3-14: (a) Original RADARSAT-2 HH-polarized image acquired on February 21, 2014. (b) Original HV-polarized image. (c) Image analysis chart reclassified into lake ice (ice concentration from 10 to 100%) and open water (ice concentration from 0 to 10%). (d) Labelled ice-water "glocal" IRGS classification.

The next scene shown in Figure 3-15 was acquired 12 hours after the last February 21 scene. This is a scene acquired in the morning around 6 am local time (descending mode) of February 22, whereas the last scene is acquired the night before at around 6 pm (ascending mode). Compared to the February 21 scene, the ice in this scene appears much brighter because the melted ice refroze as the temperature started to drop at 4am and reached the freezing point at 6 am. As shown in Figure 3-16, there was a significant melting episode before the February 21 scene was acquired as the air temperature for the previous 24 hours was greater than 1.5°C and reached 6.3°C at 1 am. Melting ice or melt ponds on the surface of the ice are likely present on the western part of the lake where the signal from the ice underneath is obscured. The low radar return of ice cover makes it difficult to

discriminate from open water in the near-range. As shown in Figure 3-15f, ice in the western part was misclassified as open water and the overall accuracy is 81.0%.

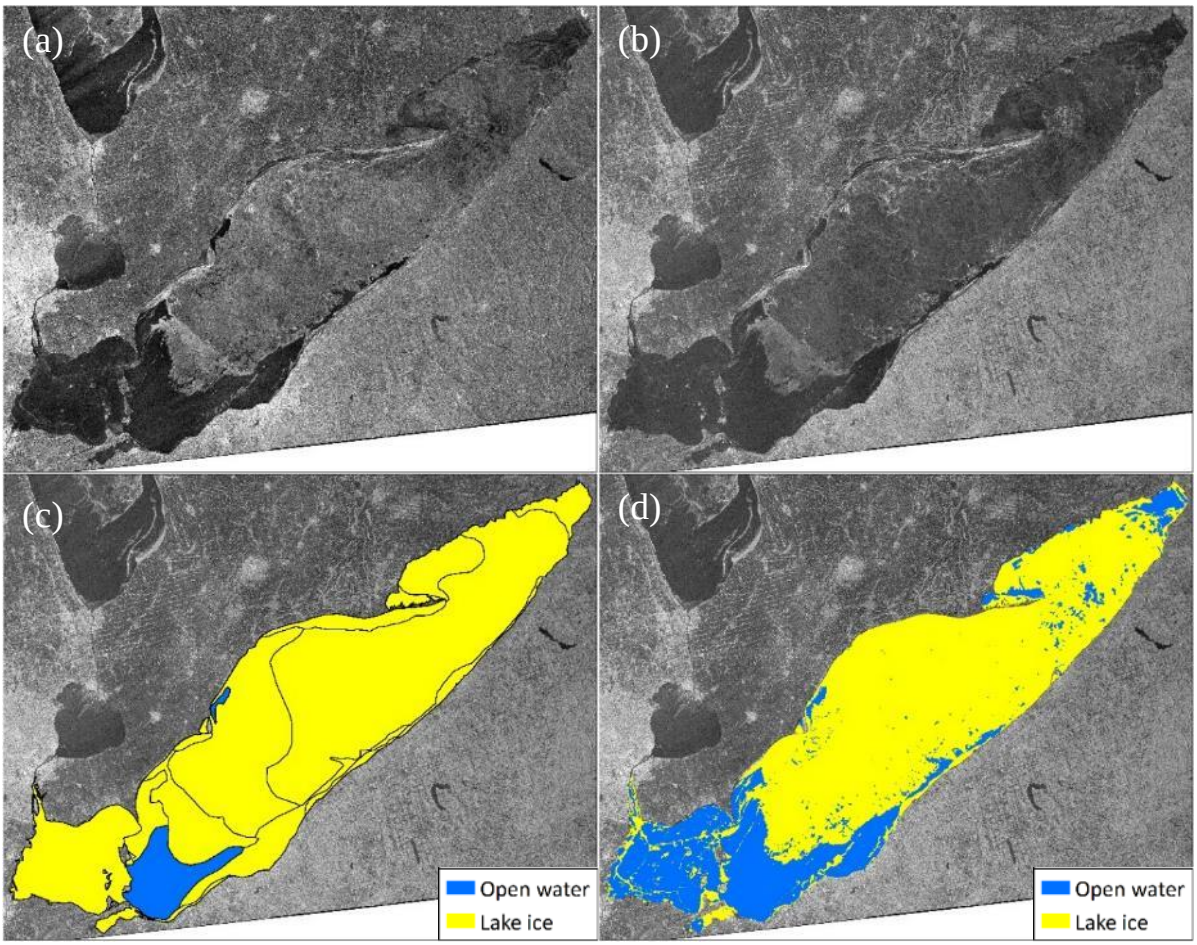

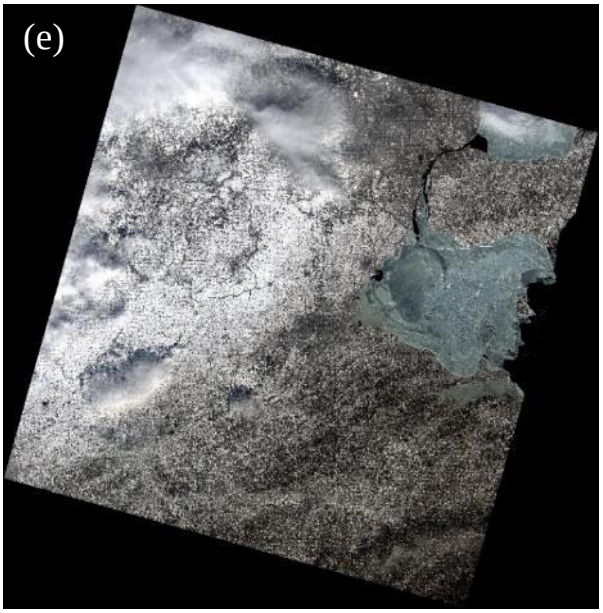

Figure 3-15: (a) Original RADARSAT-2 HH-polarized image acquired on February 22, 2014. (b) Original HV-polarized image. (c) Image analysis chart reclassified into lake ice (ice concentration from 10 to 100%) and open water (ice concentration from 0 to 10%). (d) Labelled ice-water "glocal" IRGS classification. (e) Landsat 8 image acquired on February 22, 2014.

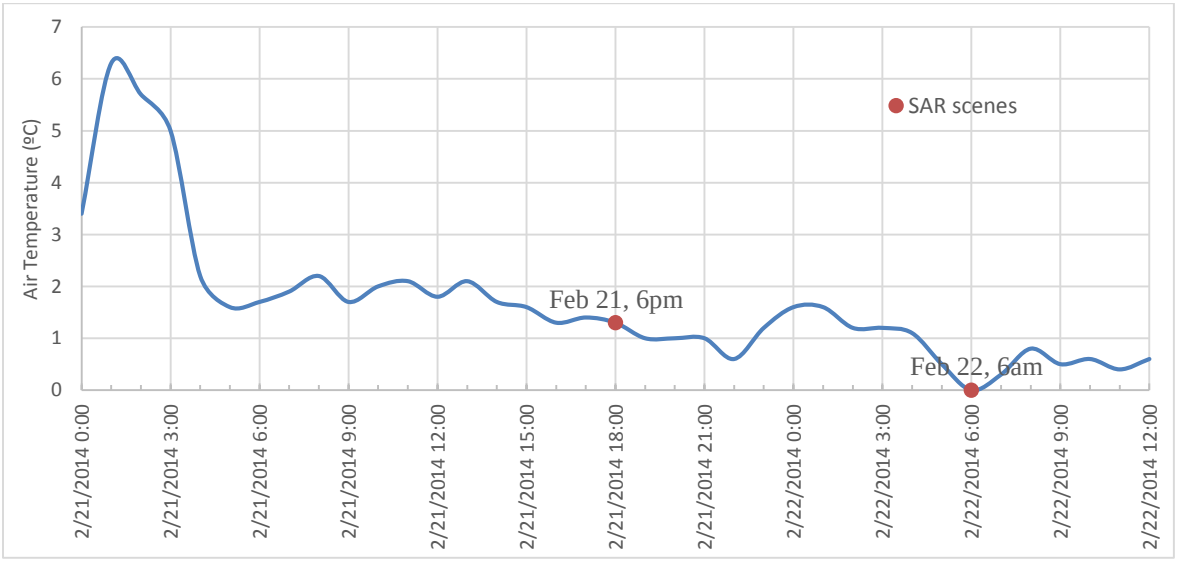

Figure 3-16: Hourly air temperature from February 21 00:00 to February 22 12:00 measured at the ERIEAU (AUT) weather station (42°15'00.4"N, 81°54'00.5"W). Local times of acquisition of the two SAR scenes are identified by red dots.

3.5.2.2 Dual-pol vs. single-pol

The advantage of using dual-pol as opposed to single-pol images is more evident for scenes acquired at small incidence angles. As mentioned earlier in section 3.5.2.1, the scene of January 15 is a near-range scene in which wind-roughed open water can appear just as bright as lake ice at HH polarization (area A in Figure 3-17a). Therefore, using only a HH image cannot discriminate some of the rougher ice types from open water (Figure 3-17d). However, HV polarization (Figure 3-17b) is less sensitive to incidence angle with open water appearing darker than the ice in area A. This provides a better backscatter contrast at the ice-water boundary. As shown in Figure 3-17e, the inclusion of both HH and HV polarizations in the algorithm produced a generally better ice-water classification result than using single polarization alone.

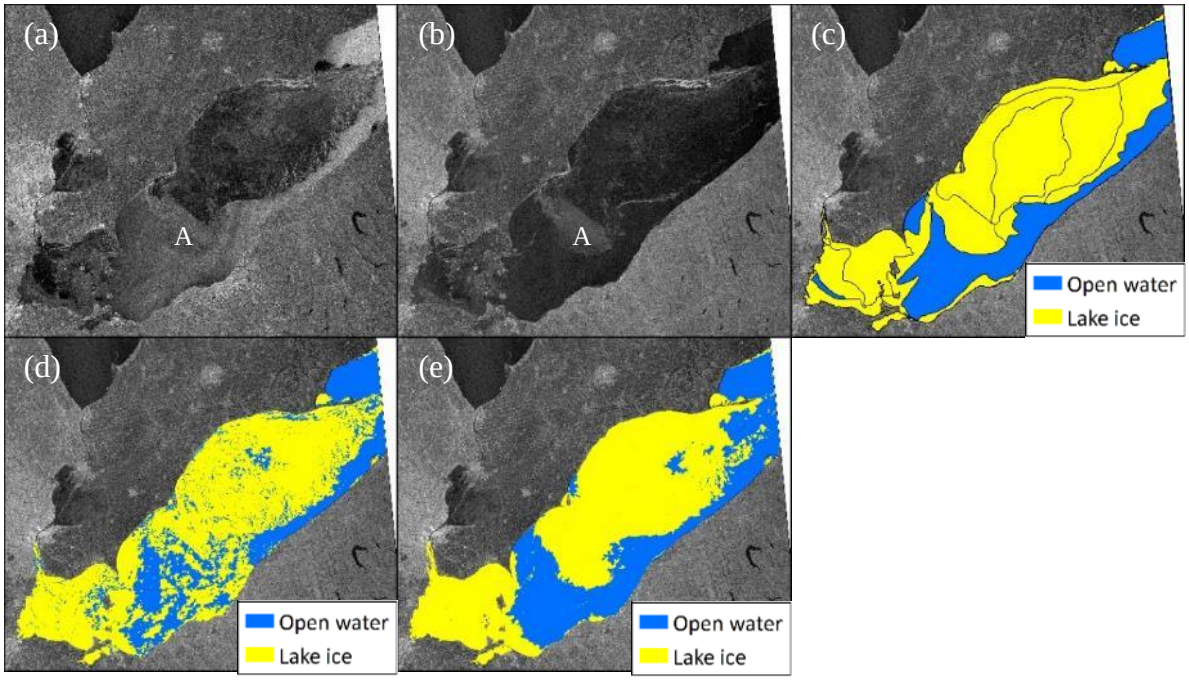

Figure 3-17: (a) Original RADARSAT-2 HH-polarized image acquired on January 15, 2014. (b) Original HV-polarized image. (c) Image analysis chart reclassified into lake ice (ice concentration from 10 to 100%) and open water (ice concentration from 0 to 10%). (d) Labelled "glocal" IRGS classification using HH polarization. (e) Labelled "glocal" IRGS classification using dual-pol images.

Most of the scenes analyzed showed that classification using single-pol or dual-pol results in similar classification accuracy. For example, the scene of April 1 shown in Figure 3-18 is a case when using dual-pol is slightly better than using HH-pol only. Although the dual-pol result (Figure 3-18e) shows a better correspondence with the image analysis chart (Figure 3-18c), the result of using single

HH-pol (Figure 3-18d) can identify more cracks between ice floes which were not delineated by the ice analyst.

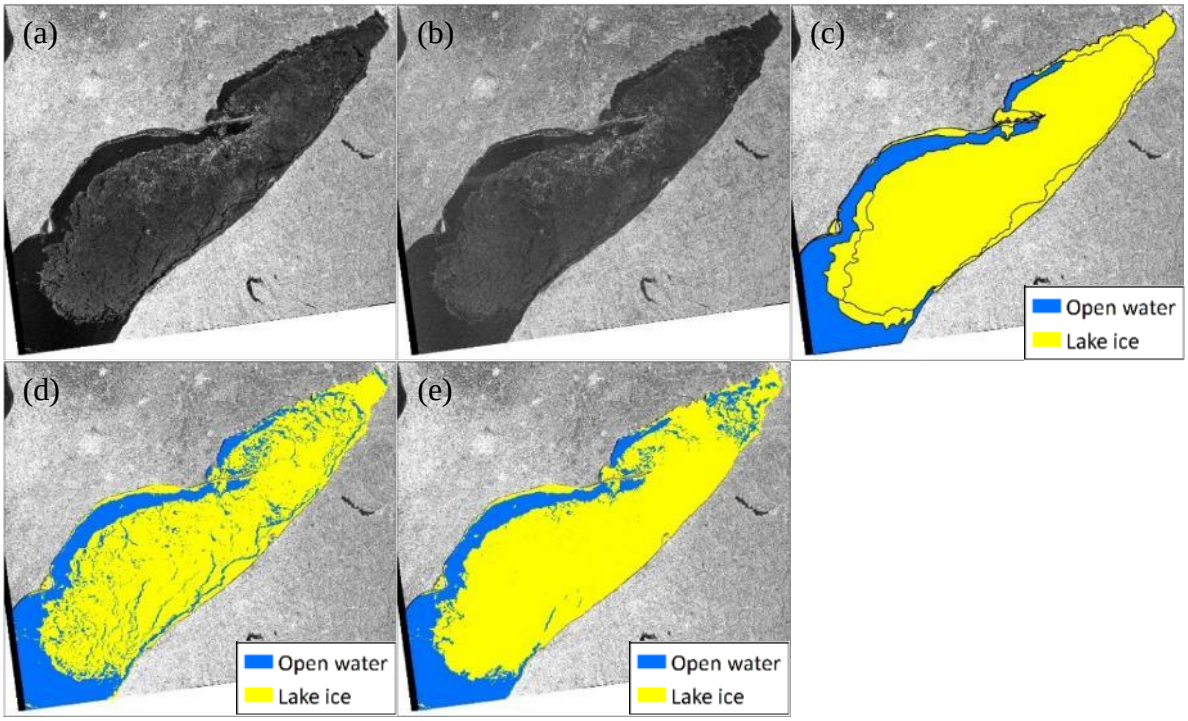

Figure 3-18: (a) Original RADARSAT-2 HH-polarized image acquired on April 1, 2014. (b) Original HV-polarized image. (c) Image analysis chart reclassified into lake ice (ice concentration from 10 to 100%) and open water (ice concentration from 0 to 10%). (d) Labelled "glocal" IRGS classification using HH polarization. (e) Labelled "glocal" IRGS classification using dual-pol images.

3.5.2.3 Ice type classification

The ice type classification result for the January 14 scene is shown in Figure 3-19. There are three ice types including thin lake ice, medium lake ice, and new lake ice in the scene. The classified ice types (Figure 3-19d) have much different distribution compared to the image analysis chart (Figure 3-19c). Some of the inconsistencies do not necessarily mean the results are erroneous because the ice expert at the CIS does not take into account small features in the image. Moreover, many of the image analysis polygons are not homogenous. They contain more than one ice type as shown in the egg code (Figure 3-19c). New lake ice is misclassified as open water due to its similar low radar return. Overall, most of the thicker ice types are correctly discriminated from open water.

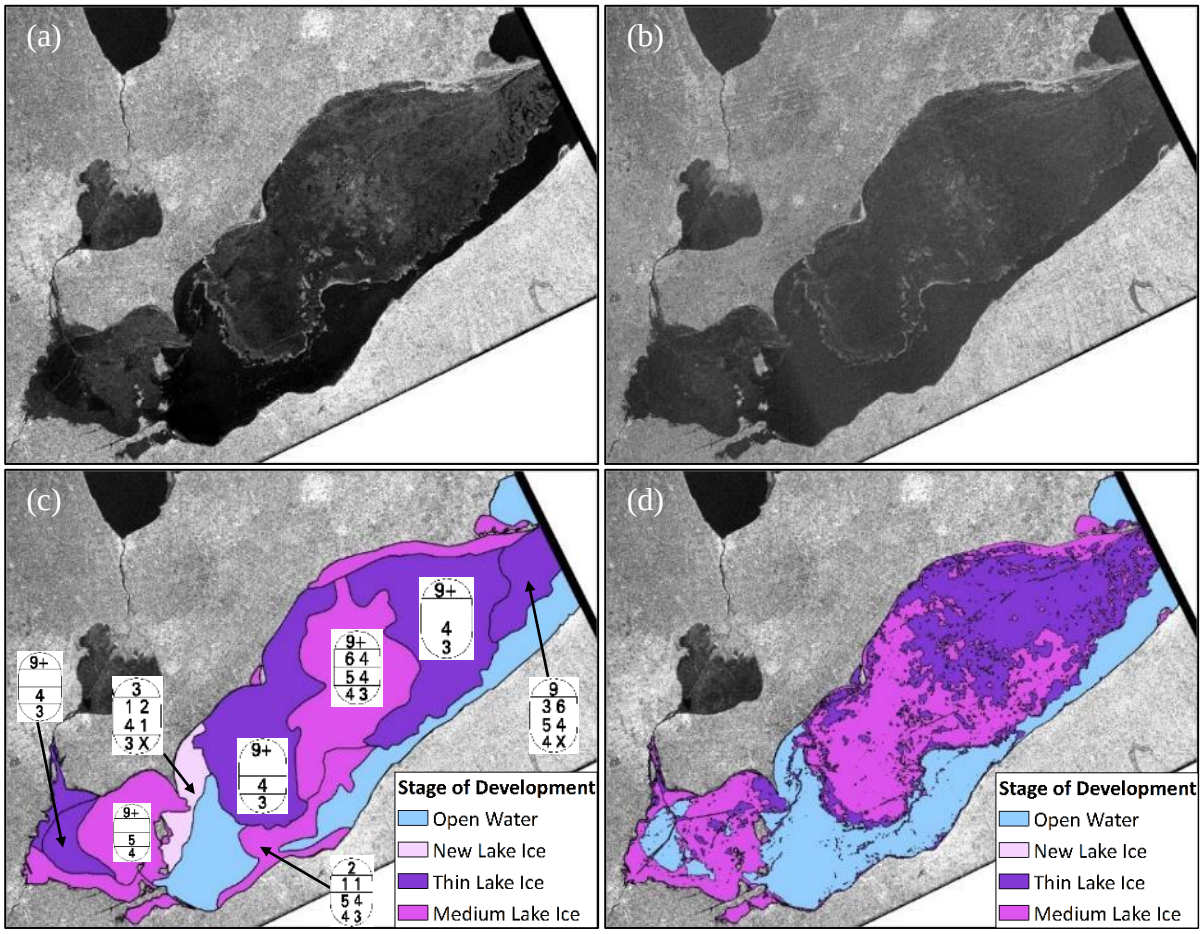

Figure 3-19: (a) Original RADARSAT-2 HH-polarized image acquired on January 14, 2014. (b) Original HV-polarized image. (c) Image analysis chart color-coded in SD. (d) Labelled "glocal" IRGS classification.

The scene of March 21 is a complicated scene that contains various ice types (Figure 3-20). The ice thickness in this scene ranges from less than 5 cm to more than 70 cm. New lake ice appears dark in the image because of its smooth surface whereas medium lake ice appears brighter with its rough surface. Thick lake ice and very thick lake ice have similar backscatter intensities and appear relatively darker than the medium lake ice. Generally, the algorithm accurately identified new lake ice, medium lake ice, and very thick lake ice. However, thick lake ice cannot be differentiated from very thick lake ice due to their similar backscatter range.

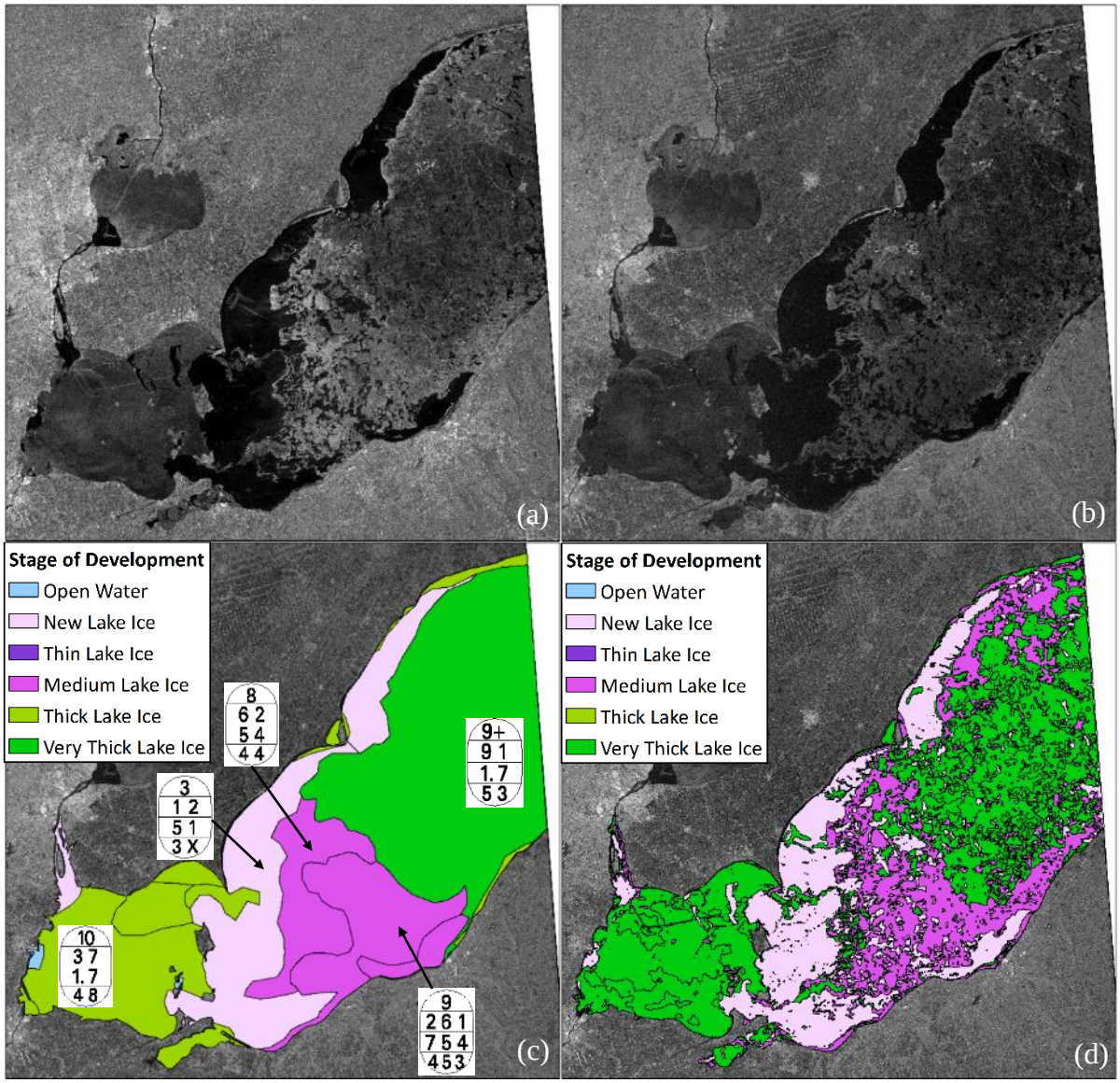

Figure 3-20: (a) Original RADARSAT-2 HH-polarized image acquired on March 21, 2014. (b) Original HV-polarized image. (c) Image analysis chart color-coded in SD. (d) Labelled "glocal" IRGS classification.

3.5.3 Classification errors

Lack of ground truth data is one of the main challenges in evaluating ice classification algorithms (Ochilov & Clausi, 2012). Since in-situ observations on large lakes like the Great Lakes is impractical and expensive, we used image analysis charts provided by the CIS who has decades of experience interpreting SAR imagery as the reference data. However, the coarse representation of image analysis charts imposes limitations in the validation process. The resolution of image analysis charts is

significantly lower than our pixel-based classification results. In order for clients to easily read the charts, ice conditions in image analysis charts are expressed for large polygons that are at least tens of square kilometers in size. Furthermore, since the image analysis charts are produced near real-time on almost a daily basis, SAR image analysis are performed quickly by ice analysts and they do not take into account small features such as cracks between ice floes. Therefore, an absolute quantitative comparison between image analysis charts and classification results is not possible.

To compare our pixel-based ice-water classification results with the region-based image analysis charts, we reclassified the charts into ice and open water using an ice concentration threshold of 10%. Here, polygons with total ice concentration larger than 10% are regarded as lake ice, otherwise are reclassified as open water. This means that even regions with 20% of ice are considered fully ice covered, which explains why most errors come from misclassifying ice as water (Table 3-3). This subjective assumption contributes to some of the discrepancy and reduces the accuracy. Considering the limitations of the validation procedure, the classification accuracy are likely more reliable than the calculated pixel-by-pixel differences with the image analysis charts. Therefore, we have also conducted the per-pixel validation using random sample points and the overall accuracy reached 90%.

Comparing ice type classification results with image analysis charts is a more challenging task than ice-water classification. The ice types in the image analysis charts are based on stage of development, and each category contains a wide range of ice thicknesses (Table 3-2). Although the CIS provides the stage of development color code, most of the polygons are heterogeneous and contain multiple ice types without identifying the exact locations of the different ice types (see egg codes in Figure 3-21). In most cases, multiple ice types are mixed together in the ice analysis polygons and small features were not included. Therefore, the quantitative assessment of the ice type classification accuracy was not performed.

Although image analysis charts are produced by ice experts, they may contain some human-made errors. The total concentration, number of classes, and ice types are assigned subjectively from visual interpretation. A quantitative assessment of the CIS visual analysis done by Shokr (2009) has indicated the existence of anomalies in image analysis charts. To ensure navigation safety, ice analysts are generally biased toward overestimation of ice concentration and assigning thicker ice types. Additionally, the interpretation of SAR images may vary between ice analysts depending on their level of expertise. Some analysts may include more details. Currently, there are seven ice analysts at the CIS in charge of the image analysis charts.

3.5.4 Limitations

3.5.4.1 Ice-water classification

There are two limitations of the "glocal" IRGS ice-water classification used in this study. One limitation is the difficulty in discriminating calm open water from new lake ice (Figure 3-19). New lake ice is a thin layer of ice that forms at the beginning of the freeze-up period. It generally has a smooth surface/ice-water interface and high optical depth allowing light to transmit to the subsurface water, which makes it visually transparent. Therefore, new lake ice can be challenging to recognize from open water in either optical or SAR imagery. Ice experts at CIS often have to rely on weather conditions to determine the presence of new lake ice. Although a robust ice-water discrimination is desirable, the very thin new lake ice is less of an issue from an operational perspective.

The presence of water on ice due to rainfall or melt is another challenge for ice-water classification. Melting snow on ice can absorb or melt ponds reflect away most of the radar signal resulting in similar low backscatter to open water. Melt conditions are also a challenging situation for ice analysts interpreting SAR images.

3.5.4.2 Ice type classification

The correlation between backscatter and different ice types is ambiguous. Each ice type can depict a large variability of backscatter that overlaps each other. Depending on the roughness at the surface and the ice-water interface, the same ice type can display very high backscatter with heavy ridging or low backscatter with a smooth surface. As shown in Figure 3-22c, the CIS ice analyst provided ridging description of the same type of ice. As they get to thicker ice types (thick and very thick lake ice), ice analysts often have to rely on freezing degree days as well as history and weather of the last few days to determine the stage of development. Therefore, it is difficult in practice to identify different ice types and estimate ice thickness based only on SAR backscatter. For further improvement, additional image characteristics such as texture features could be included (Leigh et al., 2014; Zakhvatkina et al., 2013).

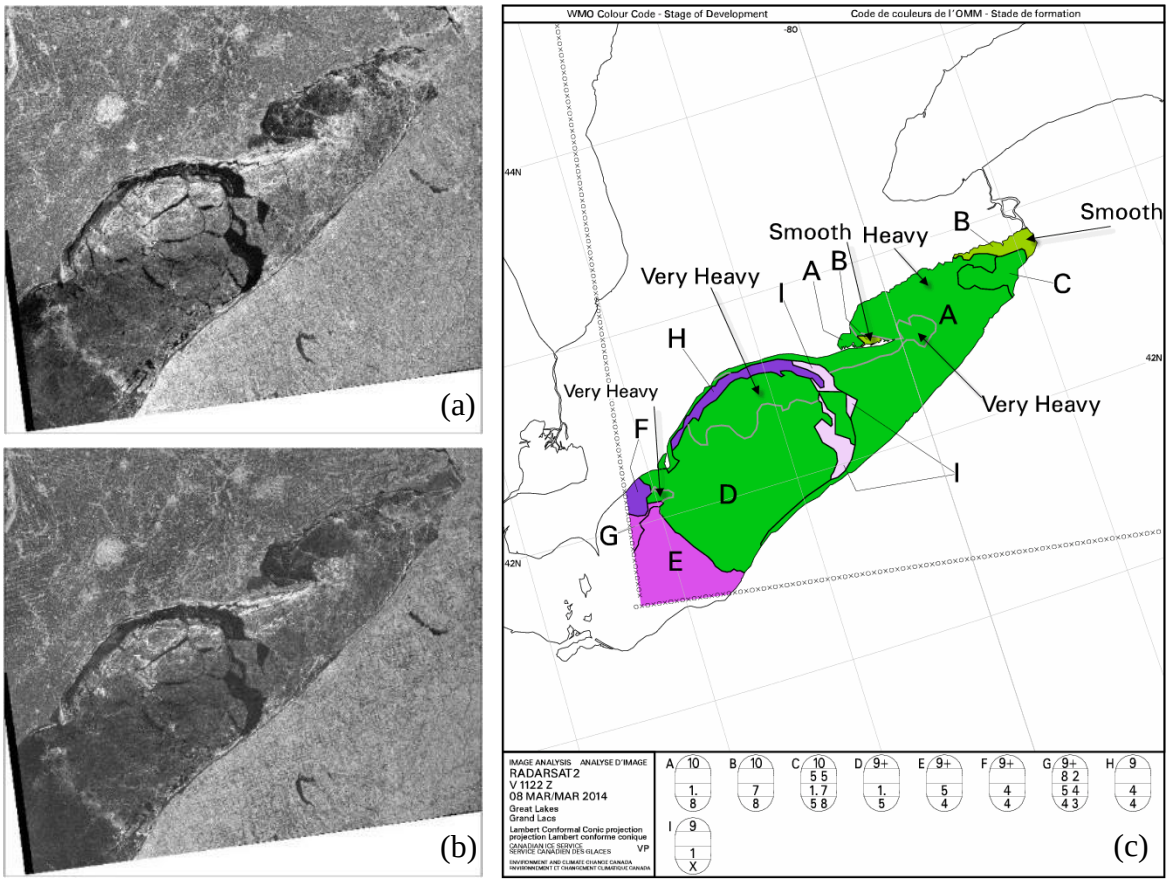

Figure 3-21: (a) Original RADARSAT-2 HH-polarized image acquired on March 8, 2014. (b) Original HV-polarized image. (c) Requested CIS image analysis chart for Lake Erie.

3.6 Conclusions

The semi-automated "glocal" IRGS classification was tested on 26 dual polarized RADARSAT-2 imagery over Lake Erie. This is hierarchical region-based approach that divides the image into small polygons and minimizes the effect of incidence angle. This unsupervised classification method identifies homogeneous regions with arbitrary classes followed by manual labeling. Validation of the classification was done via pixel-by-pixel comparison with the CIS image analysis charts. The algorithm achieved an overall accuracy of 90.2% for ice-water classification. Analysis of various case studies indicates that the "glocal" IRGS algorithm can provide a reliable ice-water classification using dual polarized images. The algorithm has difficulty distinguishing calm open water from new lake ice and decaying ice. However, the misidentification of new lake ice is not a significant drawback for operational purposes. For lake ice type classification, most thin ice types were effectively identified but thick and very thick lake ice were often confused due to the ambiguous relation between

backscatter and ice types. Texture features could be included for further improvement. Overall, our "glocal" IRGS classification results are close to visual interpretation by ice analysts and would have expected to be closer if they could draw ice charts at a more detailed level. The testing of dual- and single-pol images demonstrated the improvement of ice-water discrimination utilizing dual polarized data as opposed to single polarization, particularly for windy near-range scenes.

Although the "glocal" IRGS algorithm needs manual labelling, the whole classification process takes less than 10 minutes for each scene, which is likely to be operationally useful. The algorithm can be fully automated by implementing automatic labelling using trained models, as demonstrated by Leigh et al. (2014) for application to sea ice mapping.

3.7 Acknowledgements

The authors would like to thank Canadian Ice Service of Environment Canada for providing the Great Lakes image analysis charts. The MAGIC software was developed by the Vision and Image Processing lab (D. Clausi's group) at the University of Waterloo. This project was supported by a RADARSAT-2 Science and Operational Applications Research (SOAR) program grant from the Canadian Space Agency to C. Duguay.

Chapter 4
General Conclusions

4.1 Summary

Monitoring ice conditions and variability on the Great Lakes is crucial for marine resource management and the shipping industry. Satellite SAR systems provide high resolution and all weather sensing capabilities that make them well suited for ice mapping. For operational purposes, the CIS and NIC have been manually generating Great Lakes ice analysis charts based on mainly satellite imagery. The availability of an automated or semi-automated ice classification algorithm would benefit operational ice services. Numerous efforts have been made to automate SAR ice mapping, but little success had been achieved to date. The overall objective of this study was therefore to investigate the performance of the previously published semi-automated sea ice classification algorithm "glocal" IRGS for lake ice classification using dual polarized RADARSAT imagery.

Chapter 3 presented the results of the evaluation of "glocal" IRGS for Lake Erie ice classification using 26 dual polarized RADARSAT-2 images in 2014. The classification results were evaluated against the CIS Great Lakes image analysis charts. This study showed that the "glocal" IRGS algorithm can effectively discriminate lake ice from open water in most ice conditions, with an overall accuracy of 90.2%. Thickness-based lake ice types were effectively identified in most cases, but large overlapping backscatter range of different ice types can sometimes confuse the algorithm. Texture features could be included for further improvement of the ice type classification. The study also demonstrated a slight improvement of using dual-pol as opposed to single-pol images for ice-water separation, especially for windy near-range scenes.

In summary, this thesis demonstrated the potential of the "glocal" IRGS algorithm for operational lake ice-water classification using dual polarized SAR imagery. The classes generated from the algorithm are close to visual interpretation by ice analysts. It is a promising algorithm that can overcome a number challenges including incidence angle effect and speckle noise. Although the algorithm requires manual labelling, the whole classification process takes less than 10 minutes and is likely to be operationally useful.

4.2 Limitations

There are several limitations in this study, particularly the validation procedure. Due to the lack of ground truth data for the Great Lakes ice cover, the image analysis charts provided by the CIS were used to quantitatively evaluate the classification results. The region-based image analysis charts have much coarser representation than our pixel-based results and is challenging to compare with. Therefore, subjective ice concentration threshold was applied for direct comparison with the ice-water classification results. Evaluation of the lake ice type classification results is more difficult because most ice analysis polygons are heterogeneous and contain multiple ice types. Furthermore, the image analysis charts themselves may contain human-made errors and may vary between ice analysts.

Although the "glocal" IRGS algorithm can well discriminate open water from lake ice in most cases, it cannot effectively identify new lake ice from calm open water. New lake ice has a very low backscatter and little texture, which is similar to calm open water especially in the large incidence angles. This drawback does not pose significant risks for operational ice mapping. Another limitation of the algorithm is the difficulty in ice identification during spring melt where melting snow or melt ponds on the ice surface obscure the radar signal from the ice underneath.

The image segmentation was performed in the MAGIC software which requires a human operator to read in images, specify parameters, and export the results. Currently, the MAGIC system does not include automatic labelling so that a visual inspection is required to manually label the images. This is the main limitation for ice mapping in an operational perspective.

4.3 Recommendations for Future Work

The "glocal" IRGS algorithm tested in this study is an unsupervised approach that produces homogeneous segments with arbitrary class labels. The automatic labelling can be achieved by combining the non-labelled "glocal" results with trained supervised classification results. Leigh, Wang, and Clausi (2014) successfully implemented automatic labelling by combing the "glocal" IRGS with SVM classification using the IRGS framework. Future development of the automatic labelling in the MAGIC system would greatly improve the algorithm.

IRGS is a promising algorithm for SAR lake ice mapping. However, performing ice classification in the MAGIC software requires a human operator to manually execute each step of the process. It is recommended that the IRGS algorithm be incorporated into a processing chain that can be fully automated for operational use.

This study demonstrated the good performance of the "glocal" IRGS algorithm for lake ice-water discrimination, but its ability to identify different lake ice types is limited. For future improvement, additional image characteristics such as texture features could be considered. The low ice type classification accuracy is also partly due to the coarse representation and the sparse thickness-based ice type categories of the image analysis charts. Unlike sea ice, there is no well-defined lake ice category that captures the characteristics of each ice type. The standard terminology for lake ice used in the operational ice services are generally sparse and cannot well describe the surface conditions. Future development of a more comprehensive lake ice category would greatly benefit the lake ice studies.

References

Adams, W. P. (1976). Diversity of lake cover and its implications. *Musk-Ox, 18*, 86–89.

Adrian, R., Walz, N., Hintze, T., Hoeg, S., & Rusche, R. (1999). Effects of ice duration on plankton succession during spring in a shallow polymictic lake. *Freshwater Biology*, *41*(3), 621–632. http://doi.org/10.1046/j.1365-2427.1999.00411.x

Arkett, M., Flett, D., De Abreu, R., & Gillespie, C. (2006). Sea ice type and open water discrimination for operational ice monitoring with RADARSAT-2. *International Geoscience and Remote Sensing Symposium (IGARSS)*, 1631–1634. http://doi.org/10.1109/IGARSS.2006.421

Arp, C. D., Jones, B. M., & Grosse, G. (2013). Recent lake ice-out phenology within and among lake districts of Alaska, U.S.A. *Limnology and Oceanography*, *58*(6), 2013–2028. http://doi.org/10.4319/lo.2013.58.6.2013

Atwood, D. K., Gunn, G. E., Roussi, C., Wu, J., Duguay, C., & Sarabandi, K. (2015). Microwave backscatter from Arctic lake ice and polarimetric implications. *IEEE Transactions on Geoscience and Remote Sensing*, *53*(11), 5972–5982. http://doi.org/10.1109/TGRS.2015.2429917

Bengtsson, L. (1986). Spatial variability of lake ice covers. *Geografiska Annalar. Series A, Physical Geography*, *68*(1), 113–121.

Benson, B. J., Magnuson, J. J., Jensen, O. P., Card, V. M., Hodgkins, G., Korhonen, J., … Granin, N. G. (2012). Extreme events, trends, and variability in Northern Hemisphere lake-ice phenology (1855-2005). *Climatic Change*, *112*(2), 299–323. http://doi.org/10.1007/s10584-011-0212-8

Bernhardt, J., Engelhardt, C., Kirillin, G., & Matschullat, J. (2012). Lake ice phenology in Berlin-Brandenburg from 1947–2007: observations and model hindcasts. *Climatic Change*, *112*(3–4), 791–817. http://doi.org/10.1007/s10584-011-0248-9

Bertoia, C., Manore, M., Andersen, H. S., O'Connors, C., Hansen, K. Q., & Evanego, C. (2004). Synthetic aperture radar for operational ice observation and analysis at the U.S., Canadian, and Danish national ice centers. In C. R. Jackson & J. R. Apel (Eds.), *Synthetic aperture radar marine users manual* (pp. 417–442). Washington, DC: National Oceanic and Atmospheric Administration.

Bertoia, C., & Ramsay, B. (1998). Sea ice analysis and products: cooperative work at the US and

Canadian national ice centers. *IGARSS '98, Sensing and Managing the Environment, 18th International Geoscience and Remote Sensing Symposium, 6--10 July 1998, Seattle, Washington. Proceedings*, *4*, 1944–1947. Retrieved from http://dx.doi.org/10.1109/IGARSS.1998.703703

Blenckner, T., Jarvinen, M., & Weyhenmeyer, G. A. (2004). Atmospheric circulation and its impact on ice phenology in Scandinavia. *Boreal Environment Research*, *9*(5), 371–380.

Brown, L. C., & Duguay, C. R. (2010). The response and role of ice cover in lake-climate interactions. *Progress in Physical Geography*, *34*(5), 671–704. http://doi.org/10.1177/0309133310375653

Choiński, A., Ptak, M., Skowron, R., & Strzelczak, A. (2015). Changes in ice phenology on polish lakes from 1961 to 2010 related to location and morphometry. *Limnologica - Ecology and Management of Inland Waters*, *53*, 42–49. http://doi.org/10.1016/j.limno.2015.05.005

CIS. (2005). *MANICE: Manual of Standard Procedures for Observing and Reporting Ice Conditions* (9th ed.). Ottawa, ON: Canadian Ice Service (CIS), Meteorological Service of Canada.

CIS. (2016). Interpreting ice charts - World Meteorological Organization colour code. Retrieved from http://ec.gc.ca/glaces-ice/default.asp?lang=En&n=D5F7EA14-1&offset=2&toc=show

Clausi, D. A., Qin, A. K., Chowdhury, M. S., Yu, P., & Maillard, P. (2010). MAGIC : MAp-Guided Ice Classification System. *Canadian Journal of Remote Sensing*, *36*, 13–25. http://doi.org/10.5589/m10-008

Cordeira, J. M., & Laird, N. F. (2008). The influence of ice cover on two lake-effect snow events over Lake Erie. *Monthly Weather Review*, *136*(7), 2747–2763. http://doi.org/10.1175/2007mwr2310.1

Dibike, Y., Prowse, T., Bonsal, B., Rham, L. De, & Saloranta, T. (2012). Simulation of North American lake-ice cover characteristics under contemporary and future climate conditions. *International Journal of Climatology*, *32*(5), 695–709. http://doi.org/10.1002/joc.2300

Drai, D. (2000). *Suivi de l'évolution spatio-temporelle de couverts de glace lacustres par télédetection en micro-ondes actives (géoradar et RADARSAT)*. Université Laval. Retrieved from http://search.proquest.com.proxy.lib.uwaterloo.ca/docview/304656554?accountid=14906

Duguay, C. R., Bernier, M., Gauthier, Y., & Kouraev, A. (2015). Remote sensing of lake and river

ice. In M. Tedesco. (Ed.), *Remote Sensing of the Cryosphere* (pp. 273–306). New York: JohnWiley & Sons, Ltd.

Duguay, C. R., Flato, G. M., Jeffries, M. O., Ménard, P., Morris, K., & Rouse, W. R. (2003). Ice-cover variability on shallow lakes at high latitudes: Model simulations and observations. *Hydrological Processes*, *17*, 3465–3483. http://doi.org/10.1002/hyp.1394

Duguay, C. R., Prowse, T. D., Bonsal, B. R., Brown, R. D., Lacroix, M. P., & Menard, P. (2006). Recent trends in Canadian lake ice cover. *Hydrological Processes*, *20*, 781–801. http://doi.org/10.1002/hyp.6131

Duguay, C. R., Pultz, T. J., Lafleur, P. M., & Drai, D. (2002). RADARSAT backscatter characteristics of ice growing on shallow sub-Arctic lakes, Churchill, Manitoba, Canada. *Hydrological Processes*, *16*(8), 1631–1644. http://doi.org/10.1002/hyp.1026

Futter, M. N. (2003). Patterns and trends in southern Ontario lake ice phenology. *Environmental Monitoring and Assessment*, *88*(1–3), 431–444. http://doi.org/10.1023/A:1025549913965

Geldsetzer, T., Van Der Sanden, J., & Brisco, B. (2010). Monitoring lake ice during spring melt using RADARSAT-2 SAR. *Canadian Journal of Remote Sensing*, *36*(sup2), 391–400. http://doi.org/10.5589/m11-001

George, D. G. (2010). The impact of climate change on European lakes. In G. George (Ed.), *The Impact of Climate Change on European Lakes* (pp. 1–13). Dordrecht: Springer Netherlands. http://doi.org/10.1017/CBO9781107415324.004

Gill, R. S. (2003). SAR ice classification using fuzzy screening method. In *Workshop on Applications of SAR Polarimetry and Polarimetric Interferometry (POLinSAR)*. Frascati, Italy.

Haarpaintner, J., & Solbø, S. (2007). *Automatic ice-ocean discrimination in SAR imagery*. Norut IT-report.

Howell, S. E. L., Brown, L. C., Kang, K. K., & Duguay, C. R. (2009). Variability in ice phenology on Great Bear Lake and Great Slave Lake, Northwest Territories, Canada, from SeaWinds/QuikSCAT: 2000-2006. *Remote Sensing of Environment*, *113*(4), 816–834. http://doi.org/10.1016/j.rse.2008.12.007

Jeffries, M. O., & Morris, K. (2006). Instantaneous daytime conductive heat flow through snow on lake ice in Alaska. *Hydrological Processes*, *20*(4), 803–815. http://doi.org/10.1002/hyp.6116

Jeffries, M. O., & Morris, K. (2007). Some aspects of ice phenology on ponds in central Alaska, USA. *Annals of Glaciology*, *46*(1), 397–403. http://doi.org/10.3189/172756407782871576

Jeffries, M. O., Morris, K., & Duguay, C. R. (2012). Floating ice: lake ice and river ice. In R. S. Williams & J. G. Ferrigno (Eds.), *Satellite image atlas of glaciers of the world – state of the earth's cryosphere at the beginning of the 21st century: Glaciers, global snow cover, floating ice, and permafrost and periglacial environments* (pp. 381–424). U.S. Geological Survey Professional Paper 1386-A.

Jeffries, M. O., Morris, K., Weeks, W. F., & Wakabayashi, H. (1994). Structural and stratigraphic features and ERS 1 synthetic aperture radar backscatter characteristics of ice growing on shallow lakes in NW Alaska, winter 1991-1992. *Journal of Geophysical Research*, *99*(102), 459–471. http://doi.org/10.1029/94JC01479

Jeffries, M., Wakabayashiz, H., & Weeks, W. F. (2001). ERS-1 SAR backscatter changes associated with ice growing on shallow lakes in Arctic Alaska. In *IEEE IGARSS* (pp. 2001–2004).

Jensen, J. R. (2007). *Remote sensing of the environment: an earth resource perspective* (2nd ed.). Upper Saddle River, N.J. : Pearson Prentice Hall.

Jensen, O. P., Benson, B. J., Magnuson, J. J., Card, V. M., Futter, M. N., Soranno, P. a., & Stewart, K. M. (2007). Spatial analysis of ice phenology trends across the Laurentian Great Lakes region during a recent warming period. *Limnology and Oceanography*, *52*(5), 2013–2026. http://doi.org/10.4319/lo.2007.52.5.2013

Karvonen, J., Cheng, B., Vihma, T., Arkett, M., & Carrieres, T. (2012). The Cryosphere A method for sea ice thickness and concentration analysis based on SAR data and a thermodynamic model. *The Cryosphere*, *6*, 1507–1526. http://doi.org/10.5194/tc-6-1507-2012

Karvonen, J., Similä, M., & Mäkynen, M. (2005). Open water detection from Baltic Sea ice. *IEEE Geoscience and Remote Sensing Letters*, *2*(3), 275–279. http://doi.org/10.1109/LGRS.2005.847930

Kheyrollah Pour, H. (2011). *On the use of MODIS for lake and land surface temperature investigations in the regions of Great Bear Lake*. Waterloo, Ont. : University of Waterloo 2011. Retrieved from http://hdl.handle.net/10012/6100

Kwok, R., Rignot, E., & Holt, B. (1992). Identification of sea ice types in spaceborne synthetic

aperture radar data. *Journal of Geophysical Research*, *97*(C2), 2391–2402.

Leigh, S. (2013). *Automated ice-water classification using dual polarization SAR satellite imagery*. Waterloo, Ont. : University of Waterloo 2013. Retrieved from http://hdl.handle.net/10012/7706

Leigh, S., Wang, Z., & Clausi, D. A. (2014). Automated ice-water classification using dual polarization SAR satellite imagery. *IEEE Transactions on Geoscience and Remote Sensing*, *52*(9), 5529–5539. http://doi.org/10.1109/TGRS.2013.2290231

Leshkevich, G. (1985). Machine classification of freshwater ice types from Landsat-1 digital data using ice albedos as training sets. *Remote Sensing of Environment*, *263*(17), 251–263.

Leshkevich, G. A., & Nghiem, S. V. (2007). Satellite SAR remote sensing of Great Lakes ice cover, part 2. Ice classification and mapping. *Journal of Great Lakes Research*, *33*, 736–750. http://doi.org/10.3394/0380-1330(2007)33

Leshkevich, G., & Nghiem, S. V. (2013). Great Lakes ice classification using satellite C-band SAR multi-polarization data. *Journal of Great Lakes Research*, *39*, 55–64. http://doi.org/10.1016/j.jglr.2013.05.003

Livingstone, D. M. (1997). Break-up dates of Alpine lakes as proxy data for local and regional mean surface air temperatures. *Climatic Change* , *37*(2), 407–439. http://doi.org/10.1023/A:1005371925924

Livingstone, D. M., & Adrian, R. (2009). Modeling the duration of intermittent ice cover on a lake for climate-change studies. *Limnology and Oceanography*, *54*(5), 1709–1722. http://doi.org/10.4319/lo.2009.54.5.1709

Long, D. G., Collyer, R. S., & Arnold, D. V. (1996). Dependence of the normalized radar cross section of water waves on bragg wavelength-wind speed sensitivity. *IEEE Transactions on Geoscience and Remote Sensing*, *34*(3), 656–666. http://doi.org/doi:10.1109/36.499745

Magnuson, J. J., Robertson, D. M., Benson, B. J., Wynne, R. H., Livingstone, D. M., Arai, T., … Kuusisto, E. (2000). Historical trends in lake and river ice cover in the northern hemisphere. *Science*, *289*(5485), 1743–1746. http://doi.org/10.1126/science.289.5485.1743

Matsuoka, T., Uratsuka, S., Takahashi, A., Kobayashi, T., Satake, M., Nadai, A., … Nishio, F. (1999). A backscattering model for bubbles in lake ice and comparisons with satellite and airborne SAR data. In *IEEE 1999 International Geoscience and Remote Sensing Symposium.*

IGARSS'99 (Cat. No.99CH36293) (pp. 107–109). http://doi.org/10.1109/IGARSS.1999.773416

Maykut, G. A., & Untersteiner, N. (1971). Some results from a time-dependent thermodynamic model of sea ice. *Journal of Geophysical Research*, *76*(6), 1550. http://doi.org/10.1029/JC076i006p01550

Moore, R. K. (1983). Imaging Radar Systems. In R. Colwell (Ed.), *Manual of Remote Sensing* (2nd ed., pp. 429–474). Bethesda, Maryland: ASP&RS.

Nghiem, S. V., Leshkevich, G. A., & Kwok, R. (1998). C-band polarimetric backscatter observations of Great Lakes ice. *IGARSS '98. Sensing and Managing the Environment. 1998 IEEE International Geoscience and Remote Sensing. Symposium Proceedings. (Cat. No.98CH36174)*, 1400–1402 vol.3. http://doi.org/10.1109/IGARSS.1998.691450

Nghiem, S. V, & Leshkevich, G. (2007). Satellite SAR remote sensing of Great Lakes ice cover , part 1 . Ice backscatter signatures at C Band. *Journal of Great Lakes Research*, *33*, 722–735. http://doi.org/10.3394/0380-1330(2007)33

NOAA/GLERL. (2014). NOAA Great Lakes Environmental Research Laboratory - historical ice cover. Retrieved from https://www.glerl.noaa.gov/data/ice/#historical

Ochilov, S., & Clausi, D. A. (2012). Operational SAR sea-ice image classification. *IEEE Transactions on Geoscience and Remote Sensing*, *50*(11), 4397–4408. http://doi.org/10.1109/TGRS.2012.2192278

Qin, A. K., & Clausi, D. A. (2010). Multivariate image segmentation using semantic region growing with adaptive edge penalty. *IEEE Transactions on Image Processing*, *19*(8), 2157–2170.

Ramsay, B., Flett, D., Andersen, H. S., Gill, R., Nghiem, S., & Bertoia, C. (2004). Preparation for the operational use of RADARSAT-2 for ice monitoring. *Canadian Journal of Remote Sensing*, *30*(3), 415–423.

Robertson, D. M., Ragotzkie, R. A., & Magnuson, J. J. (1992). Lake ice records used to detect historical and future climatic changes. *Climatic Change*, *21*(4), 407–427. http://doi.org/10.1007/BF00141379

Scott, J. T. (1964). *A comparison of the heat balance of lakes in winter*. Doctoral dissertation, University of Wisconsin, Madison.

Shokr, M. (2009). Compilation of a radar backscatter database of sea ice types and open water using

operational analysis of heterogeneous ice regimes. *Canadian Journal of Remote Sensing*, *35*(4), 369–384.

Shokr, M. E., Jessup, R., & Ramsay, B. (1999). An interactive algorithm for derivation of sea ice classifications and concentrations from SAR images. *Canadian Journal of Remote Sensing*, *25*(1), 70–79. http://doi.org/10.1080/07038992.1999.10855264

Sobiech, J., & Dierking, W. (2013). Observing lake- and river-ice decay with SAR: Advantages and limitations of the unsupervised k-means classification approach. *Annals of Glaciology*, *54*(62), 65–72. http://doi.org/10.3189/2013AoG62A037

Soh, L., Tsatsoulis, C., Gineris, D., & Bertoia, C. (2004). ARKTOS: An intelligent system for SAR sea ice image classification. *IEEE Transactions on Geoscience and Remote Sensing*, *42*(1), 229–248.

Soja, A., Kutics, K., & Maracek, K. (2014). Changes in ice phenology characteristics of two Central European steppe lakes from 1926 to 2012 - influences of local weather and large scale oscillation patterns. *Climatic Change*, *126*(1–2), 119–133. http://doi.org/10.1007/s10584-014-1199-8

Sturm, M., Holmgren, J., König, M., & Morris, K. (1997). The thermal conductivity of seasonal snow. *Journal of Glaciology*, *43*(143), 26–41.

Surdu, C. M., Duguay, C. R., Brown, L. C., & Fernández Prieto, D. (2014). Response of ice cover on shallow lakes of the North Slope of Alaska to contemporary climate conditions (1950-2011): Radar remote-sensing and numerical modeling data analysis. *The Cryosphere*, *8*, 167–180. http://doi.org/10.5194/tc-8-167-2014

Truesdell, C. (1971). *The tragicomical history of thermodynamics 1822–1854* (1st ed., Vol. 4). Springer-Verlag New York.

Ulaby, F. T., Moore, R. K., & Fung, A. K. (1982). *Microwave remote sensing: Active and passive. Volume 2 - Radar remote sensing and surface scattering and emission theory* (Vol. 2). Norwood, MA: Artech House, Inc.

Ulaby, F. T., Moore, R. K., & Fung, A. K. (1986). *Microwave remote sensing: Active and passive. Volume 3 - From theory to applications* (Vol. 3). Norwood, MA: Artech House, Inc.

Vachon, P. W., & Wolfe, J. (2011). C-band cross-polarization wind speed retrieval. *IEEE Geoscience*

and Remote Sensing Letters, *8*(3), 456–459. http://doi.org/10.1109/LGRS.2010.2085417

Vant, M. R., Ramseier, R. O., & Makios, V. (1978). The complex-dielectric constant of sea ice at frequencies in the range 0.1–40 GHz. *Journal of Applied Physics*, *49*(3), 1264–1280. http://doi.org/10.1063/1.325018

Vincent, L., & Soille, P. (1991). Watersheds in digital spaces: An efficient algorithm based on immersion simulations. *IEEE Trans. Pattern Anal. Mach. Intell.*, *13*(6), 583–598.

Wang, X., & Key, J. R. (2005). Arctic surface, cloud, and radiation properties based on the AVHRR polar pathfinder dataset. Part II: Recent trends. *Journal of Climate*, *18*, 2575–2593. http://doi.org/10.1175/JCLI3439.1

Wang, X., Liu, Y., & Bao, Q. (2016). Impacts of cloud overlap assumptions on radiative budgets and heating fields in convective regions. *Atmospheric Research*, *167*, 89–99. http://doi.org/10.1016/j.atmosres.2015.07.017

Weyhenmeyer, G. a., Meili, M., & Livingstone, D. M. (2004). Nonlinear temperature response of lake ice breakup. *Geophysical Research Letters*, *31*(7), 1–4. http://doi.org/10.1029/2004GL019530

Williams, G. P. (1965). Correlating freeze-up and break-up with weather conditions. *Canadian Geotechnical Journal*, *2*(4), 313–326.

Williams, S. G., & Stefan, H. G. (2006). Modeling of lake ice characteristics in North America using climate, geography, and lake bathymetry. *Journal of Cold Regions Engineering*, *20*(4), 140–167. http://doi.org/10.1061/(ASCE)0887-381X(2006)20:4(140)

Yao, H., Rusak, J., Paterson, A., Somers, K., Mackay, M., Girard, R., … McConnell, C. (2013). The interplay of local and regional factors in generating temporal changes in the ice phenology of Dickie Lake, south-central Ontario, Canada. *Inland Waters*, *3*, 1–14. http://doi.org/10.5268/IW-3.1.517

Yu, Q. (2006). *Automated SAR sea ice interpretation*. Waterloo, Ont. : University of Waterloo, 2006. Retrieved from http://search.proquest.com.proxy.lib.uwaterloo.ca/docview/304907591?accountid=14906

Yu, Q., & Clausi, D. A. (2007). SAR sea-ice image analysis based on iterative region growing using semantics. *IEEE Transactions on Geoscience and Remote Sensing*, *45*(12), 3919–3931. http://doi.org/10.1109/TGRS.2007.908876

Yu, Q., & Clausi, D. A. (2008). IRGS : Image segmentation using edge penalties and region growing. *IEEE Transactions on Pattern Analysis and Machine Intelligence*, *30*(12), 2126–2139. http://doi.org/10.1109/TPAMI.2008.15.

Zakhvatkina, N., Korosov, A., Muckenhuber, S., Sandven, S., & Babiker, M. (2017). Operational algorithm for ice-water classification on dual-polarized RADARSAT-2 images. *The Cryosphere*, *11*(1), 33–46. http://doi.org/10.5194/tc-11-33-2017

Zakhvatkina, N. Y., Alexandrov, V. Y., Johannessen, O. M., Sandvenand, S., & Frolov, I. Y. (2013). Classification of sea ice types in ENVISAT synthetic aperture radar images. *IEEE Transactions on Geoscience and Remote Sensing*, *51*(5), 2587–2600. http://doi.org/10.1109/TGRS.2012.2212445

Appendix A

Ice-water classification result images

This appendix list the final ice-water classification results for the 12 scenes. The images are displayed in the following format:

Date of SAR scene (M/D/Y)

HH-polarized image	HV-polarized image
Image analysis chart color-coded in total concentration (CT)	Image analysis chart reclassified into lake ice (ice concentration from 10 to 100%) and open water (ice concentration from 0 to 10%)
Labelled “glocal” IRGS classification using HH polarization only	Labelled “glocal” IRGS classification using dual-pol images

1/11/2014

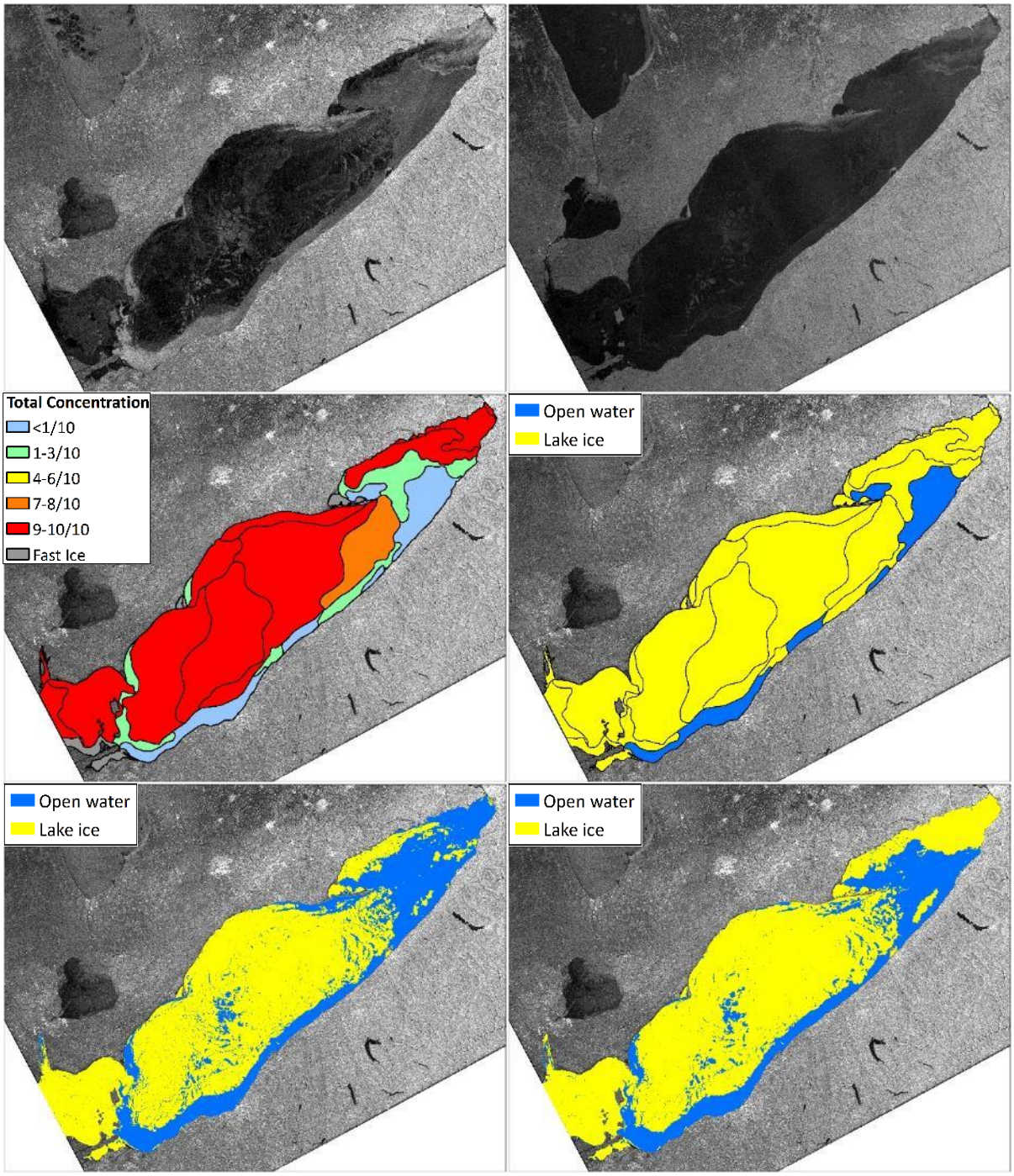
Total Concentration
<1/10
1-3/10
4-6/10
7-8/10
9-10/10
Fast Ice
Open water
Lake ice
Open water
Lake ice
Open water
Lake ice

1/12/2014

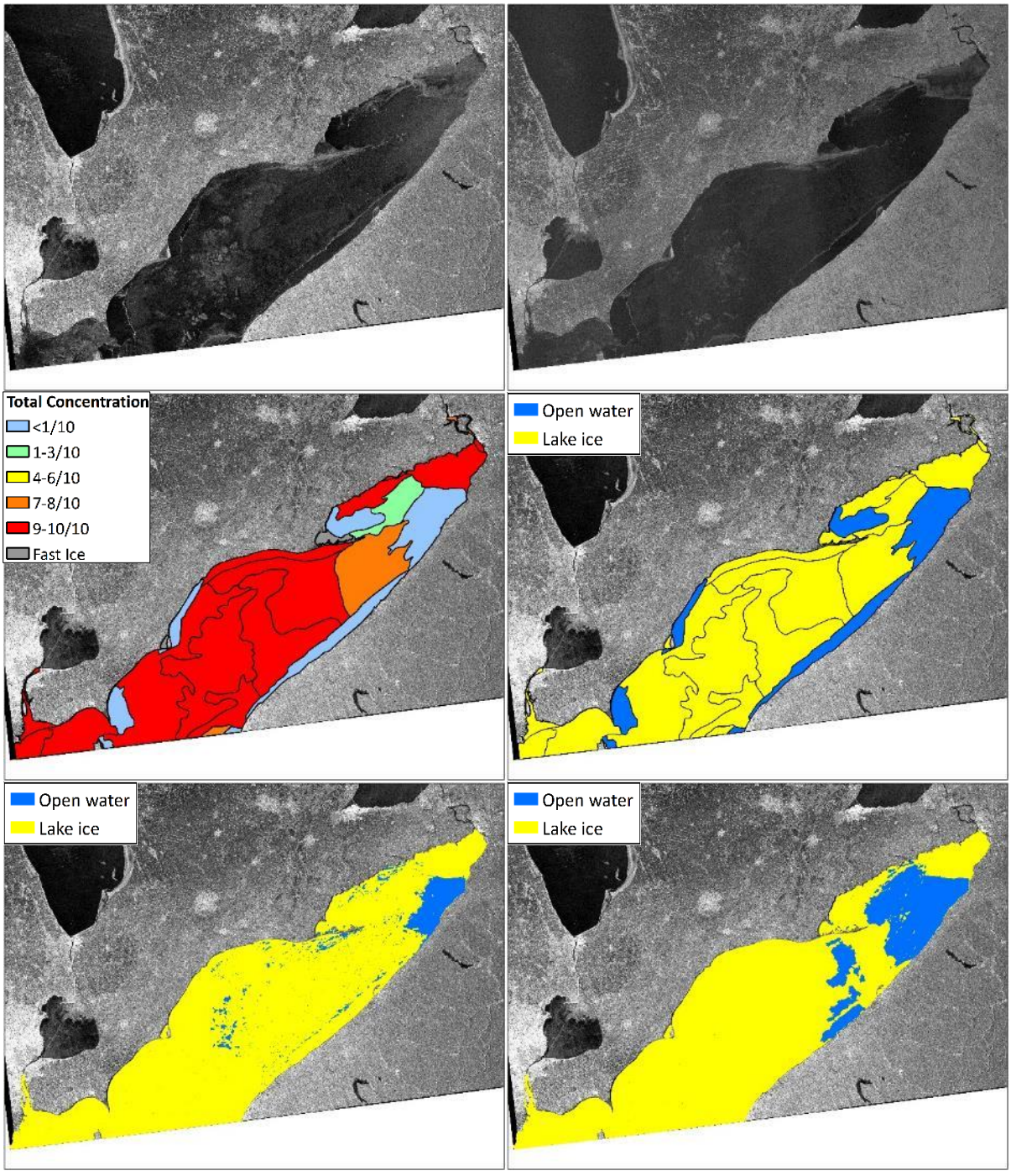
Total Concentration
<1/10
1-3/10
4-6/10
7-8/10
9-10/10
Fast Ice
Open water
Lake ice
Open water
Lake ice
Open water
Lake ice

1/14/2014

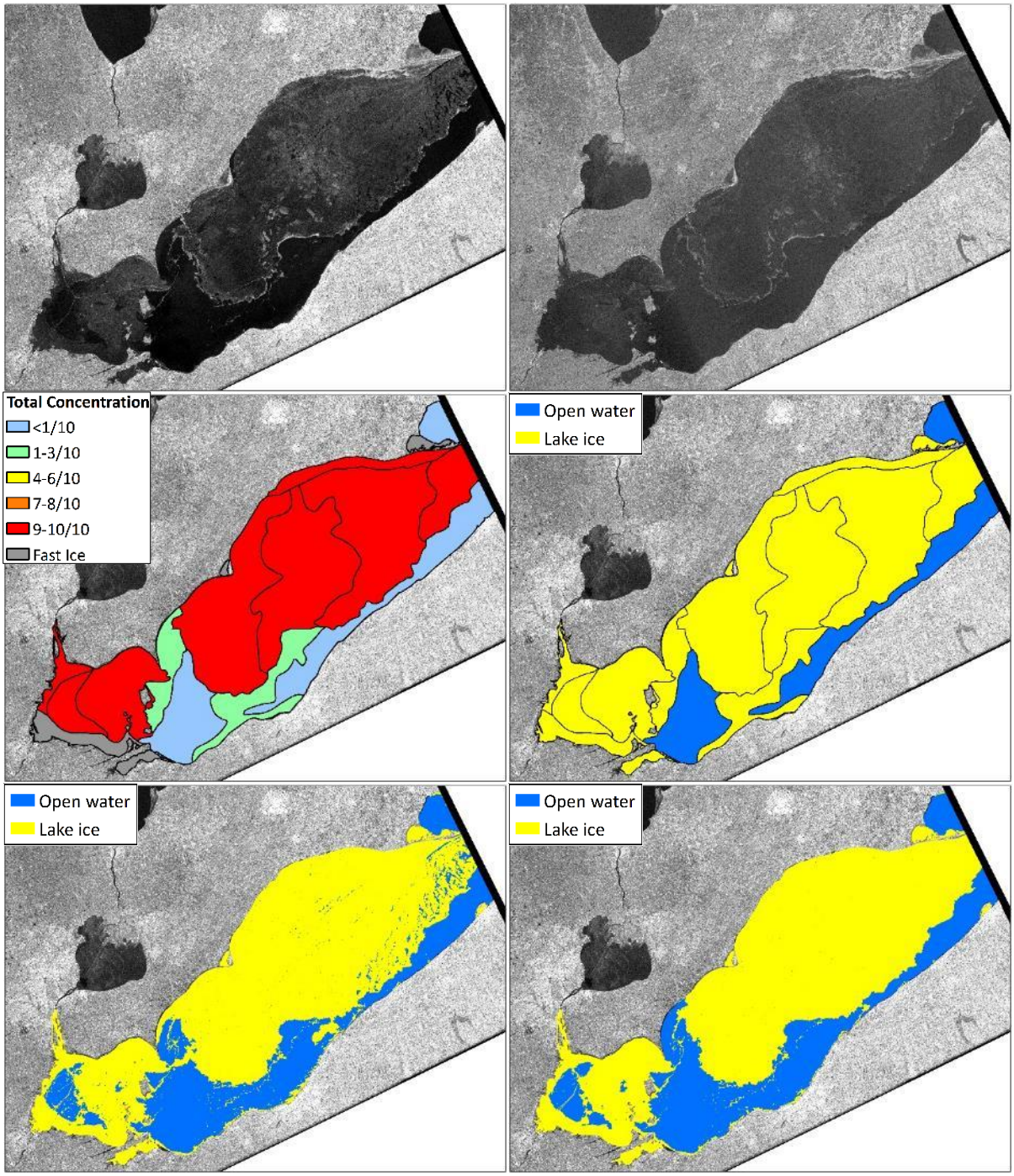
Total Concentration
<1/10
1-3/10
4-6/10
7-8/10
9-10/10
Fast Ice
Open water
Lake ice
Open water
Lake ice
Open water
Lake ice

1/15/2014

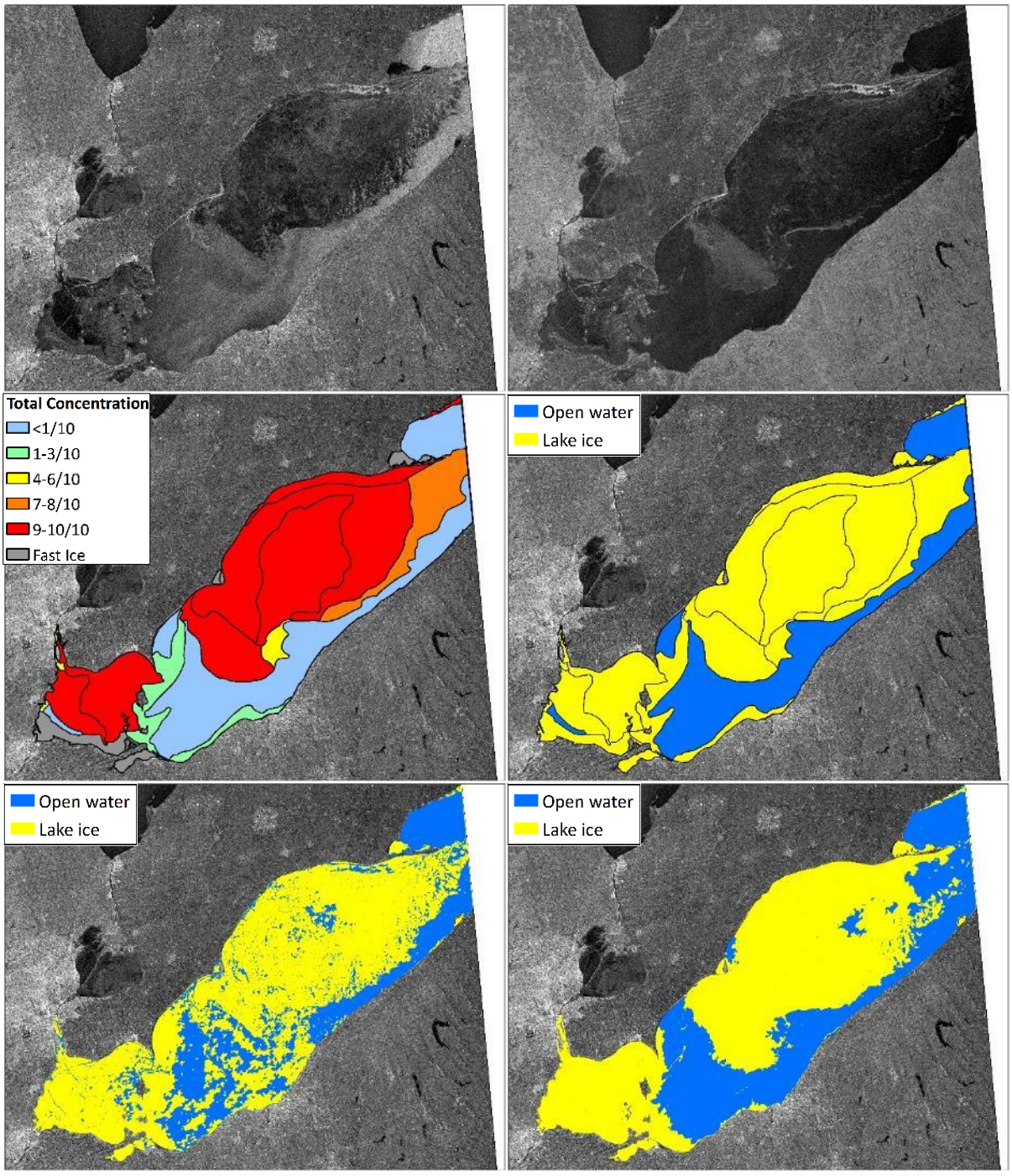
Total Concentration
<1/10
1-3/10
4-6/10
7-8/10
9-10/10
Fast Ice
Open water
Lake ice
Open water
Lake ice
Open water
Lake ice

1/18/2014

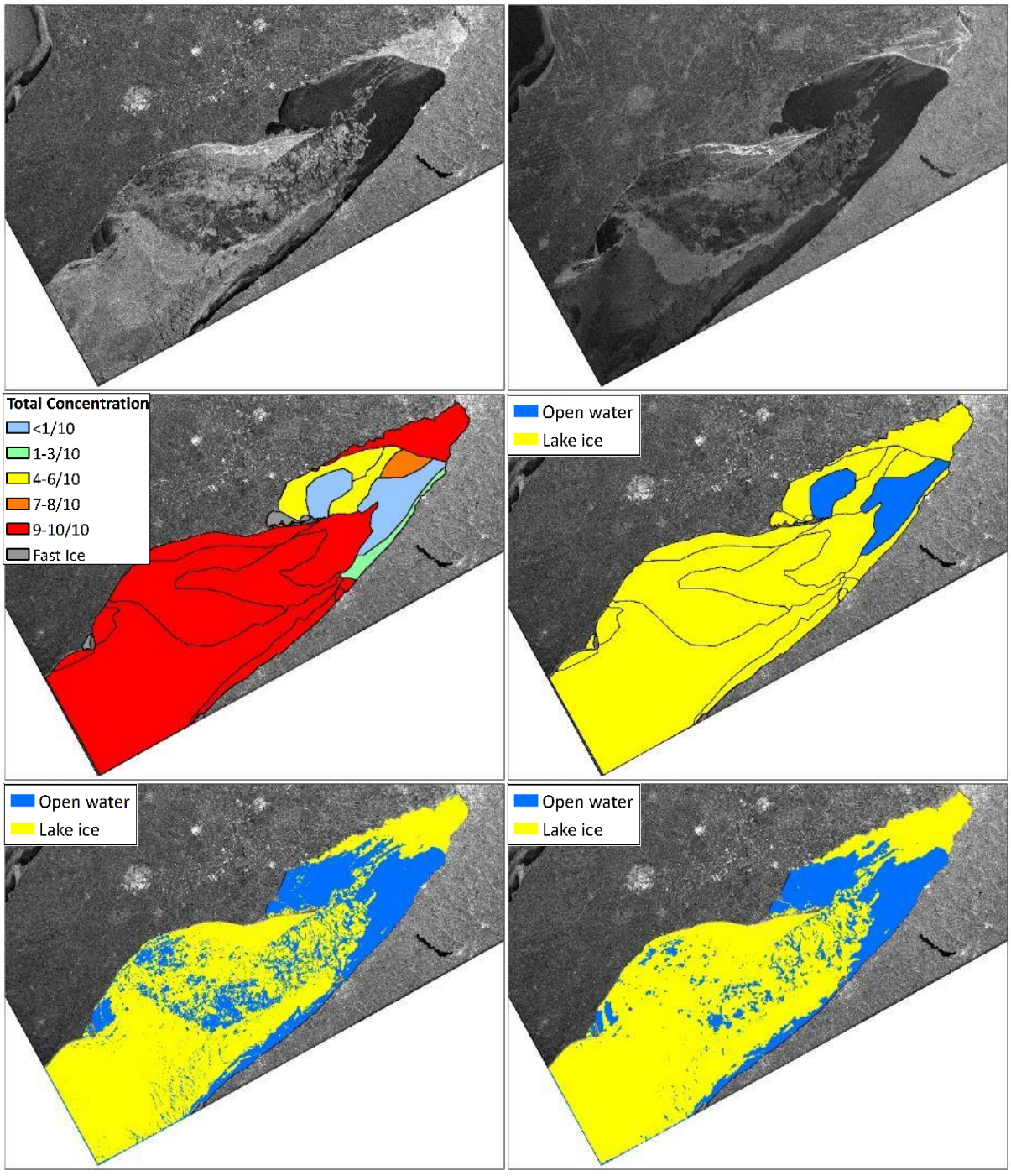
Total Concentration
<1/10
1-3/10
4-6/10
7-8/10
9-10/10
Fast Ice
Open water
Lake ice
Open water
Lake ice
Open water
Lake ice

1/19/2014

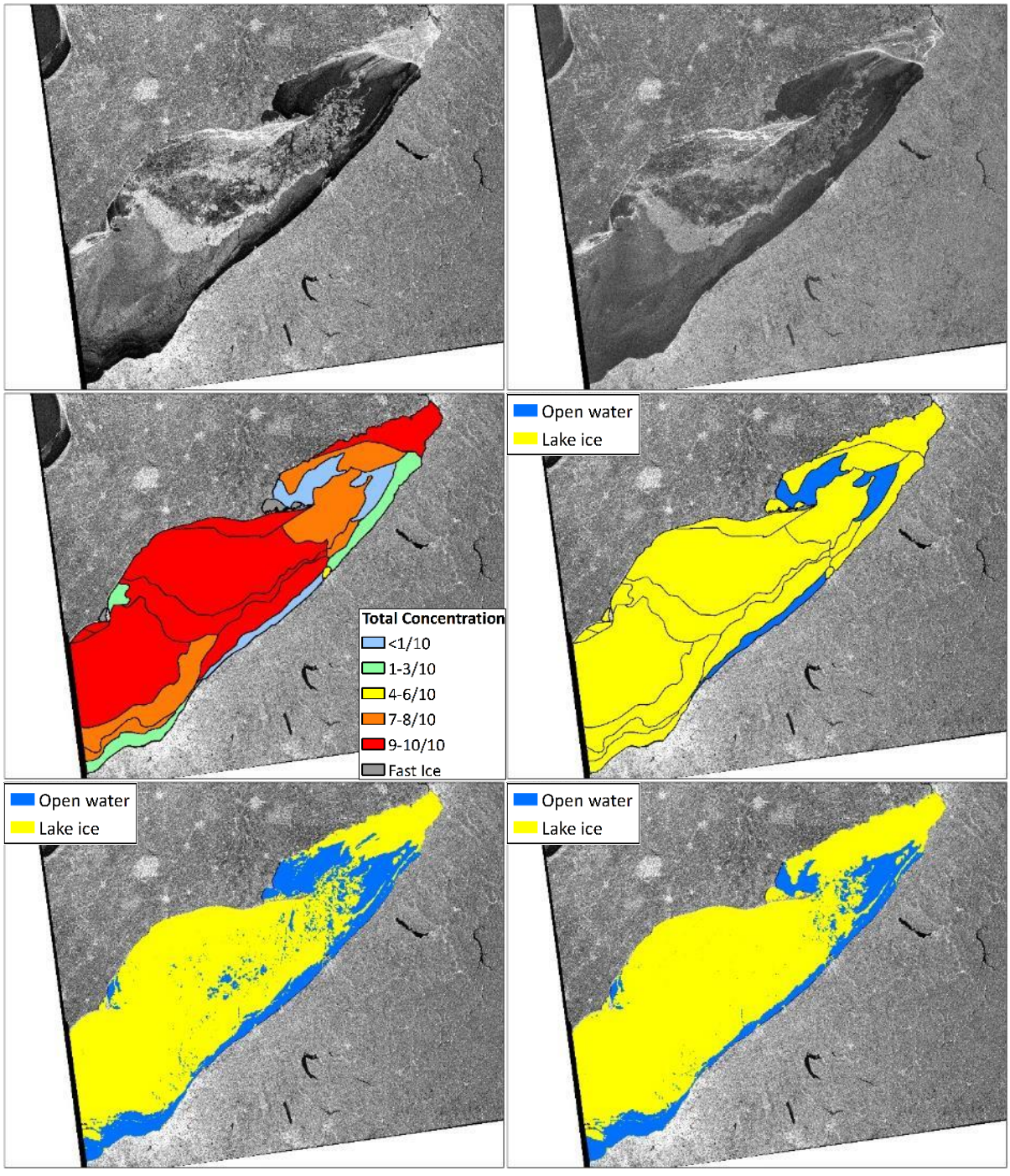
Total Concentration
<1/10
1-3/10
4-6/10
7-8/10
9-10/10
Fast Ice
Open water
Lake ice
Open water
Lake ice
Open water
Lake ice

2/21/2014

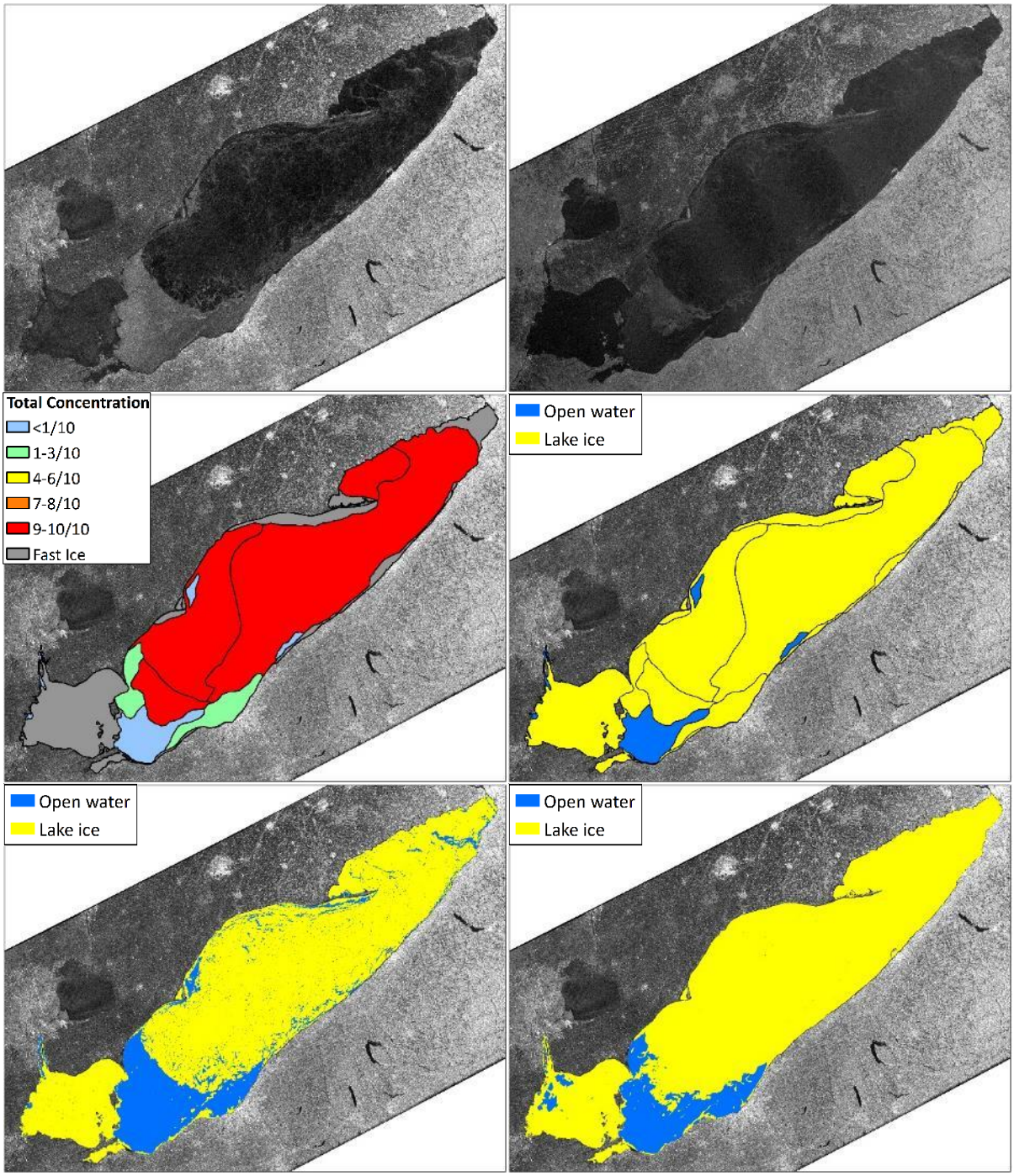
Total Concentration
<1/10
1-3/10
4-6/10
7-8/10
9-10/10
Fast Ice
Open water
Lake ice
Open water
Lake ice
Open water
Lake ice

2/22/2014

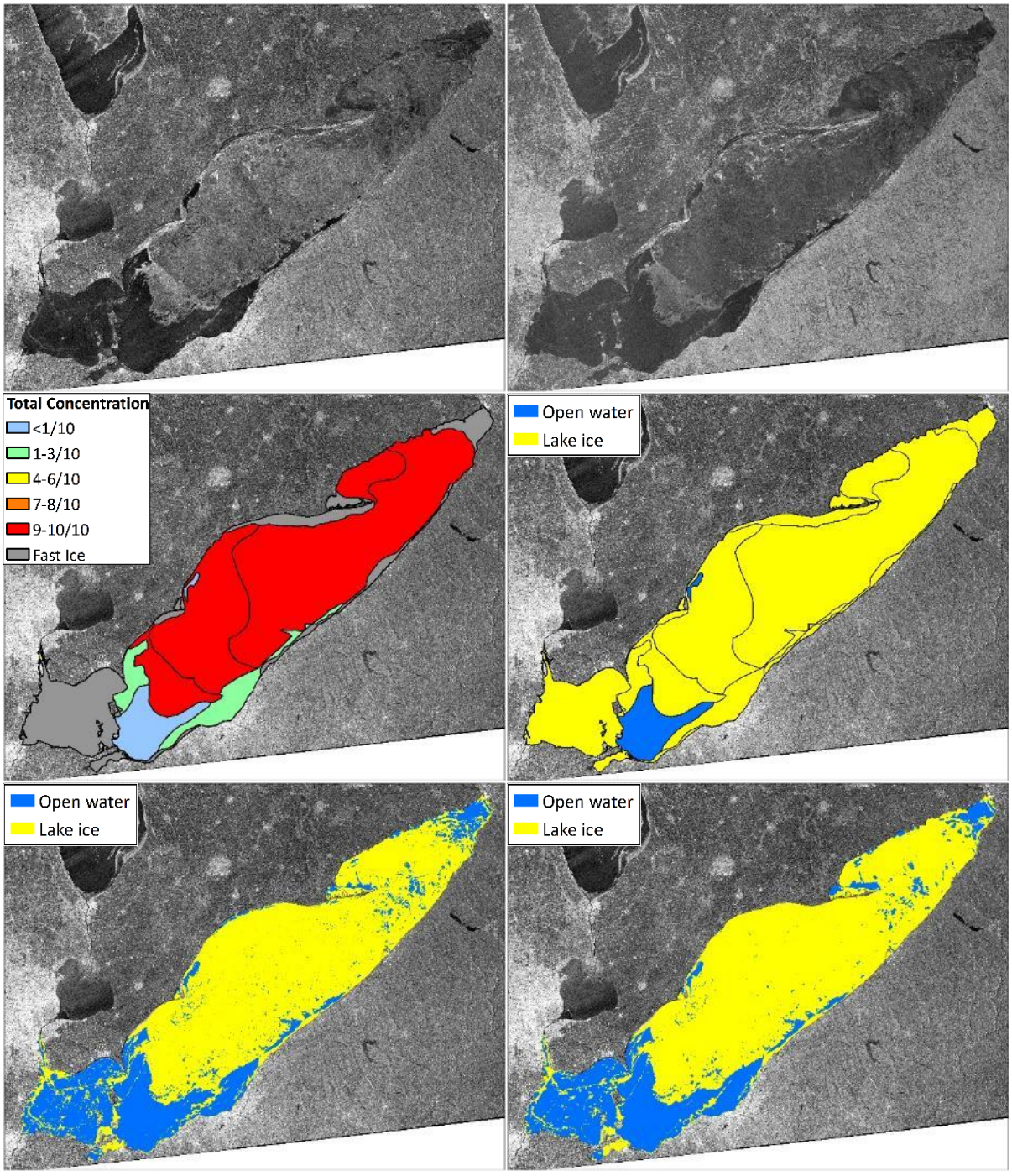
Total Concentration
<1/10
1-3/10
4-6/10
7-8/10
9-10/10
Fast Ice
Open water
Lake ice
Open water
Lake ice
Open water
Lake ice

3/25/2014

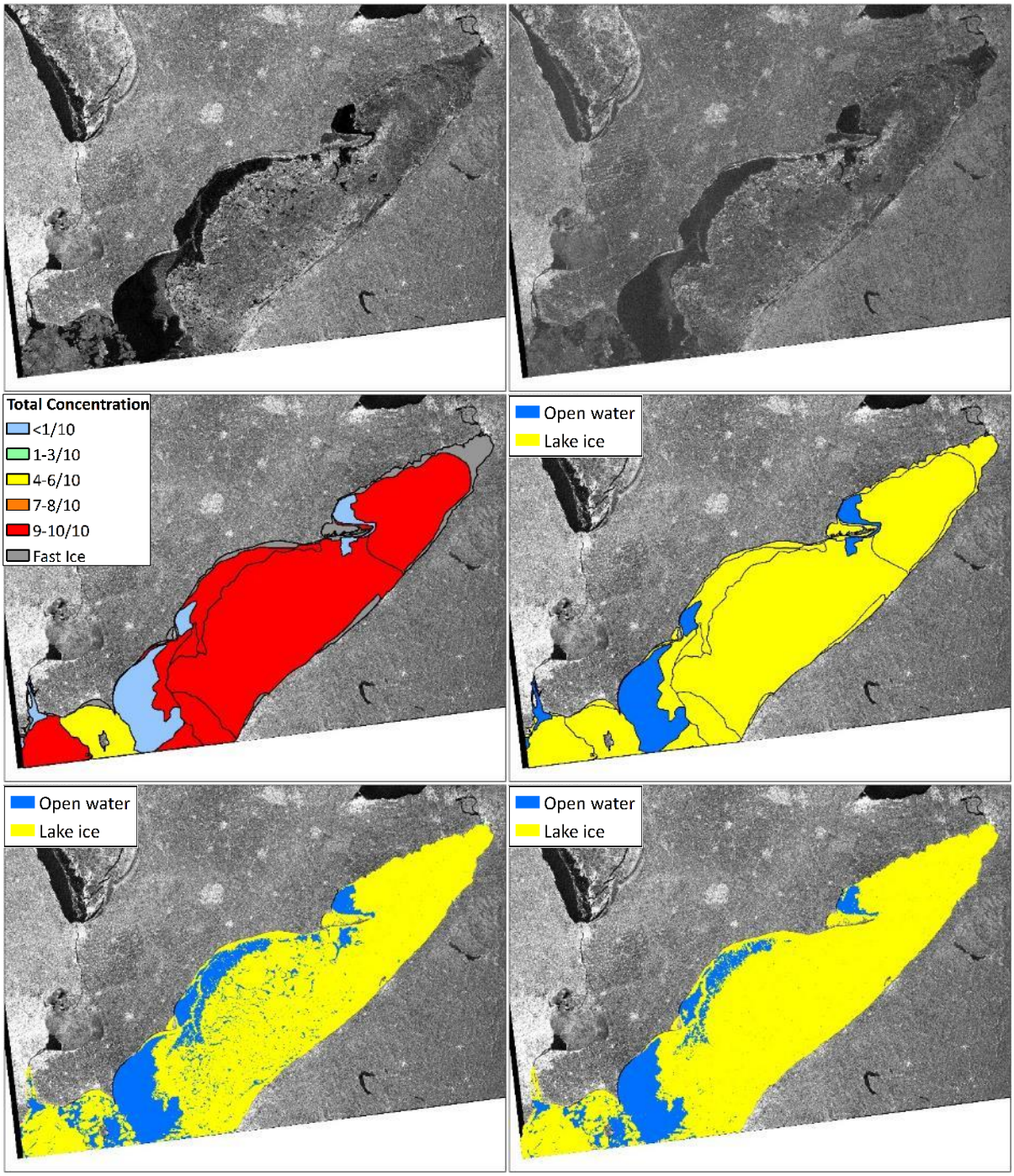
Total Concentration
<1/10
1-3/10
4-6/10
7-8/10
9-10/10
Fast Ice
Open water
Lake ice
Open water
Lake ice
Open water
Lake ice

3/28/2014

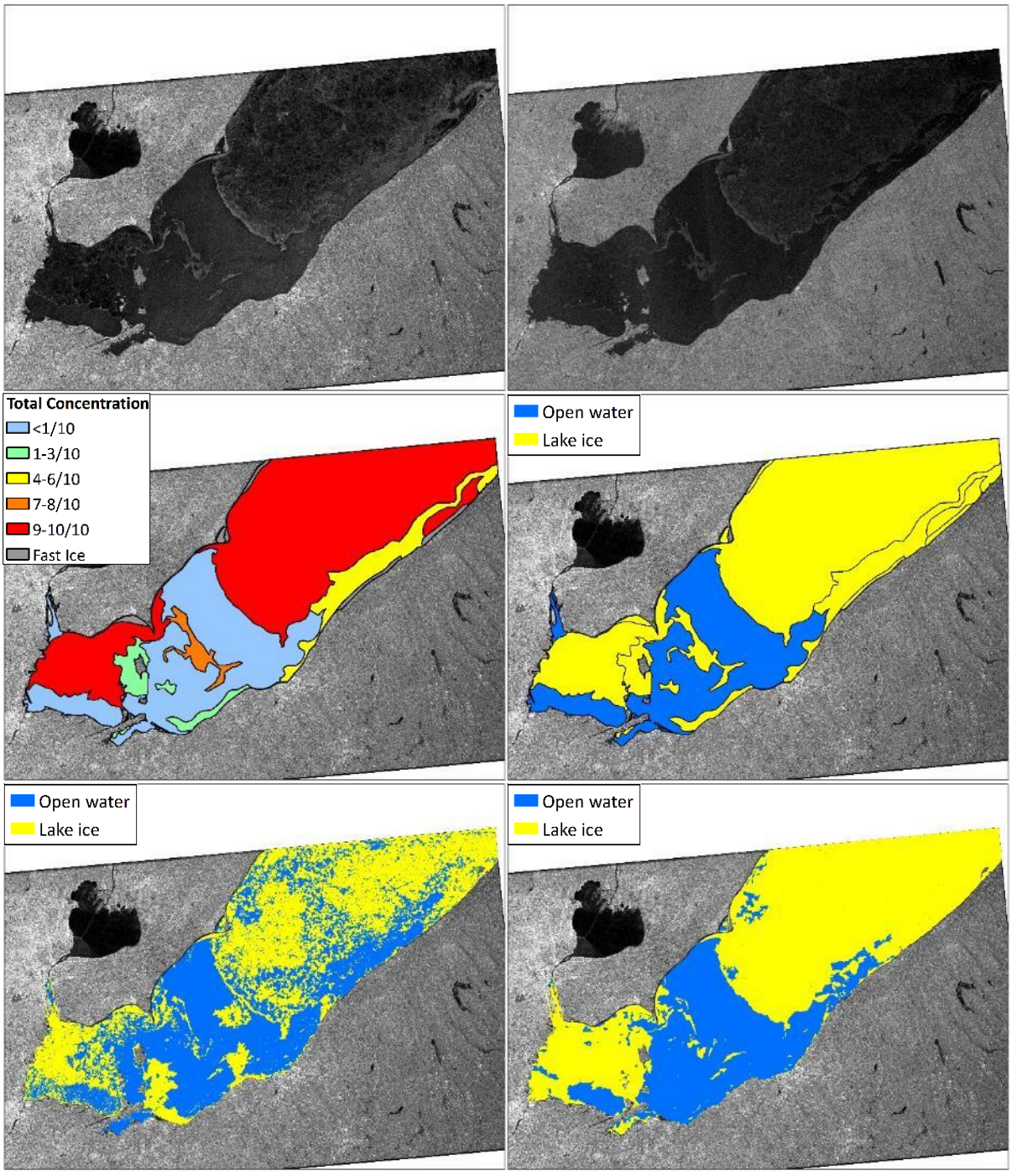
Total Concentration
<1/10
1-3/10
4-6/10
7-8/10
9-10/10
Fast Ice
Open water
Lake ice
Open water
Lake ice
Open water
Lake ice

4/1/2014

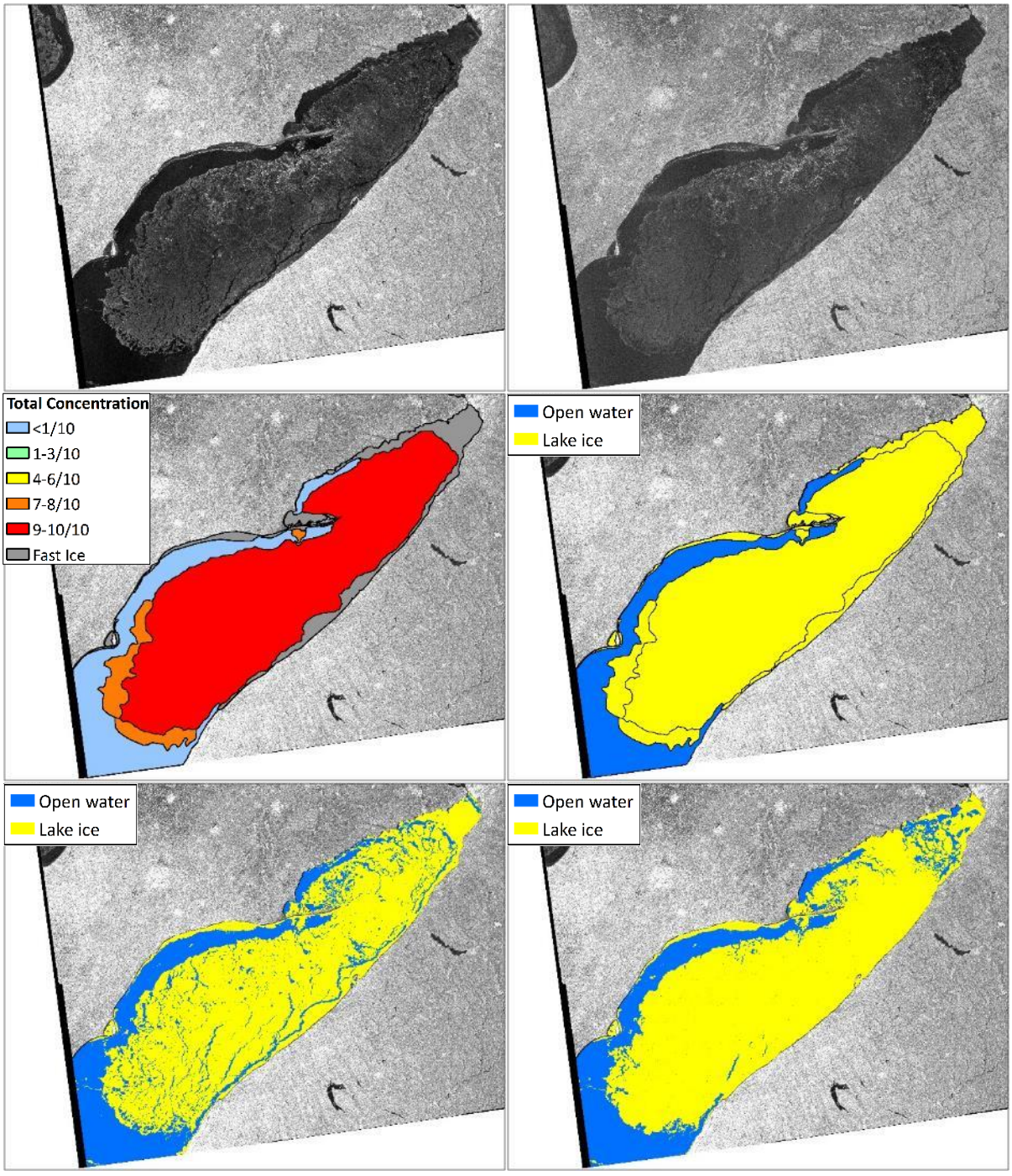
Total Concentration
<1/10
1-3/10
4-6/10
7-8/10
9-10/10
Fast Ice
Open water
Lake ice
Open water
Lake ice
Open water
Lake ice

4/4/2014

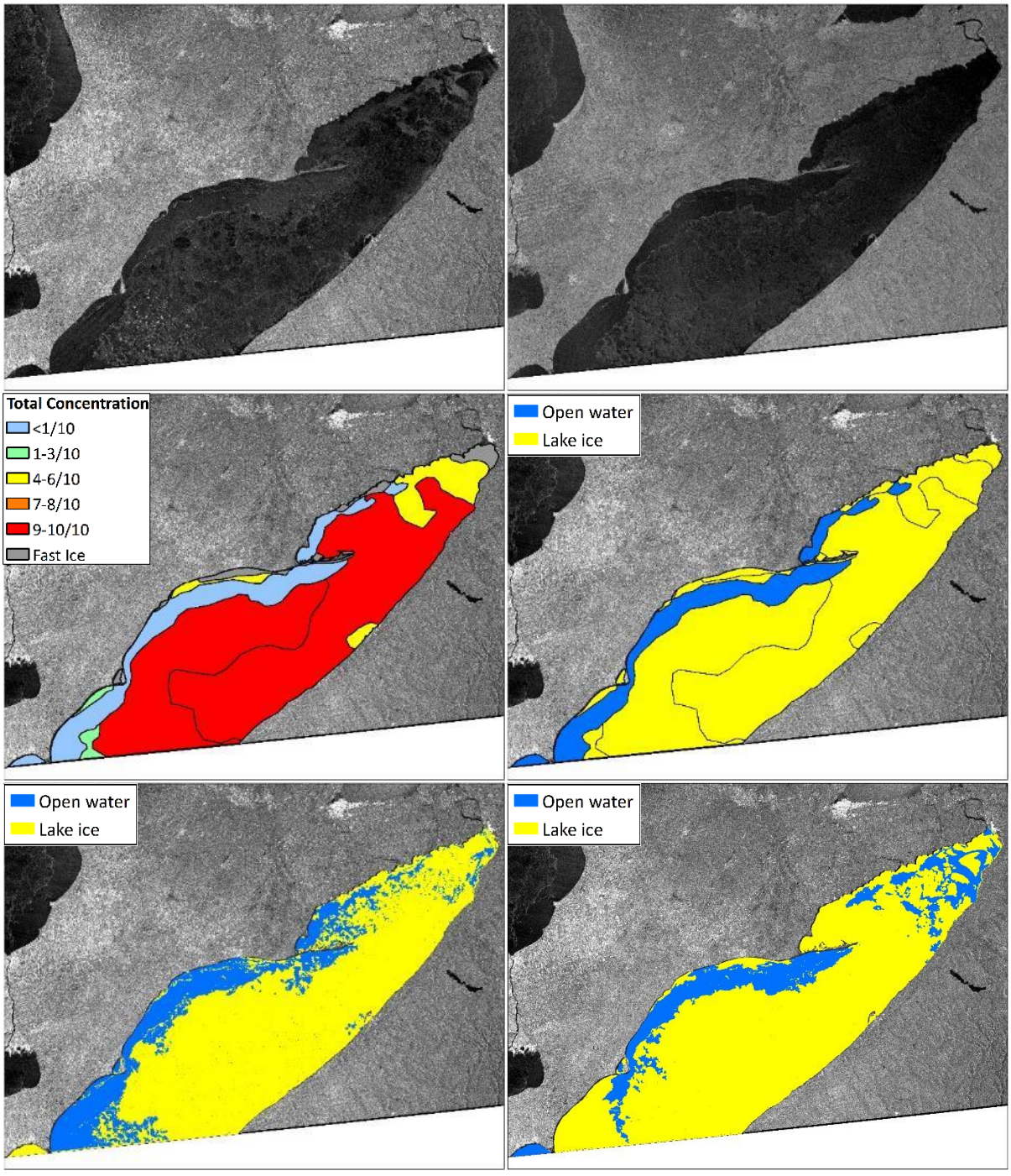
Total Concentration
<1/10
1-3/10
4-6/10
7-8/10
9-10/10
Fast Ice
Open water
Lake ice
Open water
Lake ice
Open water
Lake ice

Appendix B
Ice type classification result images

This appendix list the final ice type classification results for the 26 scenes. The images are displayed in the following format:

Date of SAR scene (M/D/Y)

HH-polarized image	HV-polarized image
Image analysis chart color-coded in stage of development (SD)	Labelled “glocal” IRGS classification using dual-pol images

1/11/2014

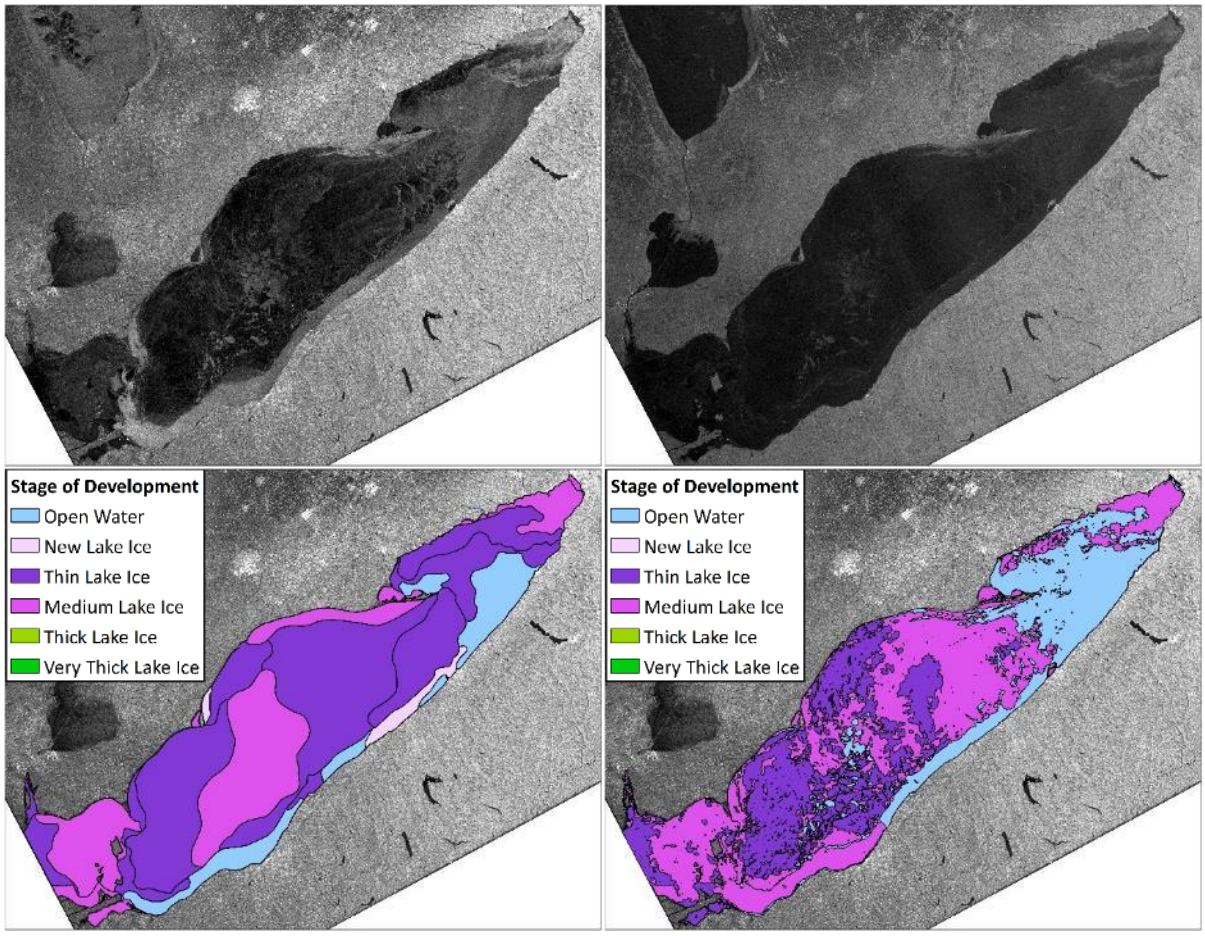
Stage of Development
Open Water
New Lake Ice
Thin Lake Ice
Medium Lake Ice
Thick Lake Ice
Very Thick Lake Ice
Stage of Development
Open Water
New Lake Ice
Thin Lake Ice
Medium Lake Ice
Thick Lake Ice
Very Thick Lake Ice

1/12/2014

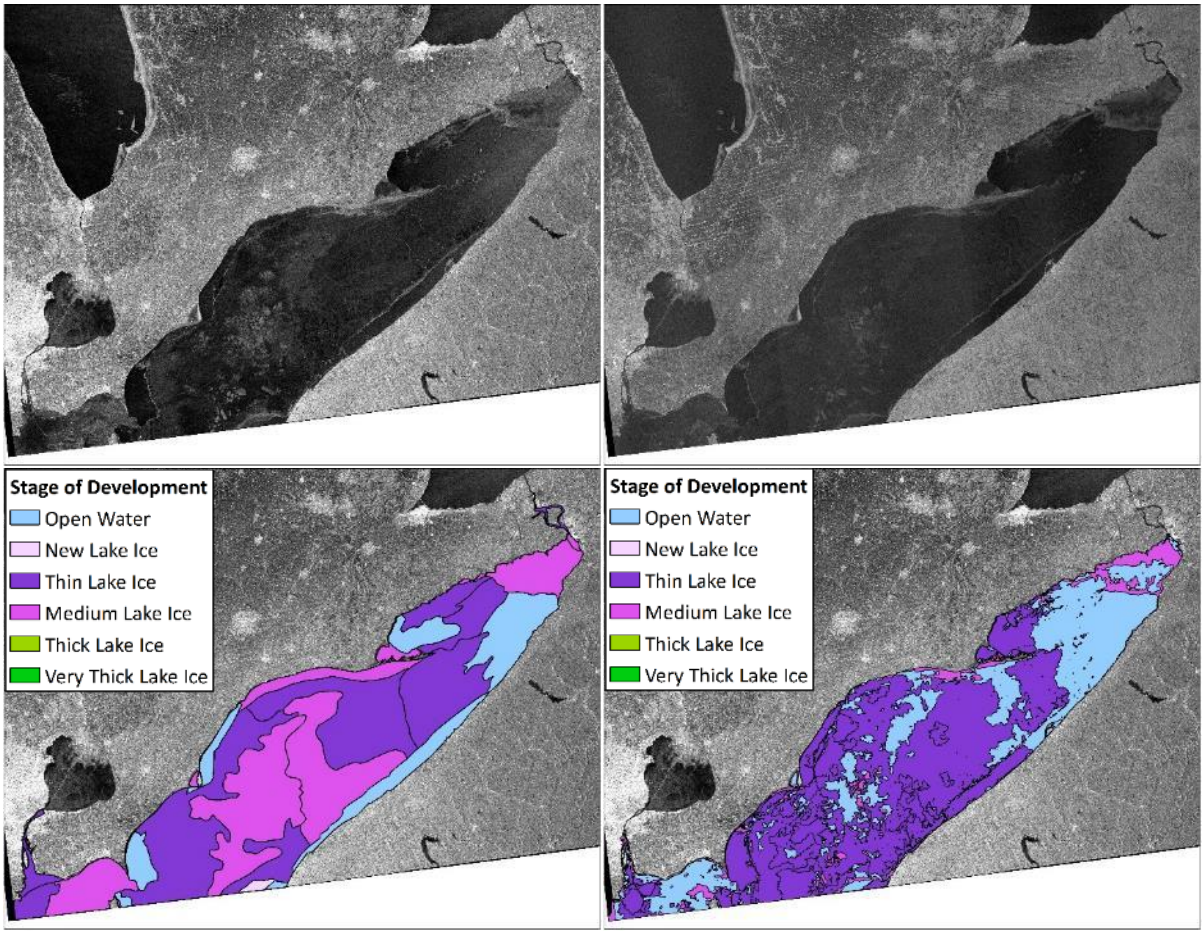
Stage of Development
Open Water
New Lake Ice
Thin Lake Ice
Medium Lake Ice
Thick Lake Ice
Very Thick Lake Ice
Stage of Development
Open Water
New Lake Ice
Thin Lake Ice
Medium Lake Ice
Thick Lake Ice
Very Thick Lake Ice

1/14/2014

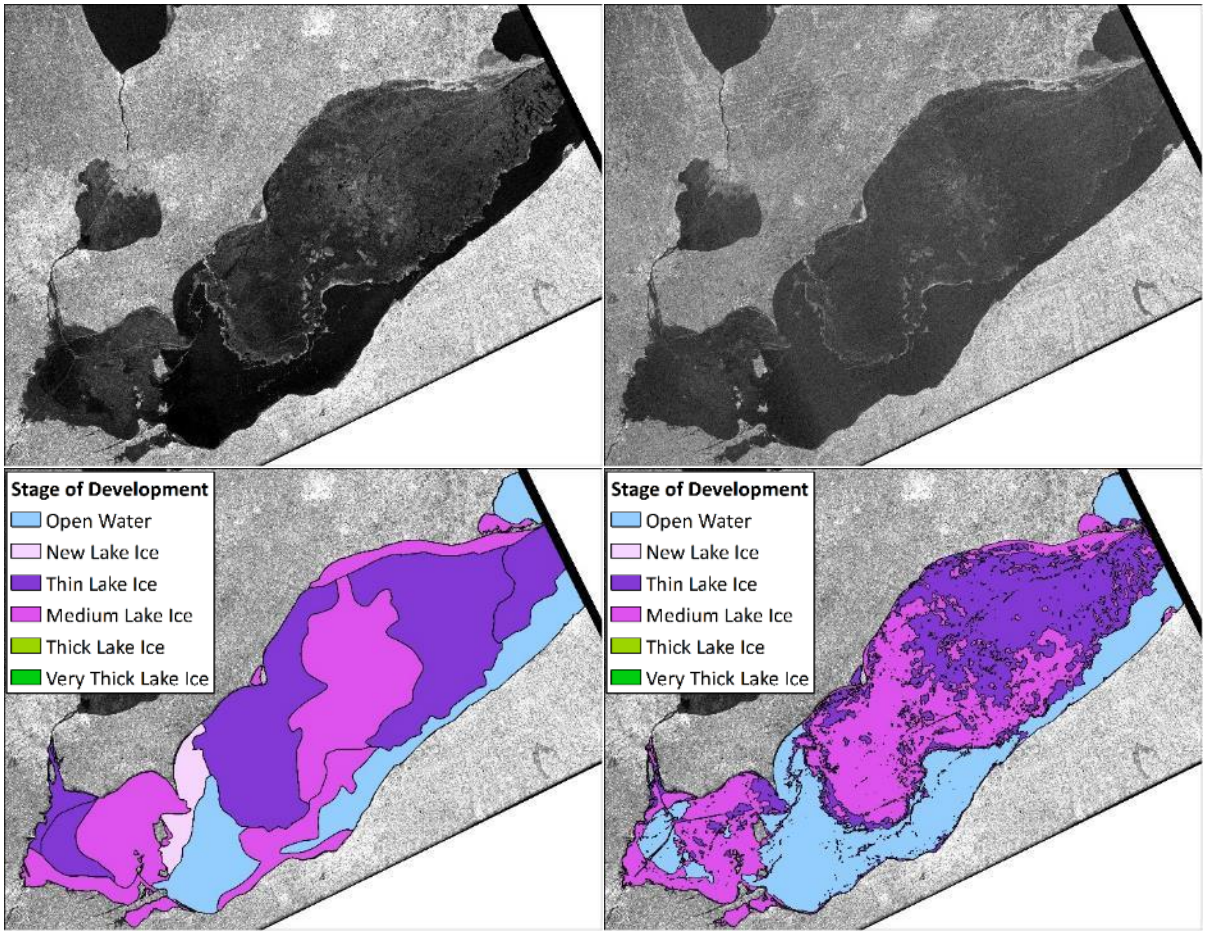
Stage of Development
Open Water
New Lake Ice
Thin Lake Ice
Medium Lake Ice
Thick Lake Ice
Very Thick Lake Ice
Stage of Development
Open Water
New Lake Ice
Thin Lake Ice
Medium Lake Ice
Thick Lake Ice
Very Thick Lake Ice

1/15/2014

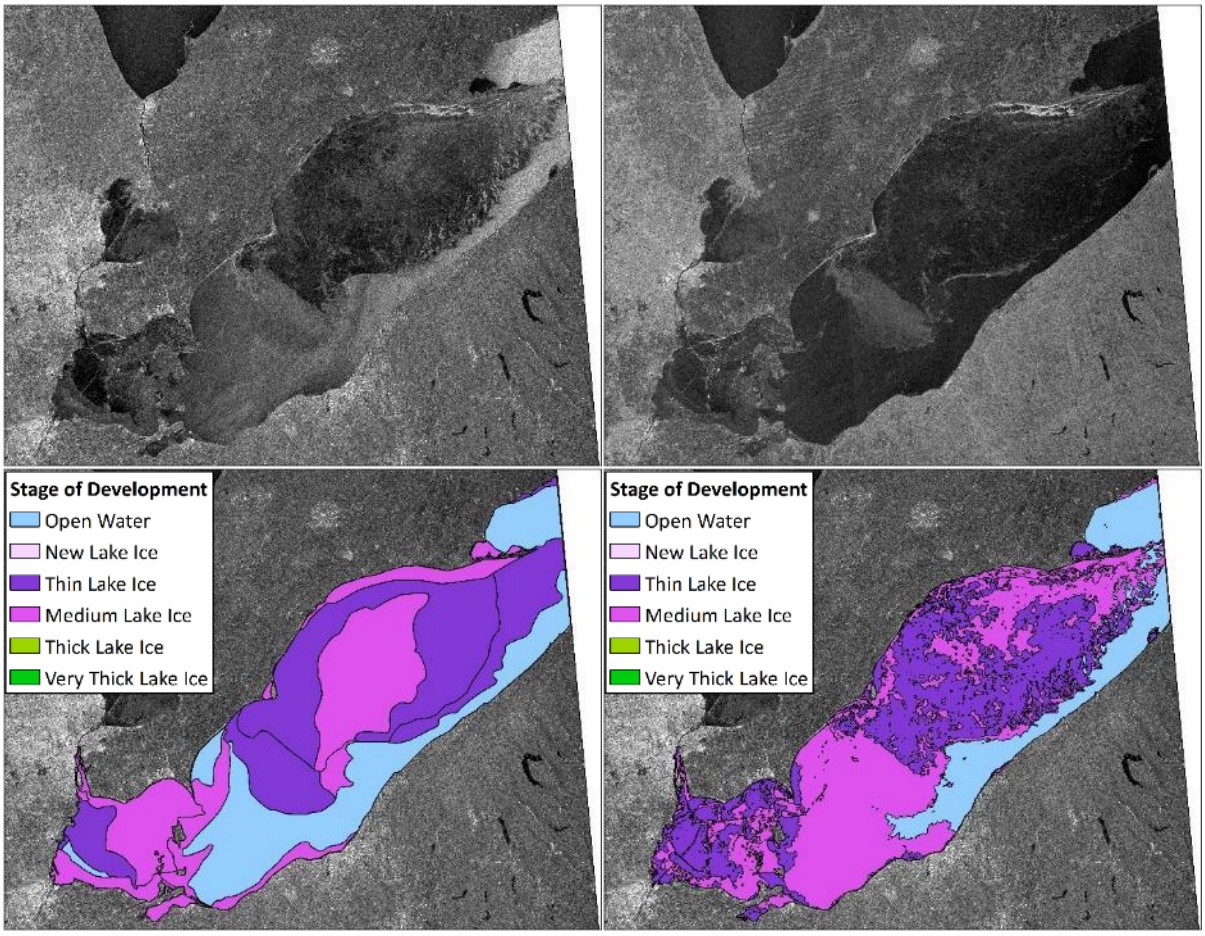
Stage of Development
Open Water
New Lake Ice
Thin Lake Ice
Medium Lake Ice
Thick Lake Ice
Very Thick Lake Ice
Stage of Development
Open Water
New Lake Ice
Thin Lake Ice
Medium Lake Ice
Thick Lake Ice
Very Thick Lake Ice

1/18/2014

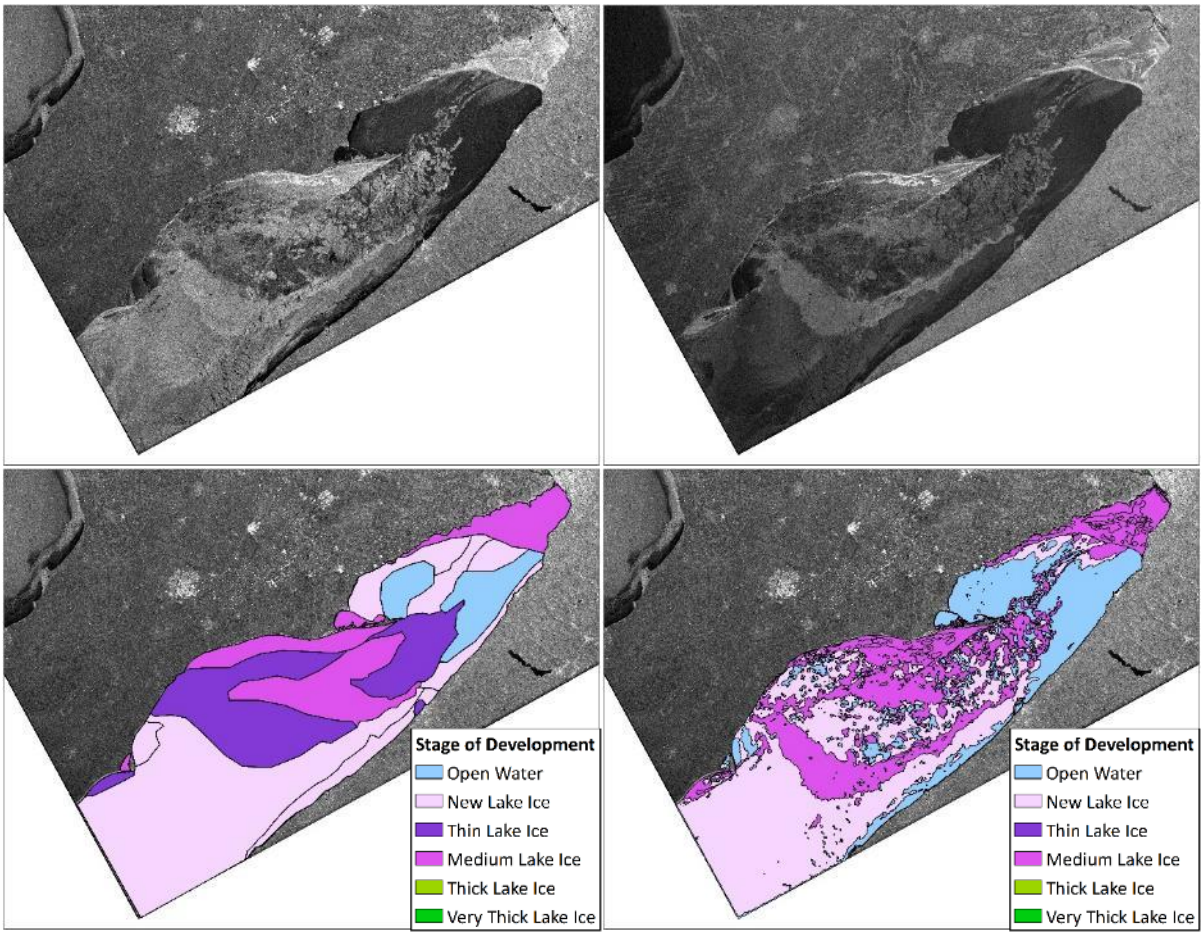
Stage of Development
Open Water
New Lake Ice
Thin Lake Ice
Medium Lake Ice
Thick Lake Ice
Very Thick Lake Ice
Stage of Development
Open Water
New Lake Ice
Thin Lake Ice
Medium Lake Ice
Thick Lake Ice
Very Thick Lake Ice

1/19/2014

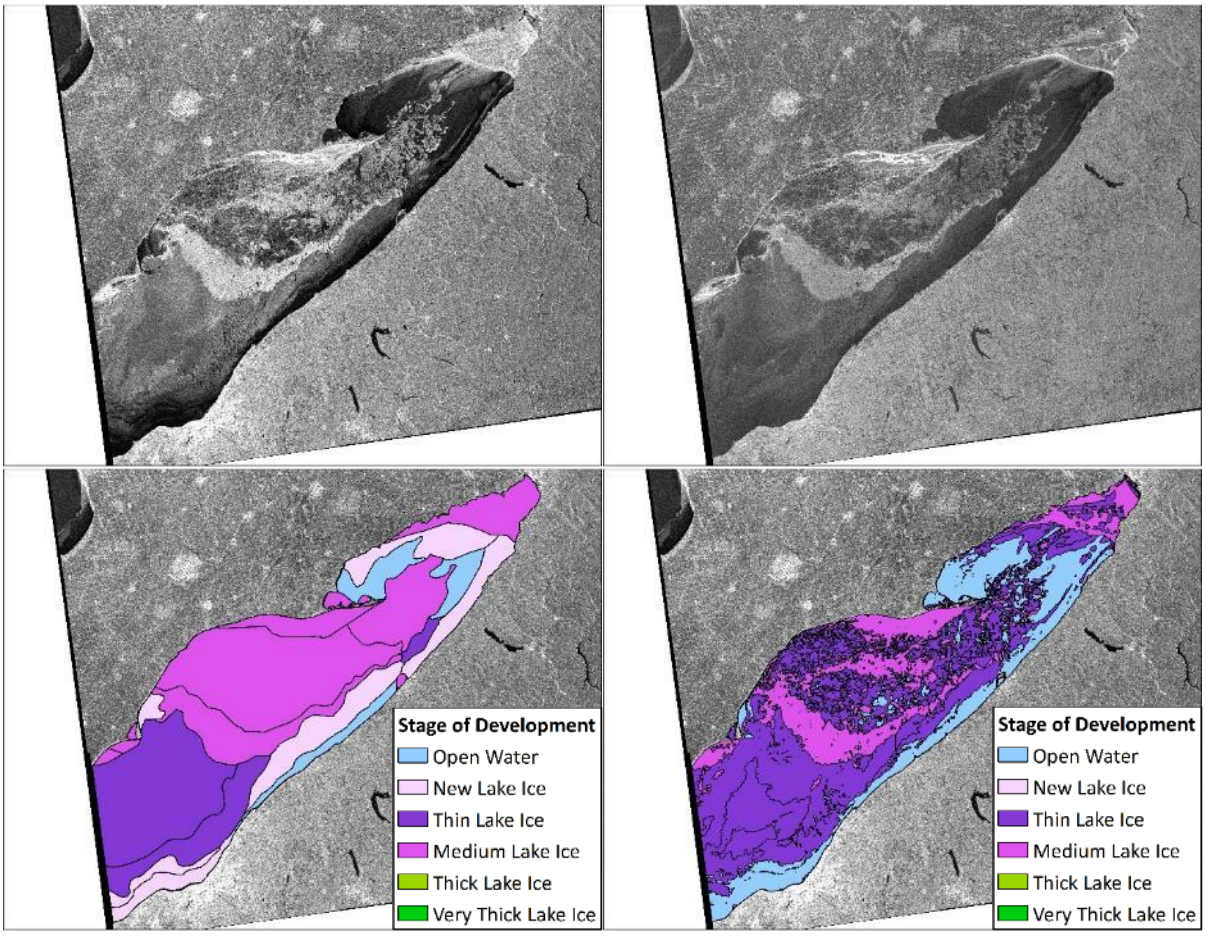
Stage of Development
Open Water
New Lake Ice
Thin Lake Ice
Medium Lake Ice
Thick Lake Ice
Very Thick Lake Ice
Stage of Development
Open Water
New Lake Ice
Thin Lake Ice
Medium Lake Ice
Thick Lake Ice
Very Thick Lake Ice

1/22/2014

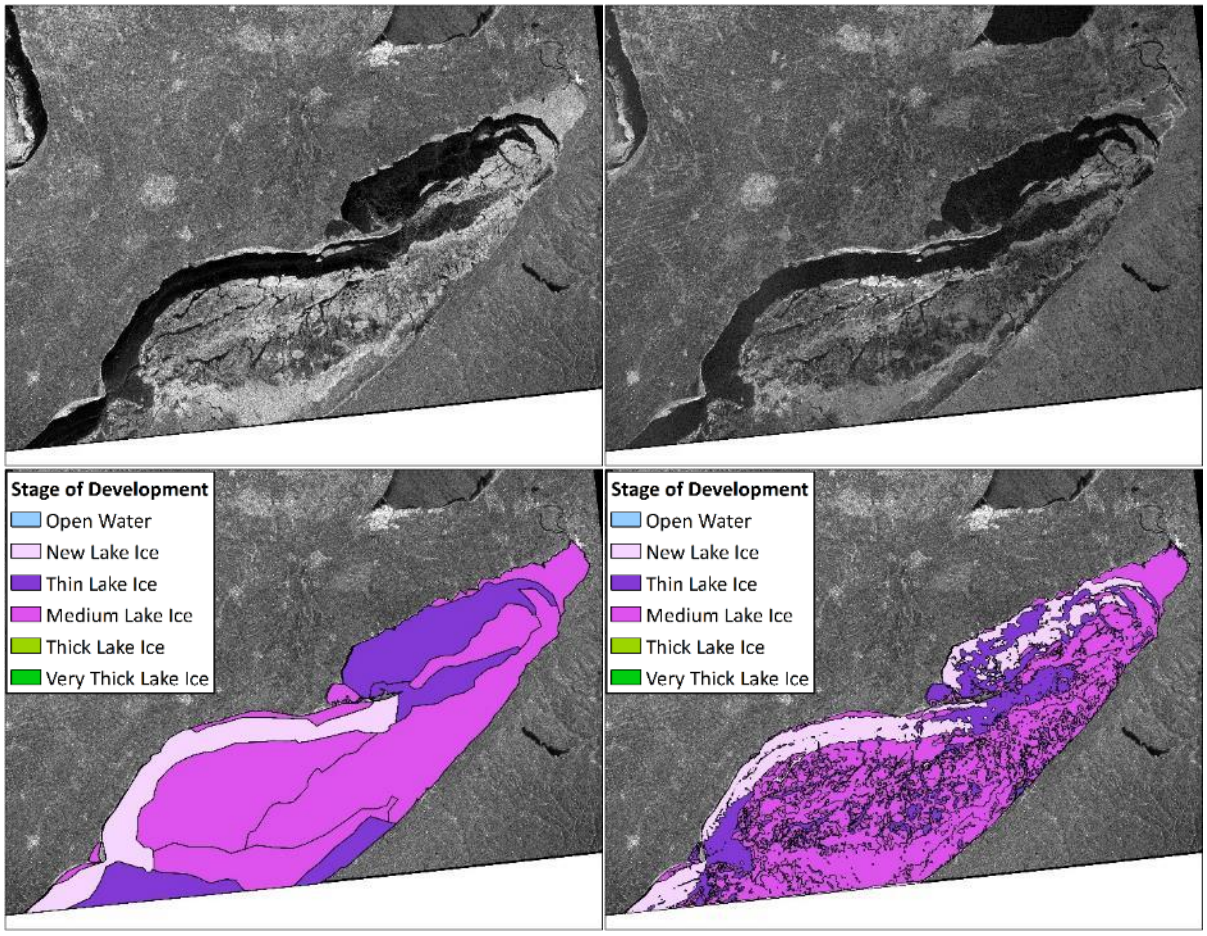
Stage of Development
Open Water
New Lake Ice
Thin Lake Ice
Medium Lake Ice
Thick Lake Ice
Very Thick Lake Ice
Stage of Development
Open Water
New Lake Ice
Thin Lake Ice
Medium Lake Ice
Thick Lake Ice
Very Thick Lake Ice

1/28/2014

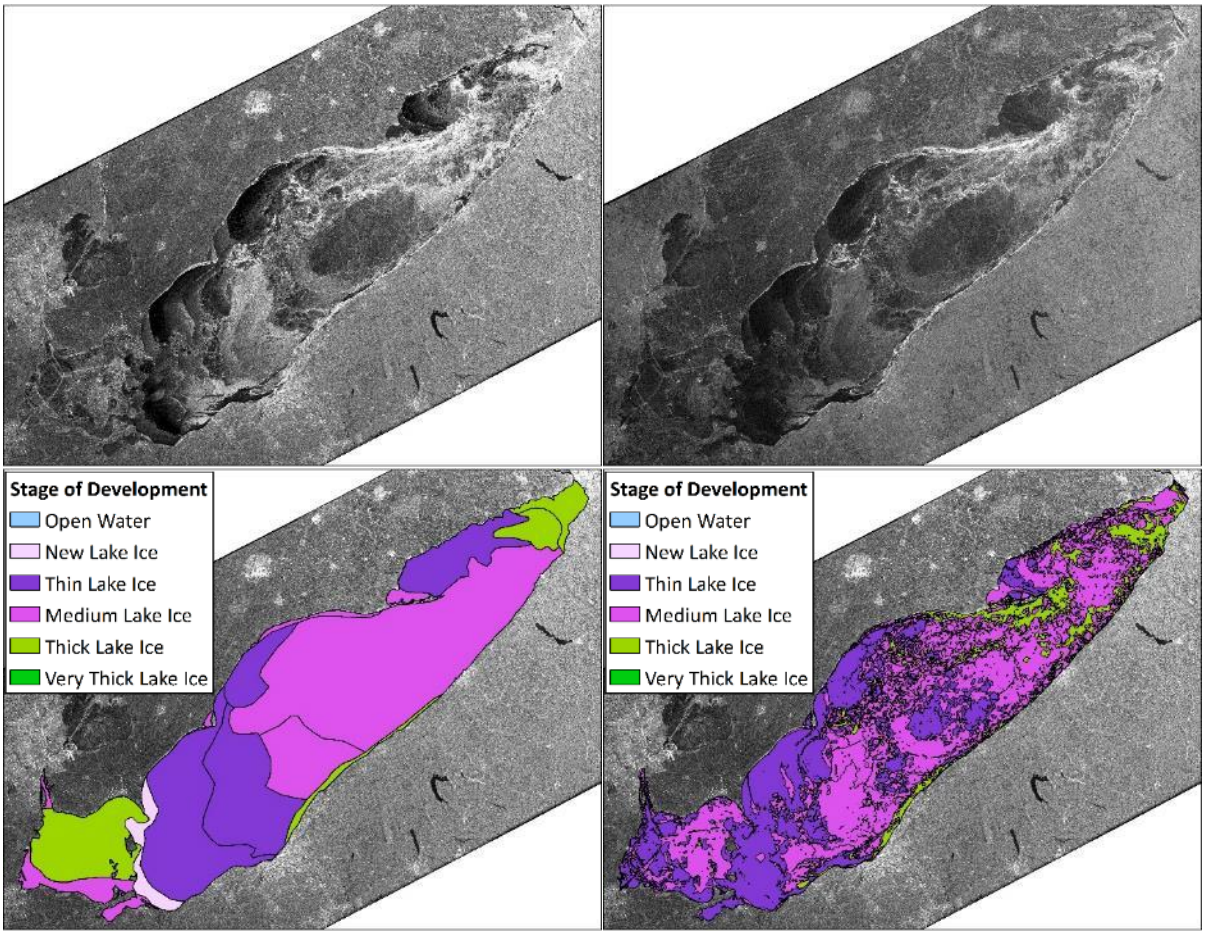
Stage of Development
Open Water
New Lake Ice
Thin Lake Ice
Medium Lake Ice
Thick Lake Ice
Very Thick Lake Ice
Stage of Development
Open Water
New Lake Ice
Thin Lake Ice
Medium Lake Ice
Thick Lake Ice
Very Thick Lake Ice

1/29/2014

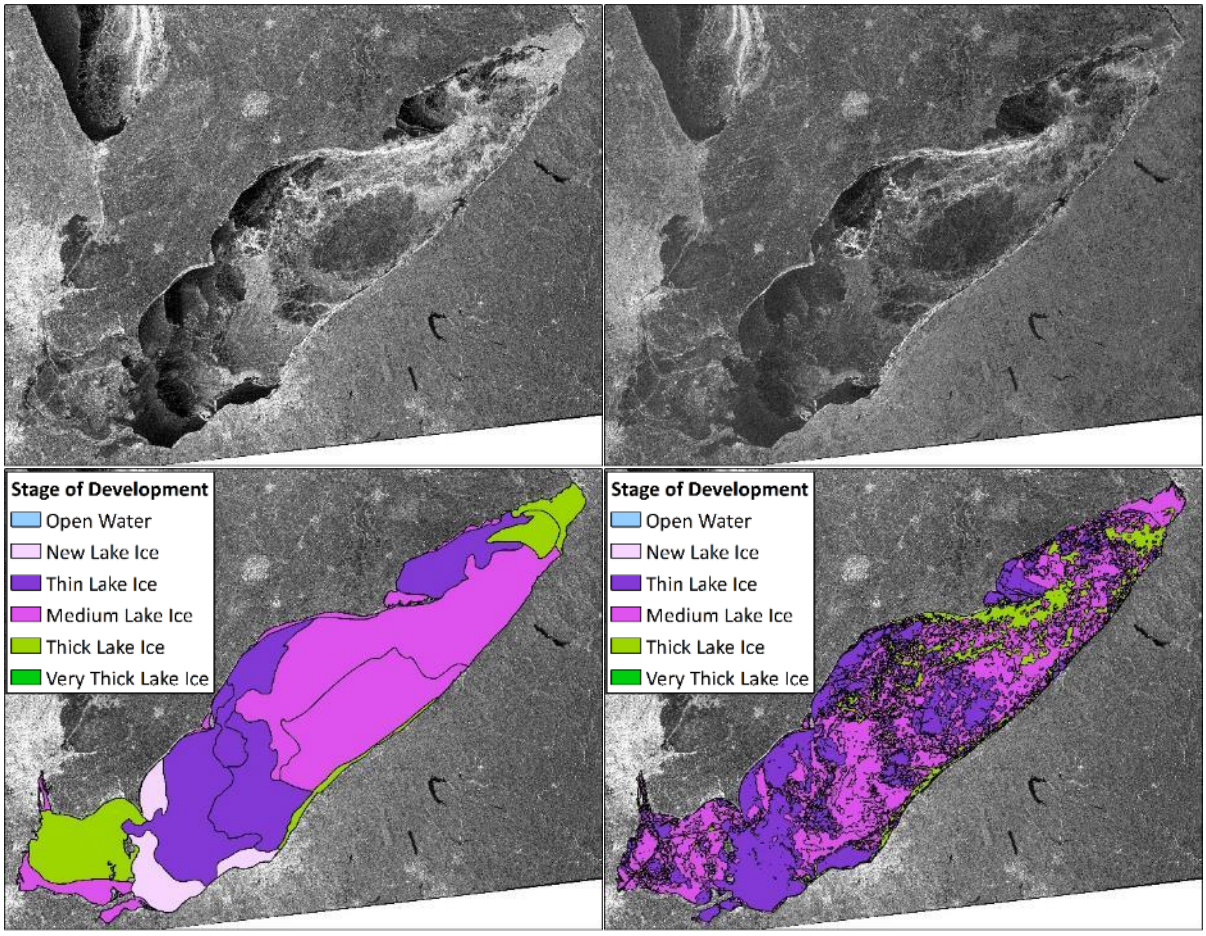
Stage of Development
Open Water
New Lake Ice
Thin Lake Ice
Medium Lake Ice
Thick Lake Ice
Very Thick Lake Ice
Stage of Development
Open Water
New Lake Ice
Thin Lake Ice
Medium Lake Ice
Thick Lake Ice
Very Thick Lake Ice

2/4/2014

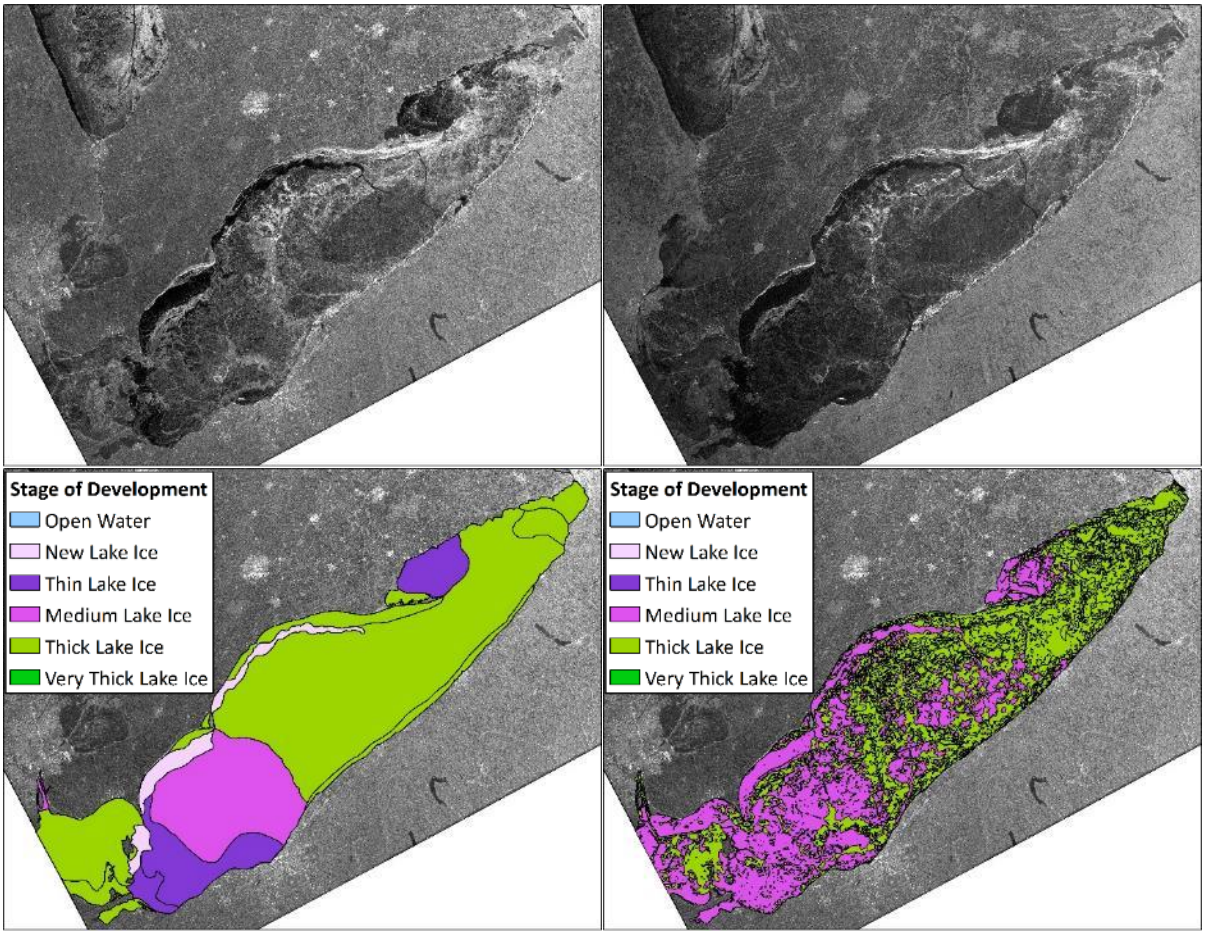
Stage of Development
Open Water
New Lake Ice
Thin Lake Ice
Medium Lake Ice
Thick Lake Ice
Very Thick Lake Ice
Stage of Development
Open Water
New Lake Ice
Thin Lake Ice
Medium Lake Ice
Thick Lake Ice
Very Thick Lake Ice

2/12/2014

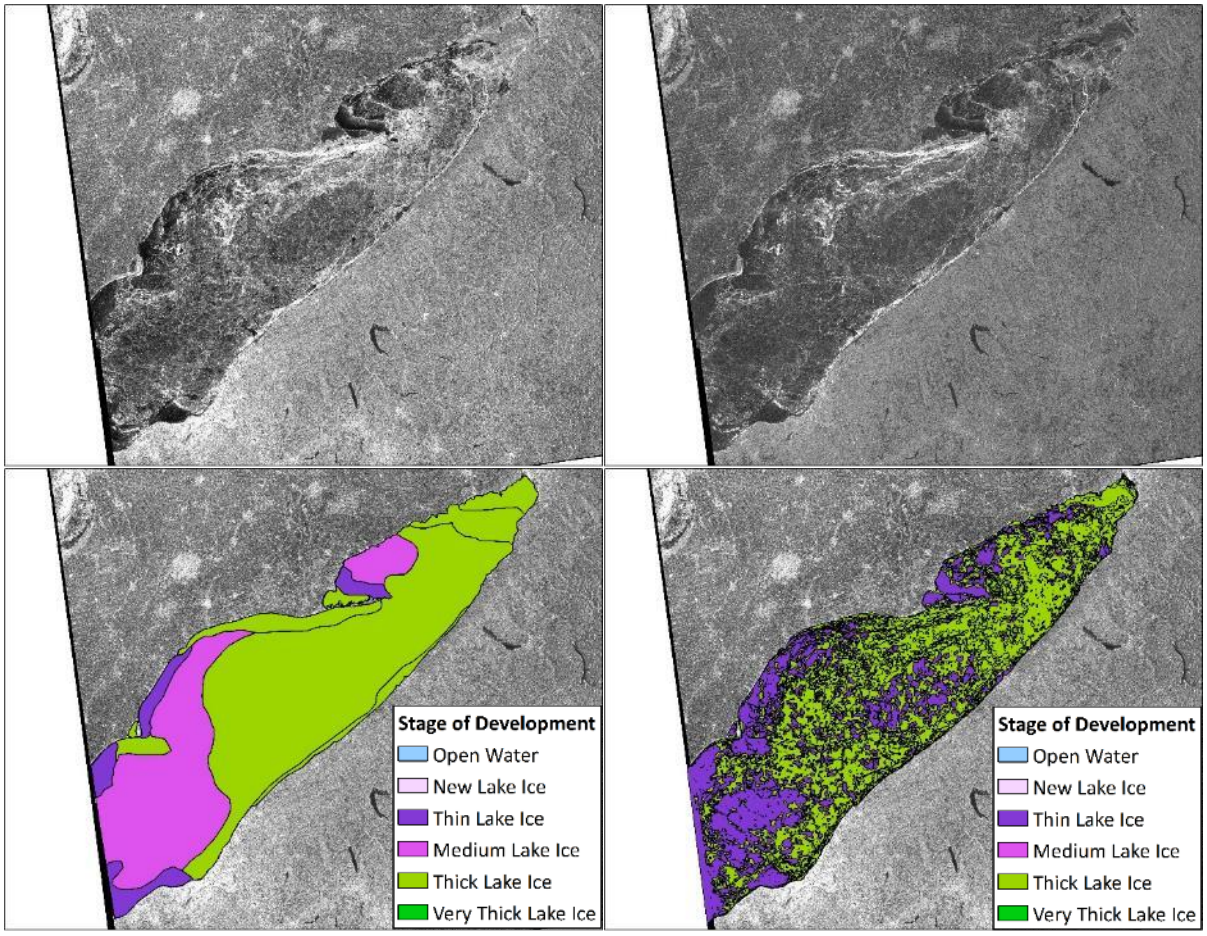
Stage of Development
Open Water
New Lake Ice
Thin Lake Ice
Medium Lake Ice
Thick Lake Ice
Very Thick Lake Ice
Stage of Development
Open Water
New Lake Ice
Thin Lake Ice
Medium Lake Ice
Thick Lake Ice
Very Thick Lake Ice

2/14/2014

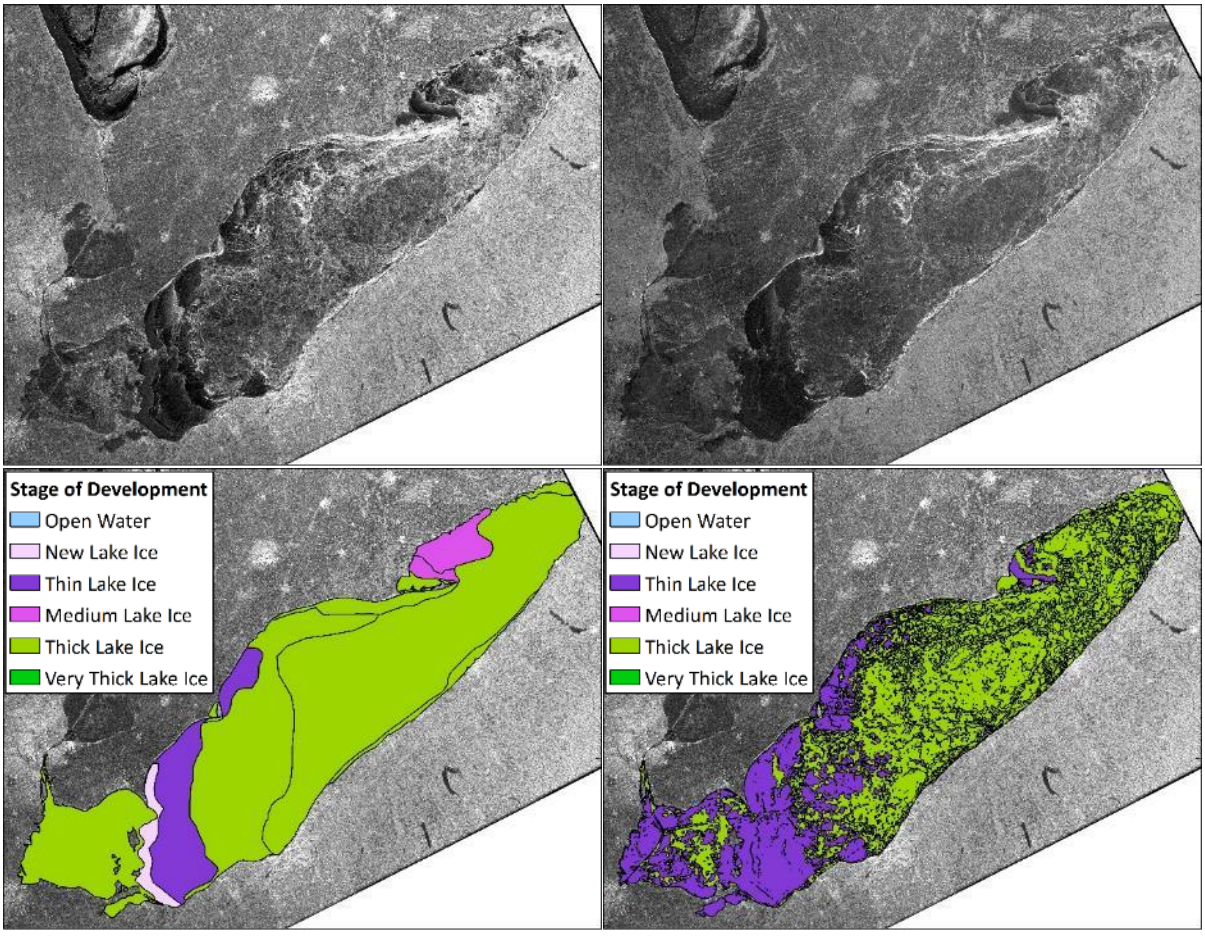
Stage of Development
Open Water
New Lake Ice
Thin Lake Ice
Medium Lake Ice
Thick Lake Ice
Very Thick Lake Ice
Stage of Development
Open Water
New Lake Ice
Thin Lake Ice
Medium Lake Ice
Thick Lake Ice
Very Thick Lake Ice

2/21/2014

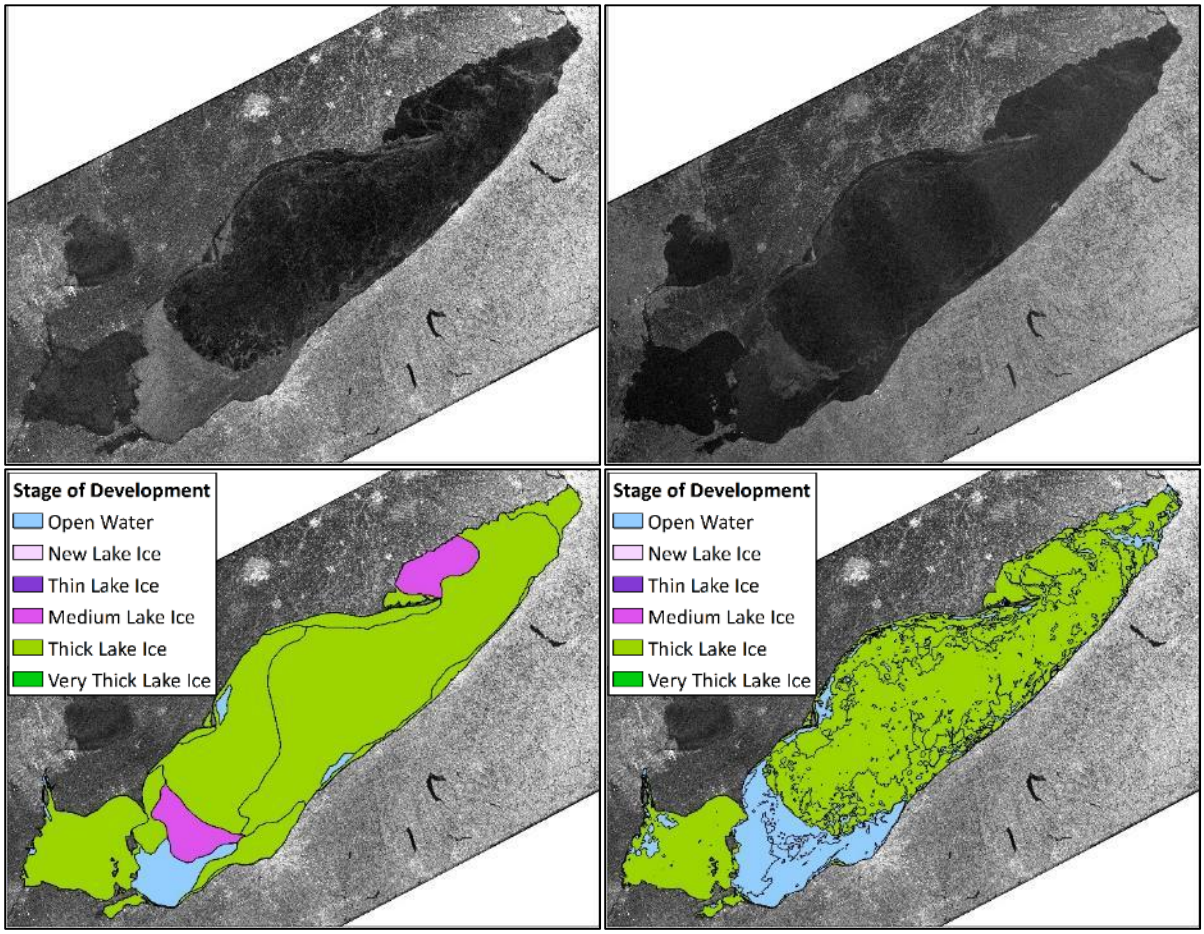
Stage of Development
Open Water
New Lake Ice
Thin Lake Ice
Medium Lake Ice
Thick Lake Ice
Very Thick Lake Ice
Stage of Development
Open Water
New Lake Ice
Thin Lake Ice
Medium Lake Ice
Thick Lake Ice
Very Thick Lake Ice

2/22/2014

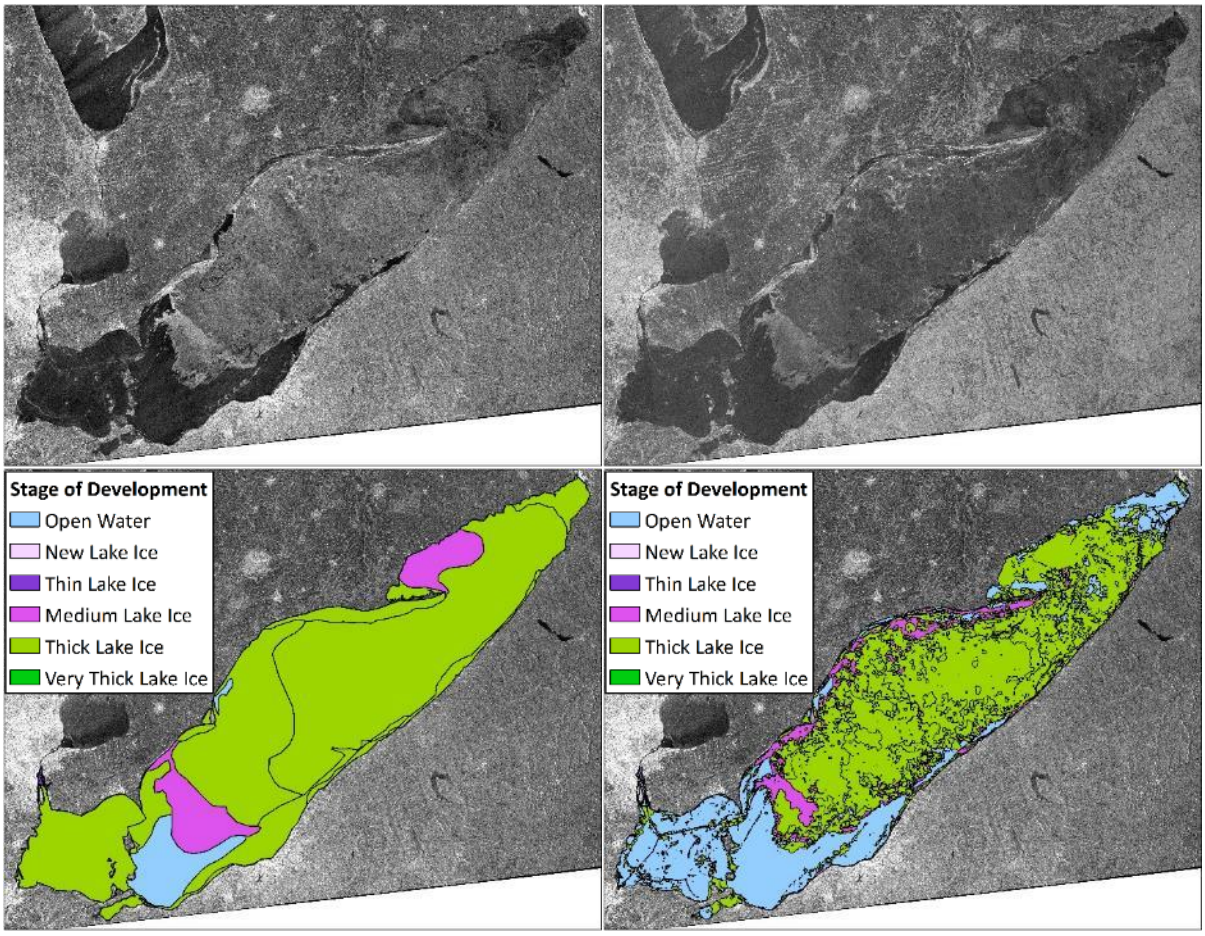
Stage of Development
Open Water
New Lake Ice
Thin Lake Ice
Medium Lake Ice
Thick Lake Ice
Very Thick Lake Ice
Stage of Development
Open Water
New Lake Ice
Thin Lake Ice
Medium Lake Ice
Thick Lake Ice
Very Thick Lake Ice

2/25/2014

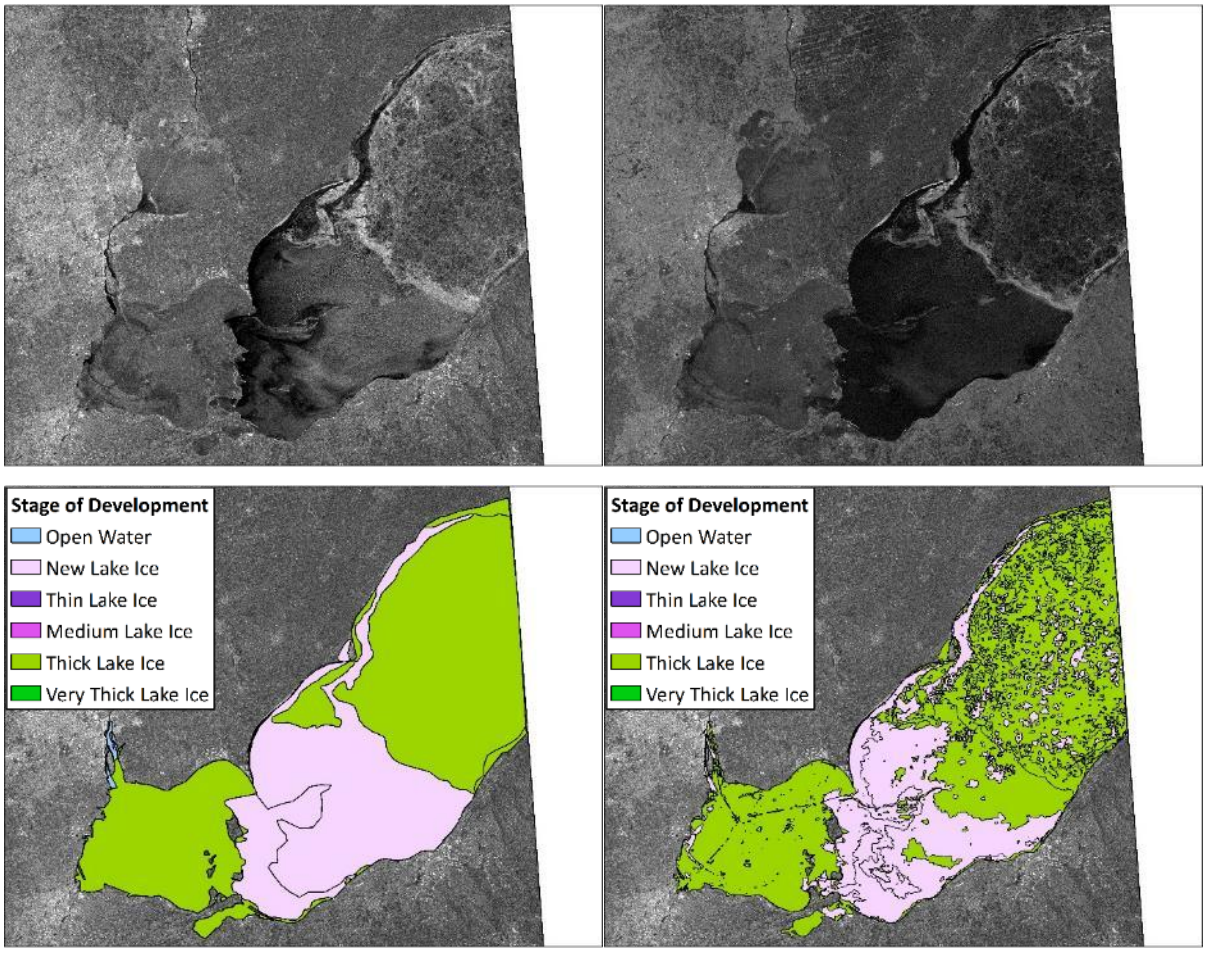
Stage of Development
Open Water
New Lake Ice
Thin Lake Ice
Medium Lake Ice
Thick Lake Ice
Very Thick Lake Ice
Stage of Development
Open Water
New Lake Ice
Thin Lake Ice
Medium Lake Ice
Thick Lake Ice
Very Thick Lake Ice

3/1/2014

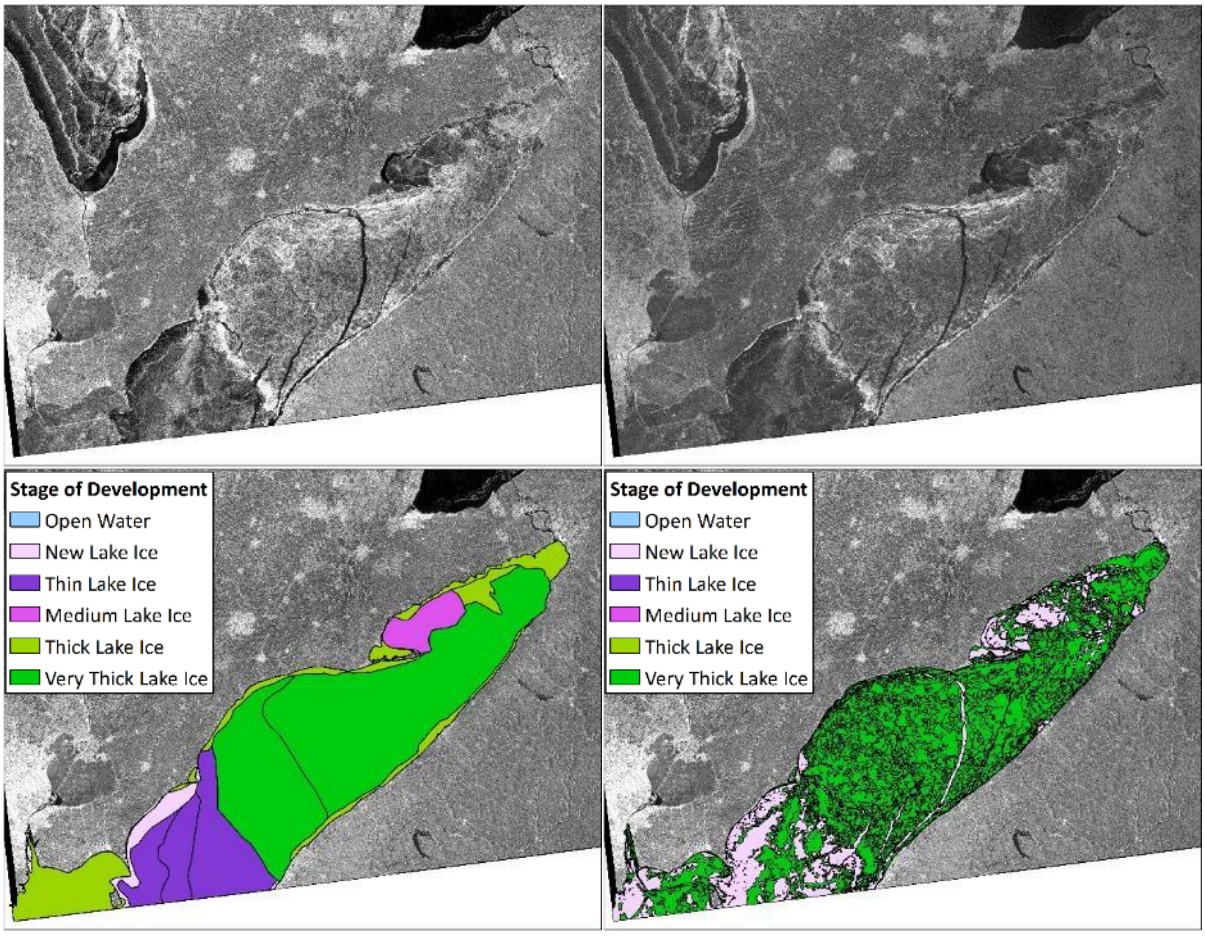
Stage of Development
Open Water
New Lake Ice
Thin Lake Ice
Medium Lake Ice
Thick Lake Ice
Very Thick Lake Ice
Stage of Development
Open Water
New Lake Ice
Thin Lake Ice
Medium Lake Ice
Thick Lake Ice
Very Thick Lake Ice

3/3/2014

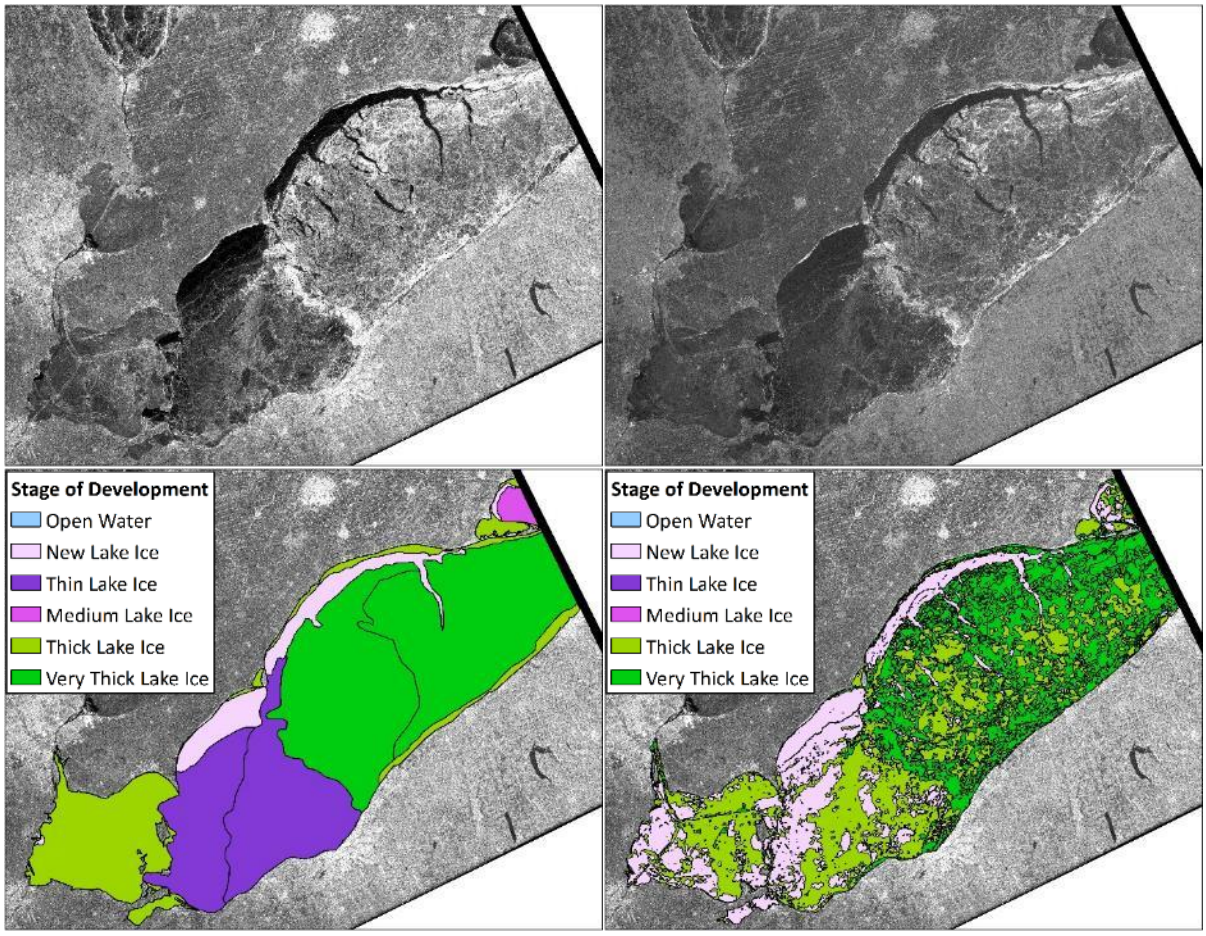
Stage of Development
Open Water
New Lake Ice
Thin Lake Ice
Medium Lake Ice
Thick Lake Ice
Very Thick Lake Ice
Stage of Development
Open Water
New Lake Ice
Thin Lake Ice
Medium Lake Ice
Thick Lake Ice
Very Thick Lake Ice

3/4/2014

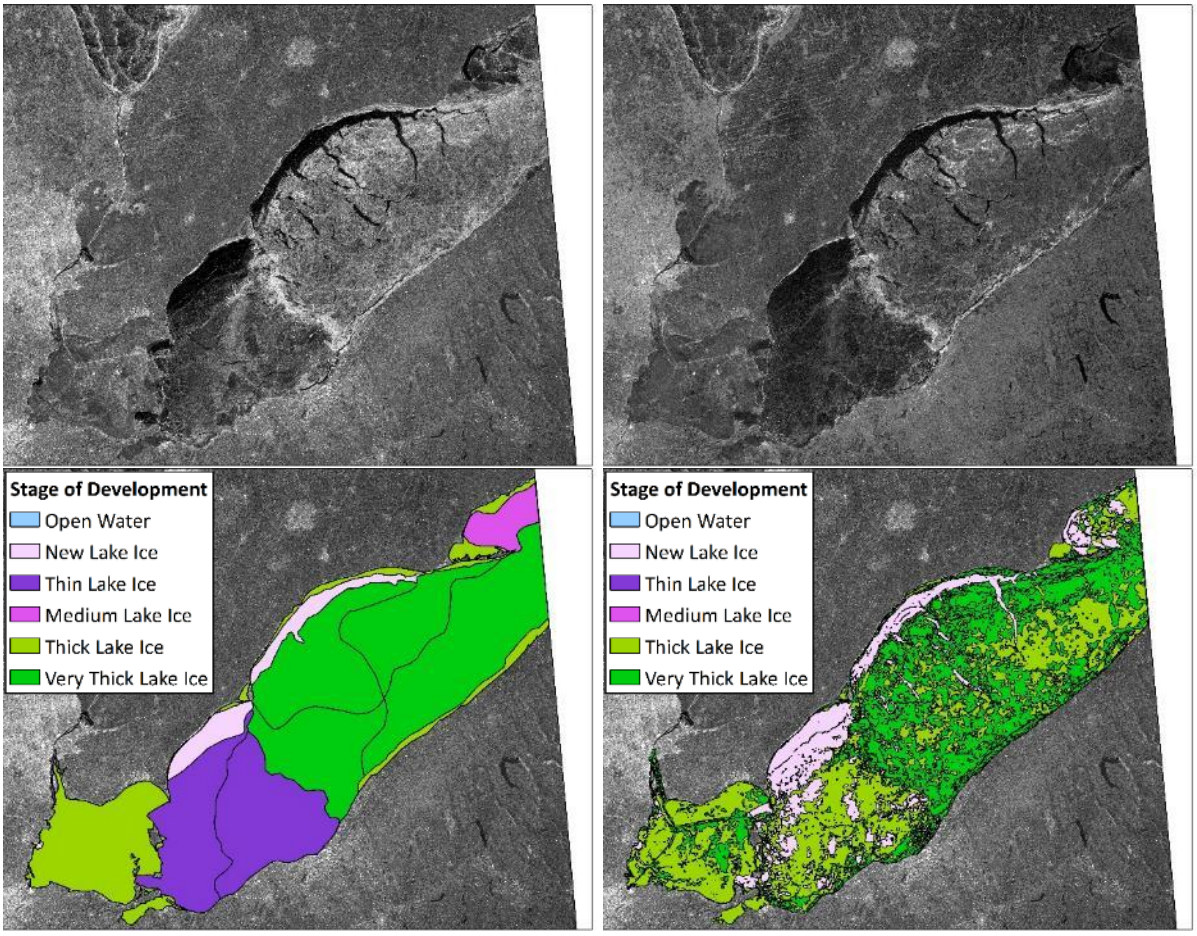
Stage of Development
Open Water
New Lake Ice
Thin Lake Ice
Medium Lake Ice
Thick Lake Ice
Very Thick Lake Ice
Stage of Development
Open Water
New Lake Ice
Thin Lake Ice
Medium Lake Ice
Thick Lake Ice
Very Thick Lake Ice

3/7/2014

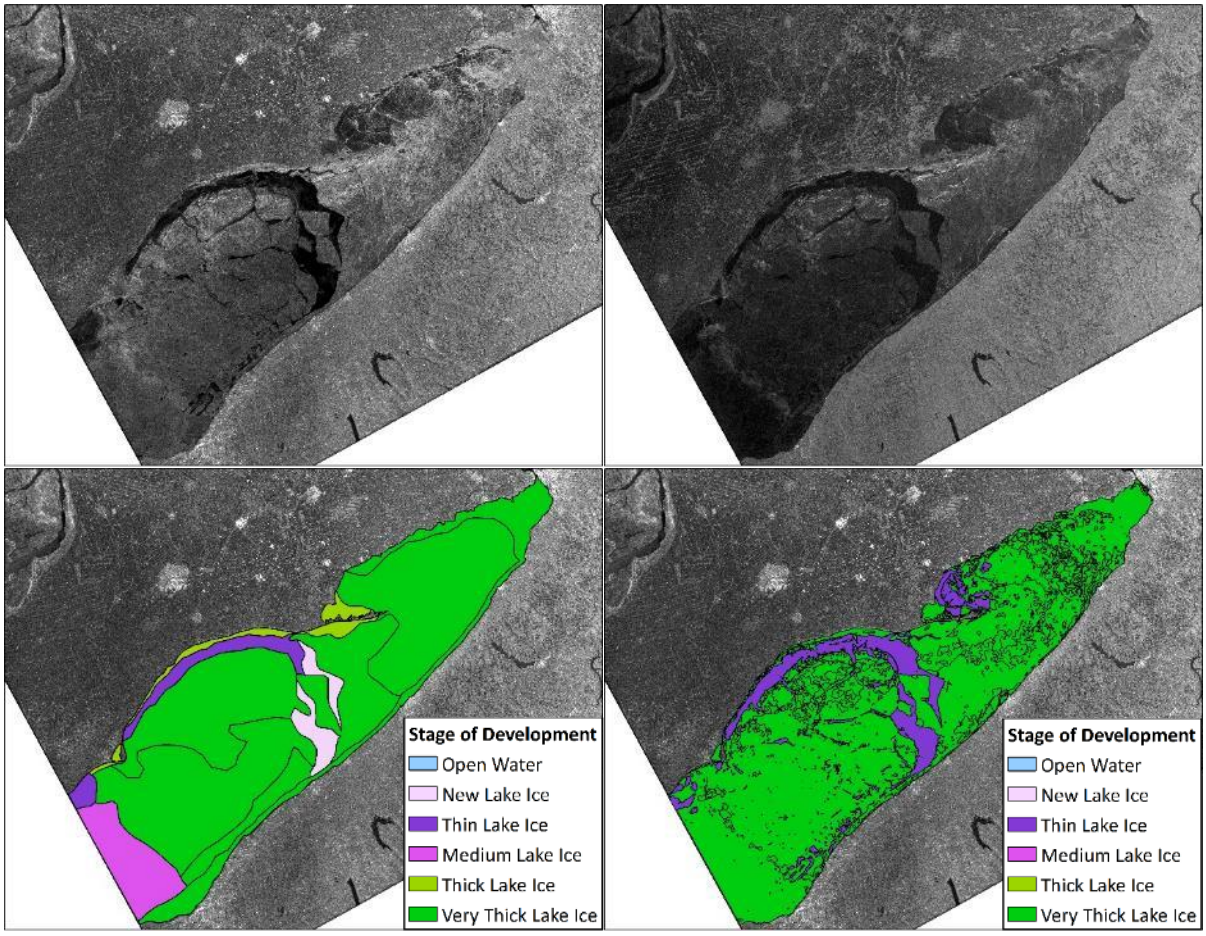
Stage of Development
Open Water
New Lake Ice
Thin Lake Ice
Medium Lake Ice
Thick Lake Ice
Very Thick Lake Ice
Stage of Development
Open Water
New Lake Ice
Thin Lake Ice
Medium Lake Ice
Thick Lake Ice
Very Thick Lake Ice

3/18/2014

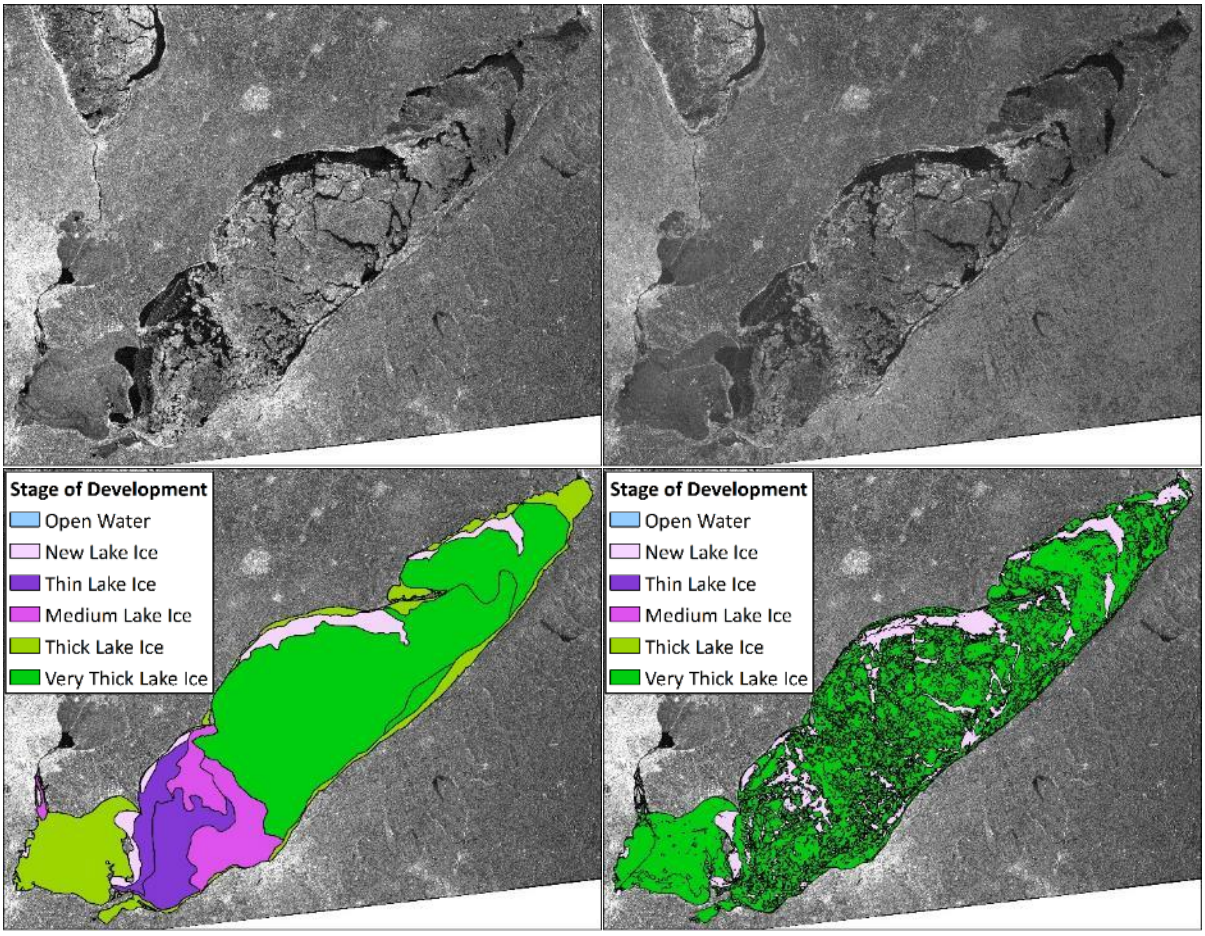
Stage of Development
Open Water
New Lake Ice
Thin Lake Ice
Medium Lake Ice
Thick Lake Ice
Very Thick Lake Ice
Stage of Development
Open Water
New Lake Ice
Thin Lake Ice
Medium Lake Ice
Thick Lake Ice
Very Thick Lake Ice

3/20/2014

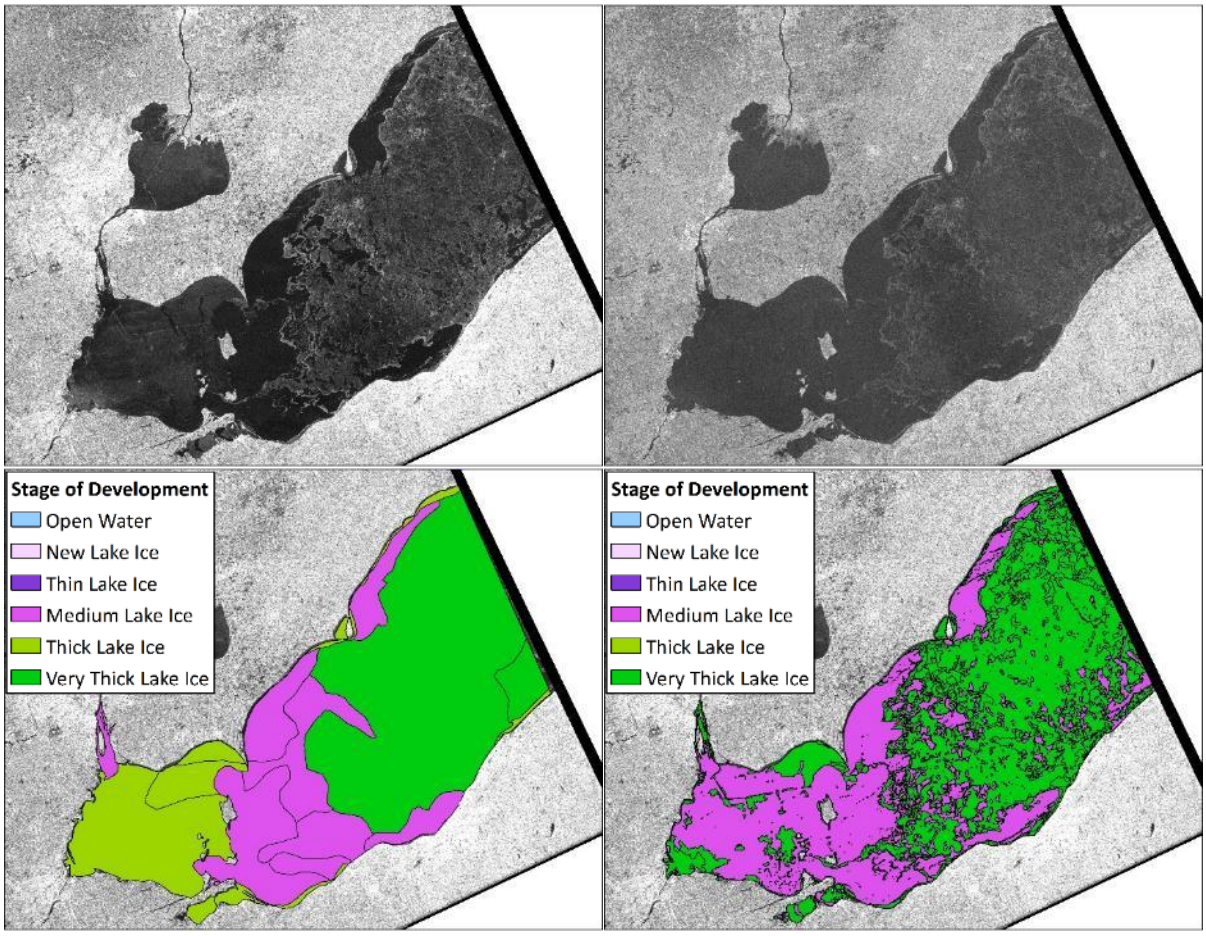
Stage of Development
Open Water
New Lake Ice
Thin Lake Ice
Medium Lake Ice
Thick Lake Ice
Very Thick Lake Ice
Stage of Development
Open Water
New Lake Ice
Thin Lake Ice
Medium Lake Ice
Thick Lake Ice
Very Thick Lake Ice

3/21/2014

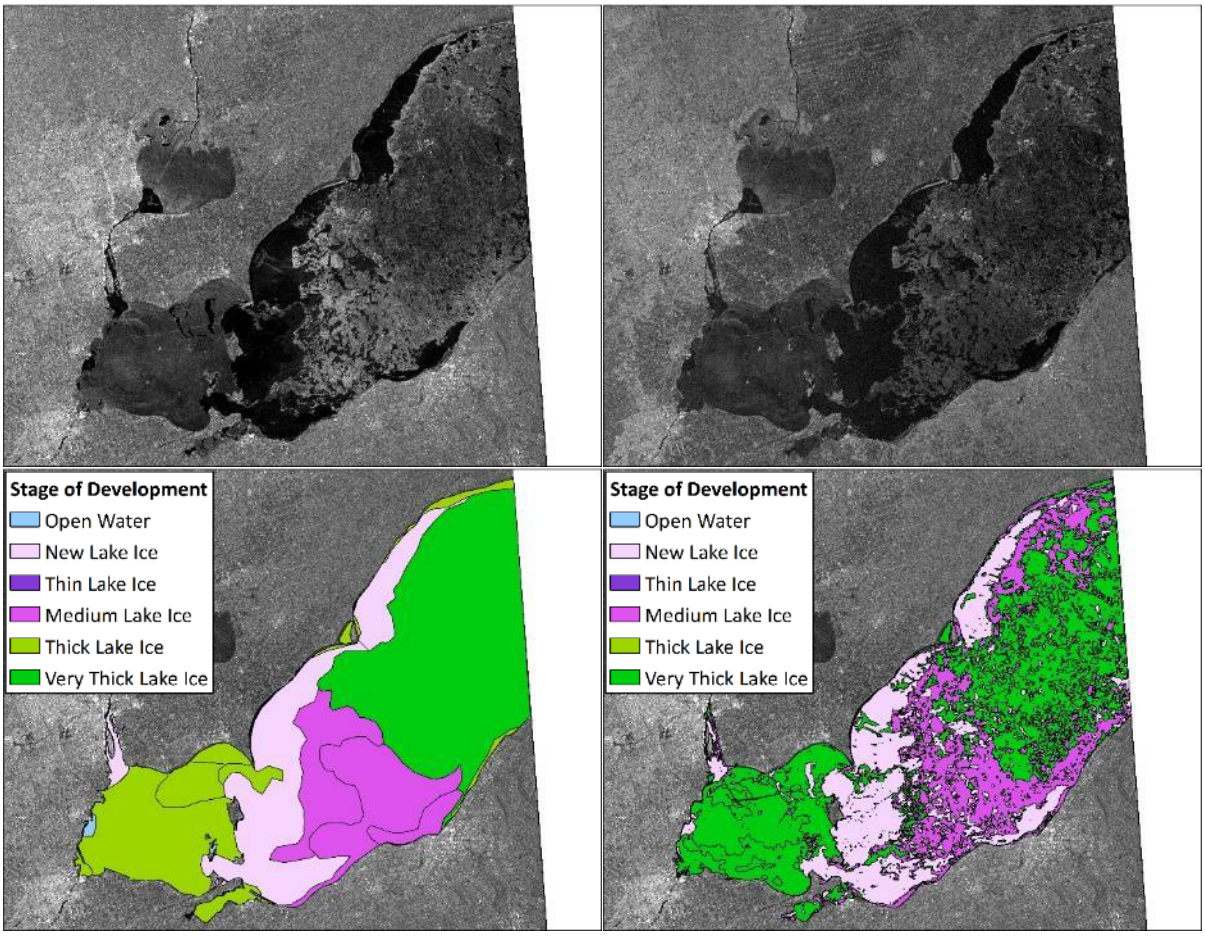
Stage of Development
Open Water
New Lake Ice
Thin Lake Ice
Medium Lake Ice
Thick Lake Ice
Very Thick Lake Ice
Stage of Development
Open Water
New Lake Ice
Thin Lake Ice
Medium Lake Ice
Thick Lake Ice
Very Thick Lake Ice

3/25/2014

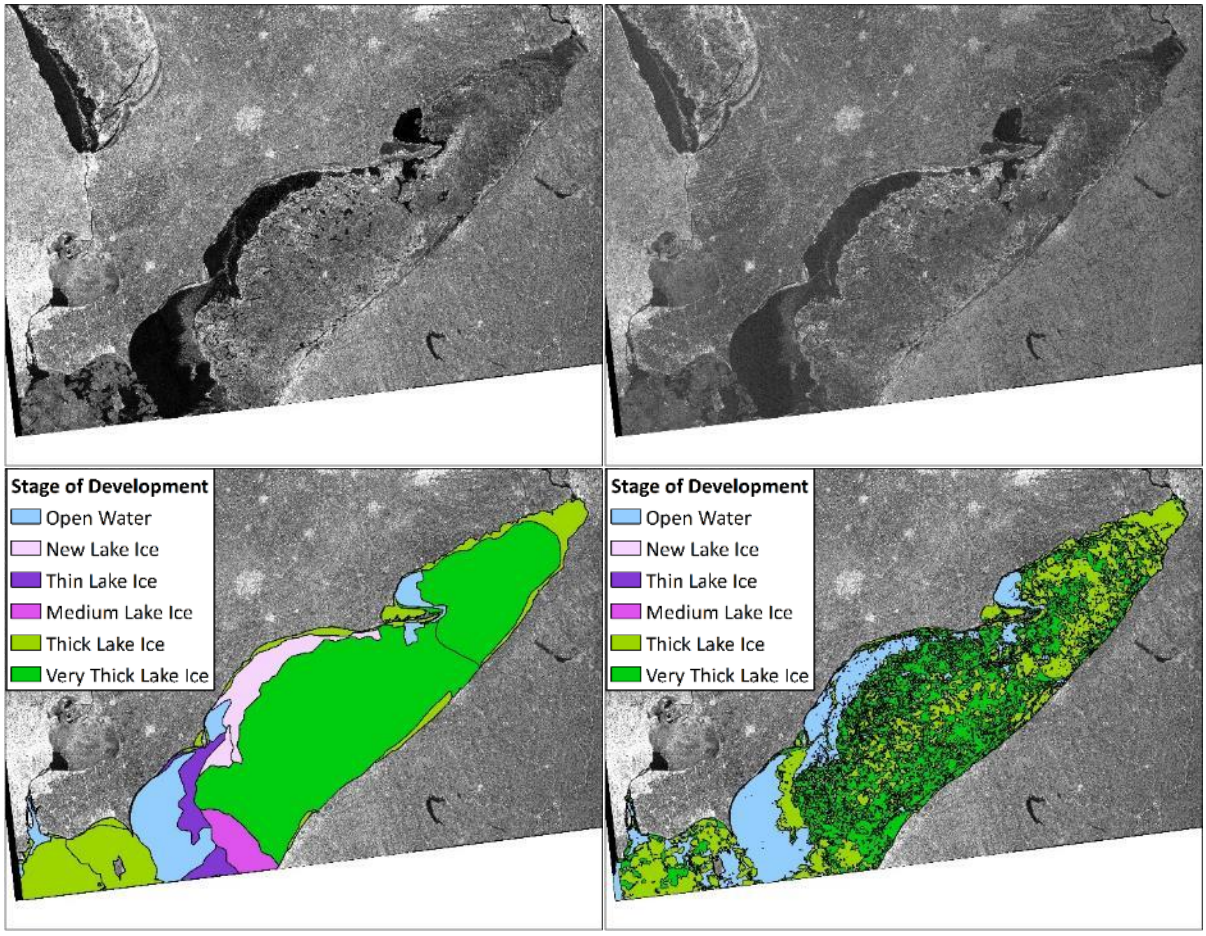
Stage of Development
Open Water
New Lake Ice
Thin Lake Ice
Medium Lake Ice
Thick Lake Ice
Very Thick Lake Ice
Stage of Development
Open Water
New Lake Ice
Thin Lake Ice
Medium Lake Ice
Thick Lake Ice
Very Thick Lake Ice

3/28/2014

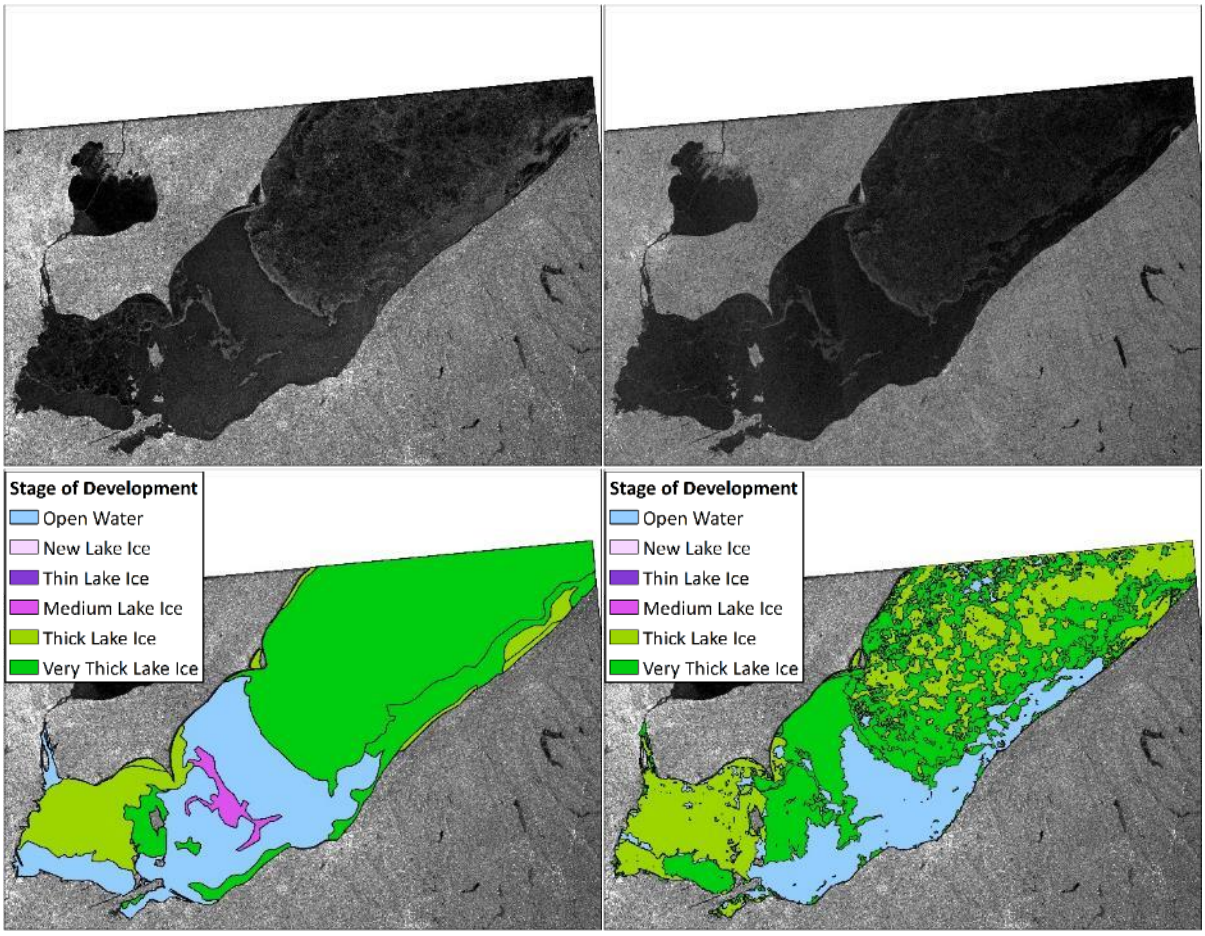
Stage of Development
Open Water
New Lake Ice
Thin Lake Ice
Medium Lake Ice
Thick Lake Ice
Very Thick Lake Ice
Stage of Development
Open Water
New Lake Ice
Thin Lake Ice
Medium Lake Ice
Thick Lake Ice
Very Thick Lake Ice

4/1/2014

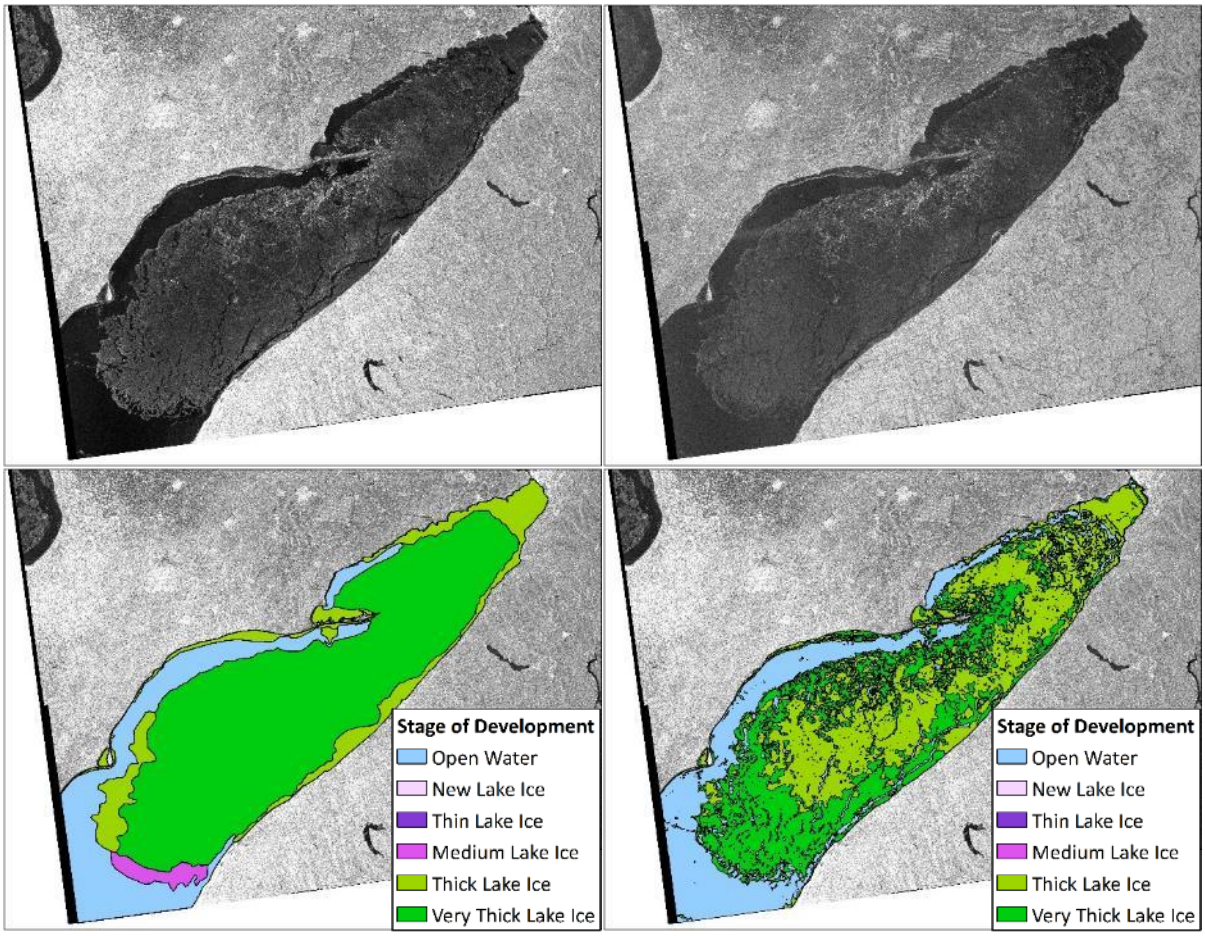
Stage of Development
Open Water
New Lake Ice
Thin Lake Ice
Medium Lake Ice
Thick Lake Ice
Very Thick Lake Ice
Stage of Development
Open Water
New Lake Ice
Thin Lake Ice
Medium Lake Ice
Thick Lake Ice
Very Thick Lake Ice

4/4/2014

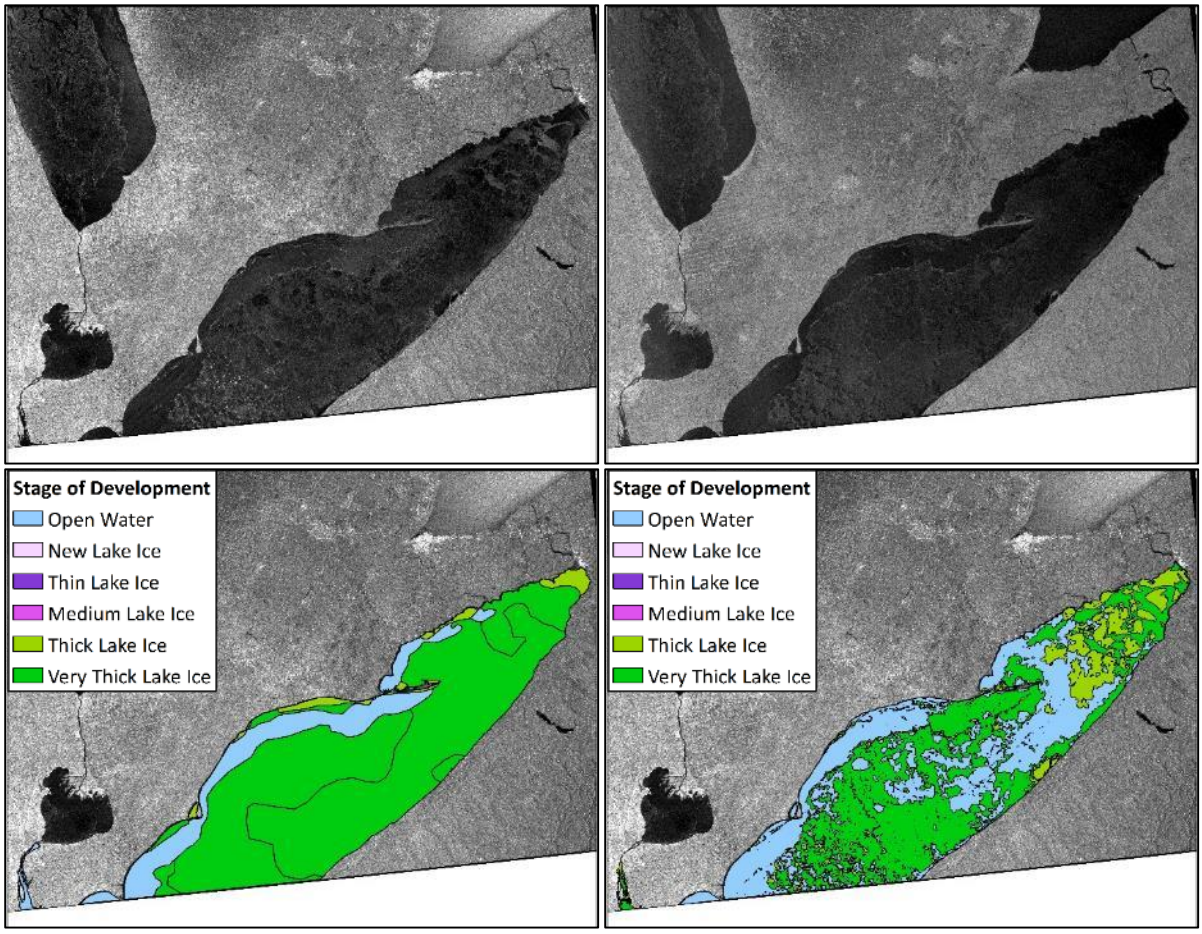
Stage of Development
Open Water
New Lake Ice
Thin Lake Ice
Medium Lake Ice
Thick Lake Ice
Very Thick Lake Ice
Stage of Development
Open Water
New Lake Ice
Thin Lake Ice
Medium Lake Ice
Thick Lake Ice
Very Thick Lake Ice